NASA Contractor Report 3031

Surface Temperatures and Glassy State Investigations in Tribology

Part I

Ward O. Winer and David M. Sanborn

GRANT NSG-3106
JUNE 1978

NASA

NASA Contractor Report 3031

Surface Temperatures and Glassy State Investigations in Tribology

Part I

Ward O. Winer and David M. Sanborn
Georgia Institute of Technology
Atlanta, Georgia

Prepared for
Lewis Research Center
under Grant NSG-3106

National Aeronautics
and Space Administration

**Scientific and Technical
Information Office**

1978

TABLE OF CONTENTS

	Page
SUMMARY	1
I. GLASS TRANSITION AND GLASSY STATE BEHAVIOR OF LUBRICANTS	6
A. Transitions by Light Scattering	6
B. Dielectric Relaxation Transition Measurements	17
C. Transitions Measured by Dilatometry	19
D. Lubricant Shear Stress-Strain Behavior in the Amorphous Glassy Region	21
E. Discussion of Results	25
II. FURTHER EXPERIMENTS IN AN EHD SIMULATOR	29
A. EHD Contact Behavior of 5P4E	30
B. Additional Investigations of the EHD Behavior of a Naphthenic Base Oil	35
C. Starvation Failure Experiments	41
III. CONCLUSIONS	46
IV. REFERENCES	48
APPENDIX: DESCRIPTION OF EXPERIMENTAL FLUIDS	51

LIST OF TABLES

Table		Page
I.	Least-square Expressions for the Glass Transition Temperature as a Function of Pressure for Experimental Lubricants Based on Formation History B. T_g in C and P_g in GPa	60
II.	Glass Transition Temperature, T_g, at Atmospheric Pressure	61
IIIa.	Temperature and Traction Measurements for Fluid 5P4E	62
IIIb.	Film Thickness Measurements for Fluid 5P4E	62
IV.	Summary of Stationary Ball Surface Temperature	63
V.	Normal Load Sharing Between Asperities and the EHD Film	64
VI.	Experimental Study of Starvation Failure of a Sapphire on Steel Ball Contact	65

LIST OF ILLUSTRATIONS

Figure		Page
1a.	Schematic Arrangement of the Light-Scattering Experiment . .	66
1b.	Schematic Arrangement of the Light-Scattering Cell. The Intensifier is attached Perpendicular to the Plane of the figure at the centerline of the cell	67
2.	Frequency Spectrum of N1 obtained by History A at 0.277 GPa and 24C. B and R represents the Brillouin and Rayleigh Components respectively (the two signal levels represent two system amplifications for clarity).	68
3.	Variation of Frequency Shift (ω_B) and Sound Velocity (V) with Pressure at 24C for Naphthenic Mineral oil (N1) (History B). Arrows indicate glass transition pressure (P_g)	69
4.	Velocity of Sound (V) as a function of Temperature at Different Pressures for Naphthenic Mineral Oil (N1) (History B). Arrows indicate Glass Transition Temperature (T_g)	70
5.	Transition Diagram for Four Experimental Fluids. Solid and Open Symbols are for Histories A and B respectively. Glassy state is to the right and below Transition lines and liquid state is to left and above transition lines based on Light-Scattering Technique	71
6.	Typical Sound Velocity as a Function of Temperature and Frequency at Constant Pressure V_∞ and V_o are limiting High and Low Frequency Sound Velocities Respectively	72
7.	Schematic of Dielectric Cell	73
8.	Permittivity (ε') of Polyphenyl Ether (5P4E) at 0.414 GPa (60 kpsi)	74
9.	Dielectric Loss Tangent (ε'') of Polyphenyl Ether (5P4E) at 0.414 GPa (60 kpsi)	75
10.	Dielectric Transition of Naphthenic Miner Oil (N1)	76
11.	Dielectric Transition of Polyphenyl Ether (5P4E)	77
12.	Dielectric ($10 \leq Hz \leq 10^6$), Low Rate Dilatometry (arrows) and Light Scattering ($Hz = 10^{10}$) Transition Data at Atmospheric Pressure	78

Figure		Page
13.	Schematic of High Pressure Dilatometer (0.35 to 1.75 GPa)	79
14.	Volume Dilatometry Transition Diagram for Polyphenyl Ether (5P4E), Naphthenic Mineral Oil (N1), Synthetic Paraffinic Mineral Oil (XRM 177F)	80
15.	Volume Dilatometry Transition Diagram for Perfluorinated Poly ether (Krytox 143-AB), Super refined Naphthenic Mineral Oil (FN 2961), Paraffinic Mineral Oil (P1) Modified Polyphenyl Ether (C-ether) (MCS-418)	81
16.	Volume Dilatometry Transition Diagram for Pentaerythritol (Advanced Ester), Polyalkyl aromatic (DN 600), Synthetic hydrocarbon (MCS 460), Tri-aryl phosphate ester (Fyrquel 150), Synthetic cycloaliphatic hydrocarbon (Santotrac 50)	82
17.	Schematic of Shear Stress Apparatus, 0.7 GPa (100 kpsi)	83
18.	Recorder Plot of Shear Stress versus Shear Strain for Polyphenyl ether (5P4E) at 0.275 GPa (40 kpsi) and Indicated Temperatures	84
19.	Elastic Shear Modulus of Polyphenyl Ether (5P4E) at 0.275 GPa in (40 kpsi) in Amorphous Glassy Region	85
20.	Ultimate Shear Stress of Polyphenyl Ether 5P4E	86
21a.	Ultimate Shear Stress for Naphthenic Mineral Oil (N1) . .	87
21b.	Ultimate Shear Stress for Naphthenic Mineral Oil (N1) . .	88
22.	Ultimate Shear Stress for Synthetic Cycloaliphatic Hydrocarbon (Santotrac 50)	89
23.	Ultimate Shear Stress for Synthetic Cycloaliphatic Hydrocarbon (Santotrac 50), Polyphenyl Ether (5P4E), Naphthenic Mineral Oil (N1) at 0.48 GPa (70 kpsi)	90
24.	Ultimate Shear Stress for the Three Lubricants at 0.59 GPa	91
25.	Schematic of High Pressure Falling Body Viscometer (0.63 GPa, 90 kpsi)	92
26.	Pressure-Viscosity Isotherm Naphthenic Mineral Oil (N1) at 40C	93

Figure		Page
27a.	Pressure-Viscosity Isotherms for Polyphenyl ether (5P4E) . .	94
27b.	Pressure-Viscosity Isotherms for Polyphenyl ether (5P4E) . .	95
28.	Pressure-Viscosity Isotherms for Perfluorinated Polyether (Brayco, 815Z)	96
29.	Low Shear Viscosity-Pressure and Dielectric Relaxation Time Isotherms for Polyphenyl Ether (5P4E) at 40C	97
30.	Transition Diagram for Naphthenic Mineral Oil (N1) and Several Methods	98
31.	Transition Diagram for Polyphenyl Ether (5P4E) and Several Methods	99
32.	Comparison of Pressure-Temperature Dependence at Constant Viscosity (μ) or Frequency (f) for Naphthenic Mineral Oil (N1)	100
33.	Comparison of Pressure-Temperature Dependence at Constant Viscosity (μ) or Frequency (f) for Polyphenyl Ether (5P4E) .	101
34.	Traction Coefficient versus Slide-roll Ratio for Polyphenyl Ehter (5P4E)	102
35.	Ball Surface Contact Center Temperature Rise for Polyphenyl Ether (5P4E)	103
36.	Film Thickness for Polyphenyl Ether (5P4E)	104
37.	Traction Coefficient as a Function of Shear Rate, Polyphenyl Ether (5P4E)	105
38.	Ball Surface Temperature Rise Along the Contact Centerline (0.011 μm R_a Roughness, P_H = 1.02 GPa, V = 0.75 m/s) for Naphthenic Mineral Oil (N1)	106
39.	Ball Surface Temperature Rise Along the Contact Centerline (0.011 μm R_a Roughness, P_H = 1.02 GPa, V = 1.00 m/s) for Naphthenic Mineral Oil (N1)	107
40.	Ball Surface Temperature Rise Along the Contact Centerline (Smooth ball 0.011 μm R_a, P_H = 1.02 GPa, V = 0.75 m/s) for Naphthenic Mineral Oil (N1)	108
41.	Ball Surface Temperature Rise Along the Contact Centerline (Smooth ball 0.011 μm R , P_H = 1.02 GN/m^2, V = 1.0 m/s) for Naphthenic Mineral Oil (N1)	109

Figure Page

42. Ball Surface Temperature Rise as a Function of Slide-Roll Ratio (-2 to +2) (Smooth ball 0.011 μm R_a, P_H = 1.02 GPa, $\bar{V}$ = 0.75 m/s) for Naphthenic Mineral Oil (N1) 110

43. Ball Surface Temperature Rise as a Function of Slide-Roll Ratio (Smooth ball 0.011 μm R_a, P_H = 1.02 GPa, $\bar{V}$ = 1.0 m/s) on Naphthenic Mineral Oil (N1) 111

44. Stationary Ball Surface Temperature Rise, pure sliding, 1.02 GPa Hertz Pressure with Naphthenic Mineral Oil (N1). 112

45. Traction Coefficient as a Function of Λ Ratio. Steel Balls with Roughnesses of 0.011, 0.076 and 0.38 μm R_a against Sapphire Flat, Naphthenic Mineral Oil, Bulk Temperature of 27C, Load and Sliding Speed Varied to Vary Lambda Ratio (Λ) 113

46. Percent Increase in Flash Temperature Due to Surface Roughness. Curve (2) corresponds to the Factor Recommended by AGMA [51] (For R_a = 0.011 μm Increase less than 1%) 114

47. Average Value and Range of Ball Surface Temperature Fluctuation versus Peak Hertz Pressure (Medium Rough Ball: 0.076 μm R_a, Fluid Naphthenic Mineral Oil (N1) . . 115

48. Average Fluid Pressure versus Peak Hertz Pressure under Partial EHD Conditions (Medium Rough Ball: 0.076 μm R_a. Fluid Naphthenic Mineral Oil (N1), Ball Sliding Speed 1.0 m/s) 116

49. Maximum Ball Surface Temperature Rise versus Sliding Speed for Steel Ball/Sapphire Flat System (Rough Ball: 0.38 μm R_a, Fluid Naphthenic Mineral Oil N1, Flat Surface Stationary, $\Lambda < 1$ except as noted) with location of conditions for Scoring Failure with Steel on Steel System 117

NOMENCLATURE

a_1, a_2	constants in regression analysis
G_∞	limiting elastic shear modulus
h_c	centerline film thickness
h_m	minimum film thickness
n	refractive index
P_{avg}	average pressure
P_{EHD}	average fluid pressure in EHD film
P_g	glass transition pressure
P_H	Hertz pressure (maximum)
R_a	average asperity height of surface roughness
T_b	ball surface temperature
ΔT_b	ball surface temperature rise, $\Delta T_b = T_b - T_{bath}$
T_{bath}	oil bath temperature
T_{bulk}	bulk oil temperature
TC	traction coefficient
T_g	glass transition temperature
ΔT_g	confidence limit on glass transition temperature
V	sound velocity
$\bar{V}$	rolling speed, $\bar{V} \equiv 1/2(V_b + V_{sa})$
V_b	ball surface velocity
V_s	sliding velocity, $V_s = \lvert V_b - V_{sa} \rvert$
V_{sa}	sapphire surface velocity
W	total load
W_{EHD}	load carried by EHD film

θ	asperity angle in EHD section and scattering angle in light scattering section
λ	wavelength of light
Λ	ratio of film thickness to composite surface roughness or wavelength of sound
σ_θ	asperity slope
Σ	slide/roll ratio, $\Sigma \equiv \frac{V_b - V_{sa}}{1/2(V_b + V_{sa})}$
ω_B	frequency shift of scattered light

SUMMARY

This is the report of research conducted in NASA Grant NSG-3106 for the period May 15, 1976 to May 15, 1977. The reserach efforts and the report are divided into two broad categories, 1) lubricant viscoelastic (or glass) transitions and lubricant rheological behavior, and 2) lubricant behavior in a simulated elastohydrodynamic contact. Both categories of effort are containuations of previous efforts in this laboratory.

The studies of lubricant viscoelastic transition and lubricant rheological behavior have fallen into several categories. These include additional low shear rate pressure viscosity measurements of the naphthenic mineral oil (N1) and the polyphenyl ether (5P4E) to pressures as high as 0.6 GPa. Viscosities as high as 10^7 Pas (10^{10} cp) have been measured and are reported. The viscoelastic transition of several lubricants has been measured by volume dilatometry to pressures as high as 1.75 GPa. Dielectric transitions have been measured at atmospheric pressure on five fluids in a frequency of 0.2 to 500 kHz and on two of those fluids in the same frequency range to pressures as high as 0.55 GPa. The dielectric transition work clearly demonstrates the shift of transition with frequency. The line of constant frequency or rate transition on a pressure-temperature diagram is essentially parallel to the curve for viscoelastic transition based on the dilatometry experiments. In addition, it has demonstrated that lines of constant viscosity also plot essentially parallel to both of the above mentioned transitions on a temperature-pressure plot. Two fluids were also

examined at elevated pressure for their viscoelastic transition based on light scattering techniques. The pressure range of the light scattering experiments was from 0.1 to 0.7 GPa. Lubricant shear stress-shear strain behavior in the amorphous glassy state was also measured to pressures of 0.7 GPa. Three fluids were examined at two pressures and various temperatures from the glass transition temperature based on dilatometry to approximately 60C below that temperature. All of these fluids demonstrated classical elastic-plastic behavior of an amorphous solid. They clearly exhibited an elastic shear modulus for strains less than approximately three percent and nearly constant ultimate shear strengths for shearing strains greater than three percent. The elastic shear modulus of one of the fluids, polyphenyl ether (5P4E), agrees well with measurements based on ultrasonic techniques that are available in the literature. The limiting shear stress of the materials range up to 90 MPa with a clear difference in this property among the three fluids examined. It appears from these investigations that many lubricants undergo viscoelastic and viscoplastic transitions in typical EHD contacts. Only in contacts with very low slide-roll ratio will the strain in the lubricant be small enough (less than 3%) for the elastic shear strain response of the lubricant to be important in determining the contact traction. In contacts with larger slide-roll ratios, and therefore larger shear strain in the lubricant, the viscoplastic transition and limiting shear stress of the material will determine the traction transmitted in the contact.

The elastohydrodynamic simulator studies conducted under this contract have consisted of infrared temperature measurement work for

both thick film and thin film elastohydrodynamic contacts with both sliding and rolling kinematics. Surface temperature measurements with the naphthenic mineral oil (N1) have been made for slide-roll ratios from -2 to +2 with film thicknesses larger than the composite surface roughness. This work has permitted the determination of the surface temperatures of the slower moving and stationary surfaces in sliding and rolling contacts. As expected the surface temperature of the stationary contact in a sliding contact is higher than that of the moving contact. For slide-roll ratios less than approximately 0.8 the surface temperatures as a function of slide-roll ratio are essentially symmetric about a zero slide-roll ratio. Measurements of surface temperature, film thickness and traction for polyphenyl ether (5P4E) have been made for slide-roll ratios of 0 to 2. In both of the above mentioned EHD studies the Hertz pressure was approximately 1 GPa. In addition, surface temperature measurements have been made in sliding contacts where the film thickness was equal to or less than the composite surface roughness. This research was in part a continuation of the rough surface temperature measurement research reported in the previous contract report. Analysis of the data has allowed the recommendation of a correction factor on flash temperature theory calculations for rough surfaces. The correction factor, based on regression analysis of the surface temperature measurement, is very similar to that recommended by the American Gear Manufacturer's Association.

Further rough surface temperature measurements were made with a severely starved sliding elastohydrodynamic contact. These experiments appeared to show that the scoring failure on a severely loaded contact

is stochastic in nature and isolated to small areas of the contact surface. Once the local scoring has occurred, local instantaneous temperatures as high as 1100 to 1200C were measured. The locally scored area will persist with high temperatures for many revolutions of the ball. It was observed that the high local temperatures were flashing synchronously with the rotation of the ball. Over the remaining area of the ball during a revolution the temperatures were relatively low (300C).

The EHD temperature measurements were subjected to a regression analysis to develop predictive equations for surface temperatures in elastohydrodynamic contacts. These equations were compared with the predictions from the Blok-Archard flash temperature analyses available in the literature. In general, the measured temperatures were less than those predicted by the Blok-Archard theories. This is thought to be because the Blok-Archard theories assumed that all energy transfer processes occur only in the Hertzian zone of the contact while in the experimental measurement system there is usually fluid surrounding the Hertzian zone to which energy is transferred. The fluid surrounding the Hertzian zone tends to act as a coolant to the Hertzian zone thereby lowering the surface temperatures in that region. As a general observation, the maximum surface temperature measured in the Hertzian zone is approximately equal to the average temperature predicted by the Blok-Archard theory. Therefore the surface temperatures in a starved contact would be expected to be higher than those observed in the contact surrounded by the lubricant.

The principal investigators wish to acknowledge the contributions

of several investigators to the research reported here; specifically Drs. Alsaad, O'Shea and Medina to the light scattering transition work, Mr. Scott Bair to the remaining rheological investigations and to the EHD equipment, and Dr. H. S. Nagaraj to the EHD investigations.

I. GLASS TRANSITION AND GLASSY STATE BEHAVIOR OF LUBRICANTS

The work started in the previous contract year has been continued and extended. The limiting low rate viscoelastic (glass) transition measurements by dilatometry and light scattering have been extended to additional lubricants and, for dilatometry, to higher pressures. A limited number of high rate transitions with light scattering have also been obtained. An apparatus for measuring dielectric transitions has been developed and used to obtain data on seven fluids at atmospheric pressure and two of them at high pressure. Another apparatus has been developed to measure the shear stress-strain behavior of lubricants under pressure and in the amorphous glassy state. This apparatus has been used to obtain data on three lubricants. Lastly, a falling body, low shear, pressure viscometer has been developed which is capable of pressures to 0.6 GPa, temperatures to 150C and viscosities to 10^7 Pas.

A. Transitions by Light Scattering[1]

The light scattering technique presented in the previous contract report (1) was employed to obtain data on two additional fluids (MCS-1218, a cycloaliphatic hydrocarbon, and N2, a polymer blend consisting of N1 + 2.2 wt. % polybutene polymer). Fluid property descriptions are

[1]The efforts of Dr. M. Alsaad and Professor D. O'Shea in conducting the work discussed in this section are acknowledged and appreciated.

found in Appendix A. Details of the experimental technique and underlying theory can be found in (1 and 2). These will be summarized here along with the results most relevant to elastohydrodynamic lubrication. More detailed data can be found in Alsaad [2]. For completeness, data on all four fluids will be included here.

A.1 Light Scattering Theory

When a laser beam passes through a transparent medium, a small portion of the light is scattering in all directions due to the optical inhomogeneities in the medium. The inhomogeneities are the result of fluctuations of the dielectric constant brought about by fluctuations of the density of the medium due to random thermal motion of the molecules [3]. The fluctuations in the dielectric constant can be separated into entropy fluctuations at constant pressure and pressure fluctuations at constant entropy. The adiabatic pressure fluctuations can be described by means of plane sound waves of thermal origin propagating in all directions. The interaction of a light wave of wave length, λ, with the sound waves in a media with refractive index, n, leads to Brillouin scattering of light by sound waves of a particular wavelength, Λ, in the direction given by the scattering angle θ and satisfying the Bragg condition:

$$2 \Lambda \sin \theta/2 = \frac{\lambda}{n} \quad . \tag{1}$$

Moreover, as a consequence of the movement of the sound waves, the frequency of the incident light is altered by the Doppler effect with respect to the original value, ω_o. This effect was first predicted by

Bruillouin [4] as

$$\omega_B = 2(nV \sin \theta/2)/\lambda \qquad (2)$$

which can be written as

$$V = \frac{\omega_B \lambda}{2n \sin \theta/2} \cdot \qquad (3)$$

Equation (3) shows that the sound velocity, V, can be determined if monochromatic light strikes the material and the frequency shift, ω_B, of the scattered light is measured for a fixed scattering angle.

In recent years, Brillouin scattering has been used in the study of polymers above and below the glass transition temperature. A change in slope of the velocity as a function of temperature or pressure, like density or specific heat, defines the glass transition and has been observed by many workers [5-9]. The change in the temperature and pressure coefficients of the sound velocity, indicating the occurrence of glass transition was observed in all lubricants investigated in this study.

A.2 Experimental Technique

The schematic arrangement of the basic components of the light scattering experiment is shown in Figure 1a and consists of an argon ion laser having a power of about 200 mw in single mode operation at

λ = 0.5145 μm, a high pressure scattering cell* (Figure 1b) containing the lubricant sample to be investigated, and a detector which permits the spectroscopic analysis of the scattered light. The scattered light is collimated by a lens and analyzed by a Fabry-Perot interferometer operating in triple pass geometry. The ring pattern from the interferometer is focused on a screen which has a pinhole in front of a photomultiplier tube (PMT), so that only the center frequency of the ring pattern is detected. One of the Fabry-Perot plates is attached to three piezoelectric stacks and can be swept in and out, thus changing the frequency that passes through the pinhole. The output signal from the PMT can be processed by a standard counting system and stored in a multichannel analyzer. The multichannel analyzer was triggered off the Rayleigh line to avoid broadening that results from drifts of the incident laser frequency relative to the interferometer pass frequency. The spectrum can also be plotted on an X-Y recorder and/or punched on paper tape.

The high pressure equipment consists of a scattering cell which was used to pressures of 0.69 GPa, a strain gage pressure transducer, a hand pump, and a 9:1 area ratio intensifier.

The four lubricants investigated were: naphthenic base oil (N1), N1 blended with 2.2 percent high molecular weight polybutene (N2), polyphenyl ether (5P4E), and cycloaliphatic hydrocarbon (MCS-1218). These oils were selected because they represent typical commercially available lubricants and research materials of current interest in

*Designed by W. B. Daniels of the University of Delaware.

the field of EHD lubrication. The fluids were passed through a millipore filter which substantially reduced parasitic light scattering and made it possible to obtain the Brillouin spectra. More detailed descriptions of the oils can be found in Appendix A.

A.3 Experimental Procedure and Data Reduction Technique

Two standard procedures were adopted to form the glass of the materials investigated. In formation history A, the glass was formed by pressurizing the samples at room temperature from atmospheric pressure until the glassy state was reached. Brillouin spectra were taken at pressure intervals of about 0.02 to 0.03 GPa. The spectra were taken 20 minutes after the pressure change was imposed. In formation history B, the pressure was increased from atmospheric to a reference pressure while the sample temperature was increased such that it remained in the liquid state. When a temperature of about 15C above the assumed glass transition for the corresponding pressure was reached, the pressure and temperature were kept constant for about 30 minutes. The sample was then cooled at constant pressure and frequency spectra were recorded at 2 or 3C intervals. Twenty minutes were allowed for the temperature to reach equilibrium before each spectrum was recorded.

This procedure was repeated at different pressures. The sample temperature was changed by controlling the voltage input to a resistance heater tape wrapped around the intensifier-cell assembly which was enclosed in an oven. The temperature was measured with a copper-constantan thermocouple in conjunction with a direct reading digital

thermometer referenced to an ice bath. The temperature was controlled to better than $\mp$ 0.1C.

All spectra were recorded at a fixed scattering angle of 90^{o}. Light scattering results of the naphthenic base oil (N1) were selected to explain the data reduction technique. Results of other experimental oils investigated were obtained in a similar manner and only their transition diagrams will be reported here.

The Brillouin spectrum of N1 recorded at 0.277 GPa and 24.4C (History A) is shown in Figure 2. It is typical in general appearance of all spectra obtained. The Fabry-Perot plate separation was 0.40 cm corresponding to a free spectral range of 37.5 GHz. The frequency shift was determined from the position of the Brillouin peaks and the sound velocity was calculated from equation (3). The refractive index needed in equation (3) was measured as a function of temperature by using a precision Abbe "60" refractometer (sodium D, line, $\lambda = 0.5896$ μm). Since it was not possible to measure the variation of the refractive index with pressure, it was assumed that $\frac{dn}{dP}$ for all experimental oils investigated has a constant value of 2.9×10^{-4} per MPa. This value was estimated from information available in the literature [10] for 5P4E. Any other estimate for $\frac{dn}{dP}$ will only shift the velocity of sound up or down without changing the location of the glass transition.

A.4 Experimental Results

Figure 3 shows the variation of the frequency shift and the sound velocity with pressure for N1 (History A). The sound velocity and frequency shift increase with increasing pressure and a change in

the slope is apparent at 0.474 GPa. This change of slope represents the glass transition P_g [5-7,9]. Results obtained by History B at different constant formation pressures are shown in Figure 4. At constant pressure the sound velocity increases as the temperature is decreased and a change in slope is observed for each formation pressure. The two portions of the sound velocity curves of Figures 3 and 4 were fit by least square regression to straight lines and were solved for their intersection to determine the glass transition. Figure 4 shows that T_g shifted to a higher temperature as the formation pressure was increased. The glass formation temperature-pressure combinations resulted in the transition diagram in Figure 5. Also included in this figure are the transition diagrams of the other experimental fluids obtained by the data reduction technique discussed above.

The glass transition temperatures and pressures for each oil were least square fitted to a straight line and the expressions obtained are given in Table I. They show that the rate of increase of T_g with pressure for N1 has the lowest value ($\simeq$ 120 C/GPa) while that of MCS-1218 has the largest value ($\simeq$ 200 C/GPa). The glass transition data obtained by History A are also shown in Figure 5 but were excluded from the fit due to the different history by which the glass was formed. However, in general, the transition obtained by History A falls on or near the transition line obtained by History B.

Figure 5 also shows the effect of the viscosity-index improver blended with the naphthenic base oil on the glass transition behavior of the blend relative to the base oil. The glass transition pressure, P_g, at room temperature for the blend occurred at 0.438 GPa compared

with 0.475 GPa obtained for the base oil. The glass transition temperature, T_g, for N2 occurred at 7.5C higher than that of N1 at 0.69 GPa. As seen from Table I, the rate of increase of T_g with pressure increased by about 10 percent from 120 to 134 C/GPa.

The longitudinal velocity of sound in the temperature and pressure ranges investigated was 2300 to 3400 m/s for N1 and N2 fluids, 2200 to 2900 m/s for 5P4E and 2600 to 3500 m/s for MCS-1218. This data can be used to determine the secant bulk modulus

$$\text{sound velocity} = (\text{modulus/density})^{1/2}$$

The velocity of sound as a function of pressure for 5P4E at comparable temperatures and history A where consistently about 3 to 4 percent higher than those reported by Dill et al. [10].

A.5 Error Analysis

The uncertainties in the absolute value of the sound velocity which arise from the uncertainties in the scattering angle, θ, the frequency shift, ω_B, and the refractive index, n, are not of great concern in the present work as the absolute value of the sound velocity is not our main concern. The quantity of interest is the intersection of the sound velocity versus temperature or pressure curves in the liquid and glassy regions which represents the glass transition for the material. This quantity is not strongly influenced by any of the above uncertainties. In obtaining all frequency spectra for each experimental fluid at different constant formation pressures, the

position of the scattering cell remained fixed and a single separation distance of the Fabry-Perot mirrors was chosen to cover the expected frequency range of the calculated velocities. This arrangement ensured that the error in the calculated velocities due to the uncertainties mentioned above for each constant formation pressure is the same for all other pressures. The influence of the above errors on the measurements is to shift the velocity-temperature or the velocity-pressure curves to higher or lower velocities without changing the location of the glass transition temperature or pressure.

The error in the location of T_g and P_g is the most important uncertainty in this work. A statistical method giving the confidence limits of the abscissa of the interseciton of two linear regressions is described in Reference [11]. This method can be used to determine the confidence limits on T_g using the liquid and the glassy linear regression expressions of the form

$$V = a + b\,T \tag{4}$$

Using the equal variance assumption, the confidence limit, ΔT_g, is equal to the difference of the two roots of the following quadratic equation

$$A\,T_g^2 + B\,T_g + C = 0 \tag{5}$$

where the coefficients A, B and C are given in Reference [11]. The 95 percent confidence limits of T_g were calculated for all lubricants investigated ΔT_g ranged from a low of 0.7 to 1.1C for N_1 to a high of from 0.7 to 3.6C for 5P4E.

An additional possible source of error in these experiments is the determination of sample pressure when the sample has gone into the glassy state. Although the pressure transducer is calibrated, it is connected to the sample cell by a passage with a small diameter. Because of fluid compressibility and transducer deformation (both small) as the pressure is increased in the sample cell some fluid motion along the passage to the transducer is required to change the pressure at the transducer. The sample scattering cell is between the pressure intensifier and the pressure transducer. Therefore as the pressure is increased in the intensifier for history A or flow from the intensifier is required to maintain constant pressure in history B, it first increases in the sample cell and then in the pressure transducer. When the material goes into the glassy state movement between the sample cell and pressure transducer is inhibited resulting in the transducer indicating a lower pressure than occurs in the cell. The magnitude of this effect is difficult to estimate and any error would be primarily in the glassy region.

A.6 Characteristic Frequency of Light Scattering Experiments

The viscoelastic or glass transition response of a material is dependent upon the frequency of the imposed environmental changes on the material. For example, in cooling experiments the glass transition temperature increases as the cooling rate is increased. For a steady periodic stress imposed on the material an increase in frequency of the

imposed stress shifts the transition to higher temperatures. The amount of shift with rate varies for different materials.

In the experiments described in this section on light scattering two widely different rates are present: a) the very low rate cooling process, and b) the high frequency inherent density fluctuations. The characteristic frequency of the density fluctuations is equal to the Brillouin frequency shift, ω_B. The characteristic time of these fluctuations is one the order of 10^{-10}s while the characteristic time of the superposed low rate cooling is greater than 10^{3}s. The difference in transition temperatures for these two quite different rates is large: about 60C for 5P4E and 160C for N1. Because of the magnitude, and limited range, of the temperatures of the experiments reported in this section, the transitions observed and reported are those corresponding to the low rate cooling process and would normally be referred to as the glass transition temperatures. The typical full range of sound velocity as a function of temperature and frequency would be like that shown in Figure 6.

Preliminary examination of two fluids in the light scattering experiment at higher temperatures and atmospheric pressure (N1 and 5P4E) has been conducted. This allowed the estimation of the high rate ($\simeq 10^{10}$ s^{-1}) transition temperatures for these fluids. These data are shown in Figure 12 in which they are seen to agree well with general relationship of transition temperature with frequency from the dielectric experiments. These data have also been entered in Figures 30 and 31. These data are preliminary in nature and more complete data will be obtained during the next year.

B. Dielectric Relaxation Transition Measurements

All properties of liquids undergo a transition in response which is a function of temperature, pressure and rate of application. Measurements described elsewhere in this report are concerned with the properties, density, viscosity, shear stress, and refractive index in the measurement of the transition. As suggested by Harrison [12] the measurement of the transition in dielectric response of the material may afford a convenient way of determining the transition characteristics of liquids over a wide frequency range. Although the correlation between mechanical property response (important to EHD) and dielectric transition is not well established [12], the relative ease with which a wide frequency range can be covered justifies the examination of the dielectric transition. Therefore an apparatus was developed in which the dielectric transitions can be measured. Five fluids (MCS 1218, Santotrac 50, Krytox, Fyrquel, Diester) have been studied at atmospheric pressure over a frequency range from 0.2 to 500 kHz and two fluids (5P4E and N1) have been studied from atmospheric pressure to 0.55 GPa over the same frequency range. Detailed descriptions of these fluids can be found in Appendix A.

B.1 Equipment

The dielectric relaxation of several lubricants was observed in the apparatus shown schematically in Figure 7. The pressure vessel was made of 4340 alloy steel. The coaxial cylindrical capacitor was calibrated in air. One terminal of the capacitor extended through an electrode of special design and the other connected to the body of the

cell. The atmospheric pressure data was taken with the capacitor removed from the pressure vessel. The high pressure data was taken with the cell in the high pressure vessel fitted with an isolating piston.

A General Radio impedance bridge with an accuracy of one percent in the frequency range of 20 Hz to 20 kHz was used to measure the loss factor and the capacitance of the capacitor-sample combination. Measurements were taken to 500 kHz with reduced accuracy. A twenty liter constant temperature bath provided steady temperature control.

B.2 Technique

The cell containing a fluid sample was pressurized to the desired test pressure while a temperature of about 60C above the expected transition temperature was maintained. Capacitance and loss factor of the capacitor were measured at various frequencies at approximately 3C intervals as the sample was cooled at the rate of approximately 0.5C/minute. The sample temperature was measured with a thermocouple in the cell wall.

B.3 Experimental Results

The permittivity and the loss tangent were plotted versus temperature. Typical examples are shown in Figures 8 and 9, respectively. The temperature at which the loss tangent was maximum at a given frequency was recorded as the transition temperature for that frequency and pressure. This transition temperature corresponded well with the midpoint temperature of the change in permittivity in most cases (Figure 8).

Dielectric transition data for N1 and 5P4E at atmospheric and

elevated pressure are shown in Figures 10 and 11, respectively. These data are also shown as lines of constant frequency along with lines of constant low shear rate viscosity on Figures 30 and 31 which show the low rate dilatometry data.

The data at atmospheric pressure for all seven fluids are shown in Figure 12 where they are compared with low rate dilatometry data and tenative high rate light scattering transition data.

C. Transitions Measured by Dilatometry

The capability in this area described in the last contract report [1] has been extended by the construction of a new apparatus capable of pressures to 1.75 GPa. This instrument is similar to those reported before [1] and is shown schematically in Figure 13. Changes in the sample volume are measured mechanically by a dial indicator attached to the piston to an accuracy of 2 μ m. The piston is equipped with Bridgeman seals at both the large and small diameter ends. The high pressure cylinder is constructed of 4340 alloy steel. Kerosene at up to 0.55 GPa is introduced into the large-bore cylinder and its pressure measured with a Heise bourdon gauge. After calibrating the equipment for seal friction, the sample pressure is calculated from the kerosene pressure and the piston area ratio. The entire dilatometer is immersed in a constant temperature bath. A temperature range of -40C to 130C is possible. The bath temperature is maintained by electric heaters and a two stage refrigeration unit. Liquid nitrogen is used for rapid cooling. Temperatures are measured both in the bath and in the high pressure cylinder wall with a thermocouple. Isothermal compression and isobaric

cooling experiments were conducted in the high pressure apparatus.

The low pressure (0.014 to 0.42 GPa) dilatometer [1] was modified to improve accuracy and ease of operation. It provides high volume sensitivity for cooling experiments. Sample pressure in this apparatus is measured by a Heise bourdon gauge actuated by kerosene which is separated from the sample by an isolator piston equipped with an O-ring seal. No seal friction correction is necessary. Volume change is measured by a magnetic core attached to the isolator piston. A linear variable differential transformer indicated the position of the core.

The atmospheric pressure dilatometer [1] was used over a temperature range of -110 to 0C. Volume changes were measured with a pipette in the top of the sealed sample holder. Methanol was used as an indicator in the pipette and was separated from the sample by a silicone diaphragm when there was the possibility of the methanol mixing with the sample. Cooling was accomplished in a methanol bath cooled by liquid nitrogen. Sample temperature was measured with a copper-constantan thermocouple in the aluminum cylinder wall.

C.1 Technique

Isothermal compression experiments were performed with the dilatometer in a constant temperature ($\pm$ 0.5 C) bath. Initial pressure is either atmospheric or well below the transition pressure estimated from previous data. Pressure increases are in steps of from 0.03 to 0.1 GPa. Final pressure and volume measurements are made after apparent equilibrium is reached (2 to 15 min.). Pressure is increased until three or four points are obtained in the glassy state where pressure

increased linearly with decreasing volume. The transition pressure is determined by extrapolating the linear portions of the pressure-volume curve to their intersection.

Isobaric cooling is performed by lowering the temperature of a propanol bath continuously with liquid nitrogen. The initial temperature is chosen well above the transition temperature estimated from previous data. Constant pressure is maintained manually to $\pm$ 1.4 MPa. The sample is then cooled and sample volume measured as a function of temperature. The transition temperature is determined by extrapolation of the linear portions of the temperature-volume curve to their intersection.

C.2 Experimental Results

In addition to the fifteen fluids reported in the previous contract report [1] the data for some fluids was extended to higher pressure and data on additional fluids were obtained. The glass transition temperatures at atmospheric pressure for several fluids based on cooling experiments are shown in Table II. The elevated pressure data are shown in Figures 14, 15 and 16. The general behavior is similar to that reported before [1].

D. Lubricant Shear Stress-Strain Behavior in the Amorphous Glassy Region

If lubricants undergo glass (or viscoelastic) transitions in EHD contacts and behave as amorphous solids in the contacts, then their large strain, shear stress-shear strain behavior in the amorphous state should be examined. An average particle in a typical EHD contact undergoes large strain ($\geq$ 10%) and therefore behavior in small strain

oscillatory experiments may not be relevant to EHD. Therefore experiments were conducted to measure the shear stress shear strain behavior of liquid lubricants under pressure and in the amorphous glassy state.

The sample was sheared to strains large enough to determine both the elastic shear modulus of the material at small strain and the ultimate or limiting shear stress. These properties were found to be functions of formation pressure and temperature below the transition temperature. Both properties continue to increase as the pressure is increased and as the temperature decreases until they begin to level off at about 50C below the transition temperature for a given formation pressure. Data has been taken on three fluids: N1, 5P4E and Santotrac 50. These limited data suggest that the maximum traction in a EHD contact is determined by the ultimate shear stress in the fluid when pressure and temperature conditions in the contact cause the material to be in the glassy state.

D.1 Equipment and Technique

An apparatus has been constructed to measure the mechanical shear properties of glassy lubricant samples to pressures of 0.7 GPa. It is shown schematically in Figure 17. The glassy sample is formed in an annular groove by cooling at elevated pressure. The groove is kept filled by a sample reservoir which is sealed from the working fluid (gasoline) by an isolator piston. The glassy material can be sheared along the midplane of the annulus by the development of a pressure difference across the driving piston. This differential pressure is

measured by two pressure transducers. The sample strain is determined by the displacement of the driving piston measured with an LVDT. Sample temperature is determined by a thermocouple imbedded in the pressure vessel wall.

At moderate working temperatures, such as those for 5P4E (-20 to 35C), and elevated pressures, the seal friction is negligible and no shearing force across the piston can be maintained when the test material is not below its glass transition temperature. However, with N1 the temperature required to go into the glassy region at moderate pressures is so low (-40C) that a correction for seal friction must be employed. The seal friction at low temperature was calibrated by using gasoline as the test fluid which has very low viscosity at the test temperature and pressure. Therefore, at the low shearing rate of the experiment, the driving force on the piston was assumed to be due to seal friction.

D.2 Experimental Results

A typical set of data taken from the x-y recorder is shown in Figure 18. The data shown are for 5P4E at 275 MPa (40 kpsi) for which the low rate glass transition temperature is 35C. The sample is first heated to 45C and pressurized to 275 MPa and then cooled to -35C. The shear stress-strain curves are then generated as the sample is allowed to heat up. As is readily observed both the shear modulus and the ultimate shear stress (maximum shear stress sustained) approach zero as the transition temperature is approached.

The elastic shear modulus from the data in Figure 18 is plotted

in Figure 19 and is seen to approach a constant value at about 50 to 60C below the transition temperature. It should also be noted that the value approached agreed well with the limiting shear modulus G_∞ obtained from ultrasonic experiments [12].

It is believed, however, that the ultimate shear stress data is more relevant to EHD traction. These data are shown in Figure 20 for the 5P4E stress-strain curves in Figure 18. These data show that the ultimate stress for 5P4E has little dependence on formation pressure but increases with temperature below the transition temperature to a nearly constant value at 50C below.

Similar experiments were performed on N1 and Santotrac 50. Only the ultimate shear stress has been plotted in Figures 21a, 21b and 22 for N1 and Santotrac 50 respectively. The pattern of behavior appears to be similar to that of 5P4E except the N1 values seem to be more dependent on formation pressure and those of Santotrac 50 increase more rapidly with decrease in temperature below T_g and are in general higher. Figures 23 and 24 compare the ultimate stress of the three lubricants at two different formation pressures and as a function of subcooling.

D.3 High Pressure Viscometry

A high pressure viscometer of the falling body type has been constructed to operate to 0.63 GPa and 150C. It is shown schematically in Figure 25. A constant shear stress of about 100 Pa is applied to the sample by a cylindrical magnetic sinker housed in a non-magnetic vessel. A linear variable differential transformer indicates the position of the sinker on a recorder. The sample is separated from the pressurizing liquid by an isolator piston. Temperature is maintained

in an air-oven. The entire viscometer is inverted to position the sinker for a test. Viscosity is determined from the time for the sinker to fall a standard distance. A correction is applied for the change in buoyancy of the sinker as the sample density changes with pressure and temperature. Since the vessel bore diameter changes with temperature and pressure, calibration must be carried out over the entire range of conditions that are to be encountered. The instrument was calibrated with bis-2-ethyl hexyl sebecate (Plexol 201 Rohm and Haas Company) using data from the ASME Pressure-Viscosity Report [13]. Viscosities to 10^7 Pas (10^{10} cp) have been measured.

This instrument has been used to measure the pressure-viscosity isotherms of fluids N1, 5P4E and Brayco[1]. These data are shown in Figures 26, 27, and 28. Descriptions of the fluids are found in Appendix A.

E. Discussion of Results

The glass (or viscoelastic) transition for several fluids has been measured over a wide range of frequencies by three different methods (dilatometry, dielectric permittivity and light scattering). The processes involved in these three methods differ in the characteristic rate at which the process and the material interact. Therefore the transition states should be continuous functions of the characteristic frequency. Figure 12 is a plot of characteristic frequency versus the

[1]The Brayco fluid was supplied by K. Demorest of NASA-Marshall Space Flight Center, Huntsville and the work performed under this contract.

reciprocal of the transition temperature for several lubricants at atmospheric pressure. The bulk of the data shown is from the dielectric experiments. Preliminary high frequency light scattering data* is shown for only two fluids. The dilatometry data is plotted along the ordinate and the characteristic frequency for these data is not clear although it is estimated to be less than 10^{-3} or 10^{-4} S^{-1}. The data therefore cover a rate range of up to 10^{14}, or 14 orders of magnitude. The agreement in trend for a fluid over this range appears to be very good. If the characteristic frequency of an EHD contact is known the temperature at which transition is expected could be determined. It must be kept in mind that the data in Figure 12 is all at atmospheric pressure and that the transition temperatures are not only functions of frequency but also pressure.

It has been argued [14] that the glass transition, and therefore conditions of constant relaxation time, should also be approximate conditions of constant low shear viscosity. This is because the relaxation time is essentially the ratio of the low shear viscosity and the limiting high rate shear modulus. The viscosity varies exponentially with both pressure and temperature while the limiting shear modulus varies only linearly and at a much lower rate. Hence the viscosity is the controlling variable. With the above in mind, low shear rate pressure-viscosity isotherms have been compared with dielectric relaxation time isotherms as a function of pressure. These are shown in

*These light scattering data are preliminary and should be repeated with more care to avoid high temperature degradation in an air environment. They are included because they appear to fit the pattern expected.

Figure 29 for 5P4E at 40C. The agreement in trend is obvious although the ratio of them is not constant.

A corollary of the above is that the pressure-temperature dependence of low shear viscosity should be the same as that of dielectric or mechanical relaxation time. The temperature-pressure transition diagrams from the dilatometry experiments are curves of constant relaxation time for the low rate dilatometry experiments. It is instructive to superpose on these diagrams lines of constant low shear viscosity and lines of constant dielectric relaxation time. This has been done for N1 and 5P4E in Figures 30 and 31, respectively. Also added to these figures are the tentative high rate light scattering data at atmospheric pressure.

The slopes of these curves appear to be the same for a given fluid at a particular pressure. The slopes have been determined at atmospheric pressure and one elevated pressure as a function of temperature and plotted in Figures 32 and 33 for N1 and 5P4E, respectively. The agreement between the experimental methods is very good particularly considering the various methods involved in obtaining these data. It is expected that high rate mechanical relaxation times will also fit the same general pattern. The slope for constant viscosity is, of course, the ratio of the pressure viscosity coefficient, α, to the temperature viscosity, β, coefficient.

Although the above data, and apparent relationships, may not be precise, they do suggest that there may be many ways of obtaining an approximate mapping of the low shear viscosity, the relaxation times,

and transition behavior of lubricants. Any of these can then be used to estimate whether a given lubricant will behave as an amorphous solid in a given EHD contact and therefore indicate which type of mechanical shear behavior of the material is most relevant for the application: low shear viscosity or ultimate shear stress of the amorphous solid. Both of these properties are functions of temperature and pressure. With these properties, and possibly the limiting elastic shear modulus, a suitable rheological model should be developed to use in EHD analysis.

II. FURTHER EXPERIMENTS IN AN EHD SIMULATOR

Four studies into the behavior of lubricated EHD contacts were conducted during this grant year which extended the previous efforts in this area. These consist of (1) temperature, film thickness and traction behavior of 5P4E over a slide-roll ratios of 0 to 2, (2) temperature measurements with the naphthenic mineral oil (N1) with negative slide-roll ratios which permit the measurement of the stationary surface in a sliding contact, (3) additional experiments and data analysis of temperatures during asperity interactions, (4) several starvation failure experiments to measure temperature excursions during local scuffing failures. These four efforts will be discussed in order.

A. EHD Contact Behavior of 5P4E

Film thickness, traction and surface temperature measurements were made on fluid 5P4E using the same equipment and technique as used in the previously reported studies of a naphthenic base fluid [1]. All measurements were taken using the smooth ball (0.011 μm R_a surface finish). This resulted in a value for Λ (ratio of film thickness to composite surface roughness) much greater than 2. Therefore, no asperity interaction was expected and none was observed.

The following property data for 5P4E at 25C was used in the data reduction: refractive index is 1.6306 at atmospheric pressure and 1.872 at 1 GPa, density is 1150 kg/m^3 at atmospheric pressure and 1470 kg/m^3 at 1 GPa. The viscosity at 37.8 C and atmospheric pressure is 3.63×10^{-4} m^2/s. This relatively high value for inlet viscosity meant that the fluid could not be circulated through the constant temperature

bath. Therefore, the lubricant reservoir was continuously replenished and its temperature monitored.

The experimental technique was essentially that used for the naphthenic fluid investigation [1]. The two surface velocities were individually controlled so that both rolling speed and the slide/roll ratio Σ could be varied. The normal load on the contact was obtained using a dead weight loading mechanism. Traction was measured by means of a strain gage load cell. Lubricant film thickness was determined using a dichromatic optical interference technique. Ball surface temperatures were measured using the infrared radiation technique previously discussed [1]. The wide band filter previously used and having a pass band from 3.3 to 5.0 μm was also used in this study. However, absorption spectra for 5P4E revealed a moderately strong absorption at 4.2 μm. This meant that the fluid, which is hotter than the ball surface, will contribute to the radiation received by the detector. In order to account for this additional radiation source, a separate experiment was performed. A very thin layer ($\sim$ 40 μm) of fluid 5P4E was placed on the upper surface of the sapphire. This fluid layer absorbed the lubricant radiation (emitted at 4.2 μm) and did not re-emit because of the low temperature level. An estimate of the effect of the lubricant emission on the ball surface temperature was then made by measuring the radiation both with and without this additional fluid layer present. It was determined that the measured ball surface temperatures could be in error up to 10C by neglecting the fluid radiation. In this estimate it has been assumed that the absorption in the fluid layer is sufficient to remove all of the contact fluid radiation.

In order to verify this, transmittance curves for fluid samples at two different temperatures were taken. No significant change in the secondary absorption band at 4.2 μm was observed. Therefore, since the ball surface radiation was measured using the wide band filter, the resulting surface temperatures will be higher (up to 10C) than the actual values. This is because there will be a radiation peak at 4.2 μm (caused by lubricant emission) which will raise the total radiation level falling on the detector.

Table IIIa shows the results of the temperature and traction measurements for fluid 5P4E. The table contains two sets of data: rolling velocities equal to 0.36 m/s and 0.50 m/s. The slide-roll ratio, Σ, was varied over a range of 0 to 2 ($\Sigma = 2$ refers to the case of a stationary sapphire and moving ball surface). The ball surface temperatures are then the moving surface temperatures. For values of $\Sigma < 0.28$, the sapphire had to be driven by a separate motor. Sufficient traction was developed for cases in which $\Sigma \geq 0.28$ such that a separate motor was not required. Experiments could not be conducted at speeds higher than 1.0 m/s because of lubricant inlet starvation. The starvation resulted in a significantly diminished film thickness and subsequent scratching of the ball surface. It is believed that starvation occurs at the higer speeds because there is insufficient time for this relatively viscous fluid to replenish the track created on the ball surface as the surface leaves the contact region.

Table IIIb shows the results of film thickness measurements for 5P4E under the same conditons as reported in Table IIIa except for a slight difference in lubricant bath temperatures.

The data given in Table III have been plotted in Figures 34 to 37. Figure 34 shows the variation of traction coefficient with slide-roll ratio for two different but constant rolling velocities. The accuracy of Σ has been estimated to be ± 0.04. Traction increases rapidly with Σ up to about $\Sigma = 0.3$. Further increases in Σ result in only a slight increase in traction. The peak in traction usually observed for nominal line contacts was not seen. Other investigations of point contacts [15,16], also show traction increasing throughout the range $0 \leq \Sigma \leq 2$.

Figure 35 shows the ball surface temperature rise as a function of slide-roll ratio at two different rolling velocities. The surface temperature is measured at the contact center. As expected the temperature rise is relatively small (about 10C) for small amounts of slip ($\Sigma \leq 0.3$) but increases rapidly with further increases in Σ. The temperature rises shown in the figure are somewhat higher than those observed for the naphthenic fluid under similar conditions. It is interesting to note that for $0 \leq \Sigma \leq 0.3$ the traction coefficient is increasing rapidly whereas the ball surface temperature remains essentially constant. On the other hand, for $0.3 < \Sigma \leq 2.0$ the traction coefficient is essentially constant whereas the surface temperature is rapidly increasing.

Figure 36 shows a plot of the film thickness values at the contact center and at the minimum film thickness location as a function of slide-roll ratio. The rolling velocity is held constant in each case. The large decrease with increasing amounts of slip is believed

to be due to the thermal reduction of the contact inlet viscosity of 5P4E. The decrease of film thickness with increasing Σ is much more pronounced than observed for fluid N1 [1].

Figure 37 shows the variation of traction coefficient with respect to the average shear rate in the Hertzian plateau region. The data shown here is the same as shown in Figure 34. Since heat generation in the fluid film is proportional to the square of the shear rate, the plot in Figure 37 indicates the variation of traction with thermal effects in the film. It can be seen from this figure that traction reaches its maximum value for shear rates $10s^{-1}$, and thereafter remains nearly constant.

It has been proposed by the authors that many lubricants go into a glassy state under normal EHD conditions [1]. Comparing the glass transition data for fluid 5P4E, presented previously in this report, with the measured surface temperatures at the contact center, it appears that under all operating conditions reported in the present work, fluid 5P4E is in the glassy state. If this is true, the fluid rheological property of interest is not viscosity, but rather the ultimate shear strength of the glassy lubricant. For the data reported here and the corresponding glass formation conditions, the calculated value of average ultimate shear stress (using the measured values of traction coefficient) agrees well with the measured values of ultimate shear strength of the 5P4E glass formed under similar conditions (45 to 50 MPa). Further, it has been observed that the traction coefficient for fluid 5P4E is about 15 to 20 percent higher than for fluid N1 under similar conditions of operation. Knowing that both fluids were

glass-like under the above operating conditions, it can be speculated at this point that the higher TC for 5P4E is due to higher values of measured ultimate shear strength for 5P4E compared with the values for the fluid N1.

B. Additional Investigations of the EHD Behavior of a Naphthenic Base Oil

B.1 Results for Negative Slide-Roll Ratios

In the previous contract report [1] the steady state ball surface temperatures were reported for a naphthenic base oil at 1.02 GPa Hertz pressure and both 0.75 and 1.00 m/s rolling velocity. Figures 38 and 39 show these results. Various amounts of sliding were introduced in these studies to cover a range of slide-roll ratio ($0 \leq \Sigma \leq 2$). The value of zero corresponds to equal ball and sapphire surface velocities, while $\Sigma = 2$ refers to a stationary sapphire and a moving ball surface.

During the past year this study of the naphthenic base oil has been extended to include negative slide-roll ratios ($-2 \leq \Sigma \leq 0$). The value of $\Sigma = -2$ refers to the condition of a stationary ball surface and a moving sapphire surface. Although the kinematics of the $\Sigma = -2$ and $\Sigma = +2$ cases are similar, the results reported for IR temperature measurements should not be the same. At $\Sigma = +2$ the recorded temperature is that of the moving surface in a pure sliding contact, whereas $\Sigma = -2$ results in the stationary surface temperature in a pure sliding contact. Other than the values of Σ, all conditions are the same as used in the previous investigation. The results are shown in Figures 40 through 43. In all cases, the smooth ball (0.011 μm R_a) was used at

a Hertz pressure level of 1.02 GPa. Comparing Figures 38 to 40 and 39 to 41, it can be seen that the temperature levels are higher for the negative Σ cases and that the shape of the temperature profiles have been altered. In the cases in which $\Sigma = +2$, the maximum ball surface temperature rise typically occurred downstream of the contact center. When $\Sigma = -2$, the maximum temperature rise occurred at the contact center.

Figures 42 and 43 show contact temperature rises for the entire slide-roll ratio range ($-2 \leq \Sigma \leq +2$). However, only the values at the contact center and the maximum values along the centerline are shown. It should be noted that results for $< = -2$ (Figures 40 to 43) depart significantly from the trends established by $\Sigma > -2$ data. The reason is simply that the results for $\Sigma = -2$ represent temperatures at a stationary point in the EHD contact. In all other cases, the ball surface being monitored is moving, both through the contact and through the detector's field of view.

Finally, Table IV and Figure 44 show the results of a number of pure sliding experiments. In all cases the temperature rise is that of the stationary surface with a stationary heat source. Figure 44 shows that the increase in temperature with sliding speed is less than linear. The energy dissipation rate in the contact is the product of traction force and sliding velocity and the temperature rise should be proportional to the dissipation rate, all other quantities remaining constant. The trend shown in Figure 44 can be explained if the traction force decreases with sliding speed. This is exactly what does occur [17,18].

B.2 The Influence of Asperity Interactions

The studies reported previously [1] using three different roughness levels for the steel balls have also been extended. Balls having roughness of 0.011 μm R_a and 0.38 μm R_a were used in traction and surface temperature rise studies. As before, proper combinations of ball roughness, rolling velocity and normal load resulted in a range of values for Λ (ratio of contact film thickness to composite surface roughness) from less than 1 to about 20.

A set of experiments was performed to see if the traction force would change significantly as the film thickness was reduced to allow asperity interactions. Figure 45 shows the traction coefficient plotted against Λ. As expected, the traction coefficient remained nearly constant for full film conditions but increased rapidly as more and more asperities carried the load.

Using both new and previously obtained contact temperature data a correlation with other experimental observations was undertaken. Surface roughness effects have been considered in the flash temperature formulas recommended by the American Gear Manufacturer's Association (AGMA) in their gear scoring criterion [19]. A multiplicative factor of $1/(1 - 0.8R_a)$ has been used for this purpose with the range of R_a being from 0.25 μm to 0.75 μm. In the literature [20-22], factors similar to the one mentioned above have been used with the coefficient accompanying R_a varying from 0.62 to 0.89. The percent increase in flash temperature predicted by these factors with surface roughness is shown plotted in Figure 46. The applicable range for the AGMA factor

is indicated in this figure. Three values of R_a corresponding to the three different types of balls used, are marked in the same figure. It can be seen that up to 40 percent increase is predicted for the rough ball (0.38 μm R_a) whereas about 7% is predicted for the medium rough ball (0.076 μm R_a). Finally, a 0.7 to 1% increase is predicted for the smooth ball (0.011 μm R_a) as compared to an ideally smooth one. An approximate comparison of the measured values with the predicted percent increase reveals a satisfactory agreement.

In order to determine an expression for the measured ball surface temperature at contact center, a surface roughness factor of the form $1/(1 - a_1 R_a)$ discussed above, was used. A multiple regression analysis of 181 data points for all three ball roughnesses resulted in the following expression for the ball surface temperature at contact center

$$\Delta T_b = 41.6\ P_H^{1.73} V_s^{.42} \left(\frac{1}{1 - 0.7R_a}\right) \qquad (6)$$

It is interesting to note that the surface roughness factor $1/(1 - 0.7\ R_a)$ obtained from the experimental data (equation (6)) is in good agreement with the factor recommended by AGMA (Curve (2) of Figure 46). In fact, the surface roughness factor obtained lies in between curves (3) and (4) in Figure 46. For the case of the smooth ball (R_a = 0.011 μm), the surface roughness factor is close to unity and the expression for ΔT_b from the equation (6) can be compared with the similar expression for ΔT_b derived earlier [1]. Even though a satisfactory agreement between the two expressions is observed, an exponent of 1.73 on P_H is obtained in equation (6) whereas an exponent of 1.34 was obtained earlier. The

apparent discrepancy between the two values is due to a considerable scatter in the data when P_H, V_s, and R_a are all considered as variables. However, when the exponents on P_H and V_s from equation (6) are compared with the theoretical pred ctions a reasonable agreement is found.

A surface roughness factor of the form $(40R_a + 1)^{a_2}$ is more convenient for correlating the experimental data. Even though there appears to be no special advantage of using the above form for the surface roughness factor, it is possible to use such a form simply for convenience. A multiple regression analysis of the same data with the surface roughness factor of the above form yielded the following expression for ΔT_b at contact center:

$$\Delta T_b = 37.8\ P_H^{1.84}\ V_s^{.31}\ (40R_a + 1)^{.18} \quad . \qquad (7)$$

The lubrication situation described in this section is characterized by the coexistence of elastohydrodynamic fluid film and interacting asperities. Such a situation is usually designated as partial elastohydrodynamic lubrication. In addition to many important parameters describing the contact, normal load sharing between asperities and EHD film is directly influenced by the degree of asperity interaction characterized by the lambda ratio (Λ).

Figure 47 taken from a report of two years ago [23] shows the difference between the DC and AC modes of operation of the IR detector. For $\Lambda < 1$ the AC signal results in an upper and a lower curve. It is believed that the upper curve corresponds to the temperature developed at an interacting asperity. The lower curve in the same figure

corresponds to the temperature of the fluid pocket (relatively low pressure region) in the neighborhood following an asperity. It can be seen from Figure 47 that the temperature of the fluid pocket (lower curve) increases up to a certain value of peak Hertz pressure (P_H), reaches a maximum, and then decreases with further increase in P_H. This can be explained as follows: even though the total load on the contact is increased, beyond a certain load, the average fluid pressure begins to decrease because the asperities share an increasing portion of the total load. In order to determine the exact proportion of the total load sheared by the asperities, normal load sharing calculations have been performed using Tallian's approach [24].

Table V shows the calculated value of the portion of load carried by the EHD film (W_{EHD}) and the corresponding average fluid pressure (P_{EHD}) at various normal loads for two different asperity slopes (σ_θ). The area of fluid pockets is assumed to be equal to the Hertzian area. This assumption is valid since the area of the contacting asperities is indeed small [25]. It can be seen (Table V) that the average fluid pressure increases with the normal load up to a certain value, reaches a maximum (depending on σ_θ), and then decreases with further increase in normal load.

Figure 48 shows a plot of average fluid pressure versus peak Hertz pressure for the medium rough ball at a sliding velocity of 1.0 m/s, corresponding to the results shown in Table V. The dotted line represents the conditions when the entire load is supported by the EHD film. At low values of Hertz pressure, the Λ ratio is greater than one

and therefore, the entire load is supported by the EHD film. As the Hertz pressure is increased, Λ decreases below one and the curve falls below the dotted line. The influence of the asperity slopes is apparent at this stage. With further increase in P_H, the average fluid pressure reaches a peak and then starts decreasing. Even though the exact value of σ_θ for the medium rough ball was not measured, the two values of 0.035($\theta = 2^o$) and 0.122 ($\theta = 7^o$) appear to be reasonable.

It therefore appears that the temperature of the fluid pocket increases with normal load up to a certain value, reaches a maximum and then decreases with further increase in normal load. This phenomenon is due to an increasing portion of the load shared by the asperities when the normal load on the contact is increased.

C. Starvation Failure Experiments

In a bearing system moving toward failure several regimes are usually encountered. A typical sequence might be full film EHD, partial EHD, boundary lubrication and finally, system failure by scoring or scuffing. Rozeanu [26] maintains that the final step to failure is always instantaneous and occurs within a few microseconds. He sees the seizure process as depending on the gradients of temperature, lubricant viscosity and the shear strength in the upper layers of the solid surfaces. Low values of these gradients promote scuffing; high values prevent it.

The experiments reported in this section were specifically directed towards determining how rapidly the final step to failure occurs. The failure criterion chosen was a local rise in temperature

above a certain level. The approach to failure was accelerated by severely starving the EHD contact.

The same experimental apparatus used in the previously reported EHD studies was used. The infrared microscope is used to measure the ball surface temperature at the contact center in a fast response mode. The fluid used in this study is the naphthenic base mineral oil N1. The balls were made of AISI 52100 with 0.011 μm R_a finish. The present investigation was limited to simple sliding with a stationary sapphire and moving ball surface. The following experimental procedure was used;

1. The system is brought into steady state operation (steady state 1) at the given speed and load conditions. The ball surface temperature at the center of the contact is measured using the IR temperature measurement technique. The traction coefficient and bath temperature also measured. This regime is comparable to that used for all previous EHD data given in this research.

2. The microscope is switched to operate in a high frequency response mode (AC mode), keeping it focused at the center of the contact. The oscilloscope is set to trigger with the signal at a level of 1/2 volt and the oscilloscope camera shutter is kept open for recording the trace.

3. The lubricant circulation and supply is stopped, thereby severely starving the contact. Still, some lubricant appears to adhere to the ball surface. With a clean cotton swab, the ball surface is cleaned as it approaches the contact.

4. This brings the system into the starved state 2. Due to increased traction under these conditions, the ball surface velocity decreases to the values used in Table VI. Operation under these conditions was found to be unsteady.

5. Shortly (approximately 15 to 30 seconds) after the system reaches the unsteady starved state 2, local failure occurs and the temperature level increases. This increase in temperature level triggers the trace on the oscilloscope. The camera shutter is closed after recording the trace. The transient temperature level is estimated by using the calibration chart for the infrared microscope.

6. Immediately after the local failure, the system reaches a state referred to as post failure state 3. This state again appears to be unsteady, in that, local failure may occur any time in the future. In fact, temperature flashes appear corresponding to the spot on the ball where initial failure occurred. Under these conditions the time averaged ball surface temperature and traction coefficient are much higher than their values in steady state 1. Due to a further increase in traction, the ball surface velocity decreases even further compared to starved state 2.

The major results from these experiments are shown in Table VI. Five different experiments are reported with sliding speeds ranging from 1.5 to 4.26 m/s and two different loads of 67 and 118.3 N. Load is maintained constant throughout each experiment and the bath temperature is monitored by a thermocouple. The ball surface velocity decreased during the test for each experiment and this is perhaps attributable to the significant increase in friction coefficient to 3 or 4 times the starting value. Because of the slow response of the velocity readout and the traction load cell, the transient values of velocity and friction coefficient could not be measured. Both the transient and the time averaged values of ball surface temperature were measured (See Table VI). Since the microscope was set to trigger with the transient temperature rise, the temperature during unsteady starved state 2 could not be recorded. It can be seen in Table VI that the transient temperature reaches very high values - sometimes

up to 1100 C. The level of transient temperature increases with increasing speed and load, as can be expected.

In addition to noting the values of the transient temperatures, an oscilloscope trace of the fast rise and decay of the transient temperature was recorded. It was found that the initial rise in temperature takes place in approximately 8 μs. This time span, when translated to distance on the surface, corresponds to the width of a single asperity. It therefore appears that failure has first occurred at a single asperity. If the system is allowed to run under these conditions, it apepars likely that many asperities may begin to fail in just the same manner, leading to an inoperable system.

These findings support Rozeanu's conjecture that the final step to failure is essentially instantaneous occurring within a few micro-seconds. The logical question arises, however, as to how does a failure in a steel/sapphire system relate to the steel/steel system. The failure of the steel/steel system should be more immediate than the other based on considerations of the relative interfacial forces present in the two cases [16,27].

In order to verify this possibility, experiments were run for a steel-on-steel system. The sapphire disc was replaced with a polished (0.006 μm R_a) AISI 52100 steel disc. Experiments were conducted at sliding speeds ranging from 0.8 to 5.0 m/s at increasing loads until scoring was encountered. For this system, scoring occurred at a sliding speed of 2.7 m/s and at a load corresponding to a peak Hertz pressure of 1.51 GPa. Under these operating conditions, and in fact even at the higher peak Hertz pressure of 1.89 GPa, the sapphire-on-steel system

was running without any signs of scoring. Indeed, the system was undergoing a successful running-in process. Figure 49 shows the location of scoring failure witnessed with a steel-on-steel system. The figure also contains information on ball surface temperature rise for a sapphire-on-steel system.

These results indicate that a system with similar materials is subject to scoring failure more readily than a system with dissimilar materials. They also emphasize the requirement of using a similar material system for studying the scoring phenomenon, which otherwise may lead to erroneous conclusions.

III. CONCLUSIONS

The glass, viscoelastic or viscoplastic transition of lubricants has been measured over a wide range of pressures, temperatures and rates for several lubricants. The different methods agree well and clearly show the change in transition temperature with pressure and frequency. The stress strain behavior of the material in the glassy state has been observed and is similar to a classical elastic-plastic model. The elastic shear modulus increases with decreasing temperature and approaches that measured by high rate ultrasonic experiments. The ultimate or maximum shear stress also increases with decreasing temperature and is believed to be the controlling shear stress in the EHD contact. The elastic portion of the curve is confined to strains of less than 5%, usually no more than 3%.

A new high pressure falling body viscometer has also been constructed which permits low shear rate viscosity measurements to greater than 10^7 Pas [10^{10} cp].

Several investigations in the EHD simulator have resulted in data on the behavior of 5P4E and N1 for slide-roll ratios ranging from -2 to +2. These data include traction, film thickness and surface temperature. They permit, for the first time in our temperature measuring research, the determination of the temperature of the slower moving surface with sliding and rolling combined. The stationary surface temperature was also determined. This work clearly shows that the stationary surface temperature is much higher than that of the moving surface. This results in conduction of thermal energy forward into the inlet zone of the contact. This can result in an inlet fluid

temperature rise and reduced film thickness particularly at high loads.

An adjustment factor for surface roughness effect on contact surface temperature was obtained from curve-fitting a large amount of data. It was found to be very similar to that recommended by the AGMA in their gear scoring criteria [19].

A limited number of experiments were performed in which local surface scuffing occurred and for which the local temperature excursion was measured. Very high temperatures (to 1100C) were observed in 8 μs or less.

IV. REFERENCES

1. Winer, W. O., and Sanborn, D. M., "Investigations of Lubricant Rheology as Applied to Elastohydrodynamic Contacts", NASA CR-2837, September 1976.

2. Alsaad, M. A., "Light Scattering Study of the Glass Transition and the Glassy State in Lubricating Oils", Ph.D. Thesis, Georgia Institute of Technology, Atlanta, Georgia, August 1976.

3. Fabelinskil, I. L., Molecular Scattering of Light, Plenum Press, New York, 1968.

4. Brillouin, L., Ann. Phys. (Paris), 17, 88, 1922.

5. Stevens, J. R., Jackson, D. A., and Champion, J. V., "Evidence for Ordered Regions in Poly(n-butyl) Methacrylate from Light Scattering Studies", Molecular Physics, 29(6), 1893, 1975.

6. Coakley, R. W., Mitchell, R. S., Stevens, J. R., and Hunt, J. L., "Rayleigh-Brillouin Light Scattering Studies on Atactic Polystrene", A paper presented at the American Physical Society Conference, Atlanta, Georgia, April 1976.

7. Jackson, D. A., Pentecost, H. T. A., and Powels, J. G., "Hypersonic Absorption in Amorphous Polymers by Light Scattering", Molecular Physics, 23(2), 425, 1972.

8. Juang, Y., and Wang, C., "Brillouin and Rayleigh Scattering in Polybutadiene", 61, 1868, 1974.

9. Mitchell, R. S., and Guillet, J. E., "Brillouin Scattering in Amorphous Polymeric Solid", J. Polym. Sci.: Polym. Phys. Ed., 12, 713, 1974.

10. Dill, J. F., Drake, P. W. and Litovitz, T. A., "The Study of Viscoelastic Properties of Lubricants Using High Pressure Optical Techniques", ASLE, 18(3), 202, 1975.

11. Filliben, J. J., and McKinny, J. E., "Confidence Limits for the Abscissa of Intersection of Two Linear Regressions", J. Res. Nat. Bur. Stand. (U.S.), 76B (Math. Sci.), 179, 1972.

12. Harrison, G., The Dynamic Properties of Supercooled Liquids, Academic Press, 1976.

13. ASME, Pressure-Viscosity Report I, II, A Report Prepared by the ASME Research Committee on Lubrication, New York, ASME, 1953.

14. McKinny, J. E., and Goldstein, M., "PVT Relationships for Liquid and Glassy Poly(Vinyl Acetate)", Journal of Research of the NBS-Physics and Chemistry, 78A, 331, 1974.

15. Wedeven, L. D., "Traction and Film Thickness Measurements Under Starved Elastohydrodynamic Conditions", Trans. ASME., Journal of Lubrication Technology, Series F, No. 2, pp. 321-329, April 1975.

16. Nagaraj, H. S., "Investigation of Some Temperature-Related Phenomena in Elastohydrodynamic Contacts Including Surface Roughness Effects", Ph.D. Thesis, Georgia Institute of Technology, December 1976.

17. Sanborn, D. M., "An Experimental Investigation of the Elasto-hydrodynamic Lubrication of Point Contacts in Pure Sliding", Ph.D. Thesis, University of Michigan, 1969.

18. Sanborn, D. M. and Winer, W. O., "Fluid Rheological Effects in Sliding Elastohydrodynamic Point contacts: II - Traction", Trans. ASME, Journal of Lubrication Technology, 93, pp. 342-348, 1971.

19. American Gear Manufacturer's Association (AGMA), "Gear Scoring Design Guide for Aerospace Spur and Helical Power Gears", AGMA Information Sheet 217-.01 (Prepared by Lemanski, A. J.), October 1965.

20. Dudley, Darle W., Practical Gear Design, McGraw-Hill Book Company, Inc., New York, 1954.

21. Kelley, B. W., "A New Look at the Scoring Phenomena of Gears", Trans. Soc. Automotive Engineers, 61, pp. 175-188, 1953.

22. Kelley, B. W., and Lemanski, A. J., "Lubrication of Involute Gearing", Proc. Inst. Mech. Eng., 182, Part 3A, pp. 173-184, 1967-1968.

23. Nagaraj, H. S., Sanborn, D. M., and Winer, W. O., "Effects of Load, Speed, and Surface Roughness on Sliding EHD Contact Temperatures", Trans. ASME, Journal of Lubrication Technology, 99, No. 2, pp. 254-262, April 1977.

24. Tallian, T. E., "The Theory of Partial Elastohydrodynamic Contacts", Wear, 21, pp. 49-101, 1972.

25. Greenwood, J. A., and Williamson, J. B. P., "Contact of Nominally Flat Surfaces", Proc. Roy. Soc. Lond., 295, Series A, pp. 300-319, 1966.

26. Rozeanu, L., "Friction Transients (Their Role in Friction Failures)", Trans. ASLE, 19, 4, pp. 257-266, 1976.

27. Bowden, F. P., and Tabor, D., Friction and Lubrication of Solids - Vol. II, Oxford University Press, London, 1964.

APPENDIX

DESCRIPTION OF EXPERIMENTAL FLUIDS

The following table summarizes the oils investigated in this research and gives characteristic data for each oil.

Experimental Fluids

Symbol	Description
N1	Naphthenic Base Oil (R-620-15)
N2	N1 + 2.2 percent Polybutene (LF-5346)
N3	Blend of N1 and 4% Polyalkylmethacrylate (PL-4523)
Nap 2	Naphthenic Base OIl (R-620-16)
P1	Paraffinic Base Oil (R-620-12)
FN 2961	Super Refined Naphthenic Mineral Oil
XRM 177F (lot 4)	Synthetic Paraffinic Hydrocarbon
Mobil 1	Synthetic Paraffinic Motor Oil
Santotrac 50	Synthetic Cycloaliphatic Hydrocarbon Traction Fluid
5P4E	Five-ring Polyphenyl Ether
MCS 418	Modified Polyphenyl Ether (C-ether)
MCS 460	Synthetic Hydrocarbon
MCS 1218	Cycloaliphatic Hydrocarbon
FYRQUEL 150 R&O	Tri-Aryl Phosphate ester
DN-600	Polyalkyl Aromatic
S1-Diester	Diester-Plexol 201 di-2-ethyl hexyl sebecate (PL 5159)
S2	Polybutene (LF-5193)
Krytox 143-AB	Perfluorinated polyether
Brayco, Micronic 851Z	Perfluorinated polyether
Advanced Ester	Based on Pentaerythritol (Aeroshell Turbine Oil 555 Base Oil)

Symbol:	N1	
Source:	Sun Oil Company	
Type:	Naphthenic Base Oil R-620-15	
Properties:	Viscosity at 37.8C, m^2/s	24.1×10^{-6}
	Viscosity at 98.9C, m^2/s	3.73×10^{-6}
	Viscosity Index (ASTM D-2270)	-13
	Flash Point, C	157
	Pour Point, C	-43
	Density at 20C, Kg/m^3	915.7
	Average Molecular Weight	305

Symbol:	N2	
Type:	Blend of N1 and 2.2% Polybutene (LF-5346)	
Blend properties:	Viscosity at 37.7C, m^2/s	81.6×10^{-6}
	Viscosity at 98.8C, m^2/s	11.9×10^{-6}
Source of Polymer:	American Oil Company	
Properties of Polymer:	Density at 25C, Kg/m^3	865.6
	Viscosity at 37.7C, m^2/s	8040×10^{-6}
	Viscosity at 98.8C, m^2/s	637×10^{-6}
	Viscosity Index	123.5
	Flash Point, C	240
	Diluent Oil Content, percent	80
	Diluent Oil Viscosity at 37.7C, m^2/s	18×10^{-6}
	Polymer number average molecular weight	25,000

Symbol:	N3	
Type:	Blend of Ni and 4% Polyalkylmethacrylate (PL-4523)	
Blend properties:	Viscosity at 37.7C, m^2/s	182×10^{-6}
	Viscosity at 98.8C, m^2/s	27×10^{-6}
	Pressure viscosity coefficient (atmospheric pressure slope)	
	at 37.7C, GPa^{-1}	10.7
	at 98.8C, GPa^{-1}	8.27
Source of Polymer:	Rohm and Haas Company	
Properties of Polymer:	Viscosity Average Molecular Weight	1.65×10^6
	Viscosity m^2/s at 98.9C	773×10^{-6}
	Consists of 19% Polymer in solution with a paraffinic hydrocarbon	

Symbol:	Nap 2	
Source:	Sun Oil Company	
Type:	Naphthenic Base Oil R-620-16	
Properties:	Viscosity at 37,8C, m^2/s	114×10^{-6}
	Viscosity at 98.9C, m^2/s	8.08×10^{-6}
	Viscosity Index (D2270)	< 0
	Density at 20C, Kg/m^3	930.3
	Average Molecular Weight	357
	Refractive Index	1.5173
	Pour Point C	-23

Symbol:	P1	
Source:	Sun Oil Company (R-620-12)	
Type:	Paraffinic Base Oil	
Properties:	Viscosity at 37.8C, m^2/s	33.7×10^{-6}
	Viscosity at 98.9C, m^2/s	5.4×10^{-6}
	Density at 25C, Kg/m^3	860.2
	V.I. (ASTM D-2270)	103
	Pour Point, C	-15
	Average molecular weight	404
	Flash point, C	216

Symbol:	FN 2961	
Source:	Humble Oil and Refining Company	
Type:	Super Refined Naphthenic Mineral Oil	
Properties:	Viscosity at 37.8C, m^2/s	78×10^{-6}
	Viscosity at 98.9C, m^2/s	8.2×10^{-6}
	Viscosity at 148.9C, m^2/s	3.3×10^{-6}
	Density at 15.6C, Kg/m^3	887
	Pour Point, C	-34

Symbol:	XRM-177-F (Lot 4)	
Source:	Mobil	
Type:	Synthetic Paraffinic Hydrocarbon	
Properties:	Viscosity at 37.8C, Pas	376×10^{-3}
	Viscosity at 98.9C, Pas	31.6×10^{-3}
	Pour Point, C	< -40
	Density 37.8C, Kg/m^3	838.9

Symbol:	Mobil 1	
Type:	Synthetic Paraffinic Hydrocarbon	
Source:	Mobil Oil Company	
Properties:	Viscosity at 204.4C, m^2/s	1.69×10^{-6}
	Viscosity at 148.9C, m^2/s	3.04×10^{-6}
	Viscosity at 98.9C, m^2/s	7.50×10^{-6}
	Viscosity at 37.8C, m^2/s	44.67×10^{-6}
	Viscosity at -17.8C, m^2/s	1.284×10^{-3}
	Viscosity at -28.9C, m^2/s	3.812×10^{-2}
	Viscosity at -40C, m^2/s	14.122×10^{-3}

Symbol:	Santotrac 50	
Source:	Monsanto Company	
Type:	Synthetic Cycloaliphatic Hydrocarbon Traction Fluid	
Properties:	Viscosity at 37.8C, m^2/s	34×10^{-6}
	Viscosity at 98.9C, m^2/s	5.6×10^{-6}
	Pour Point, C	-37
	Density at 37.8C, Kg/m^3	889
	Flash Point, C	163
	Fire Point, C	174
	Specific Heat at 37.8C, J/Kg·K	2332
	Additive package includes: Antiwear (zinc dialkyl dithiophosphate), Oxidation inhibitor, Antifoam, VI Improver (Polymethacrylate).	

Symbol:	5P4E	
Type:	Five-ring Polyphenyl Ether	
Source:	Monsanto Company	
Properties:	Viscosity at 37.8C, m^2/s	363×10^{-6}
	Viscosity at 98.9C, m^2/s	13.1×10^{-6}
	Density at 22.2C, Kg/m^3	1205
	Density at 37.8C, Kg/m^3	1190
	Flash Point, C	288
	Pour Point, C	4.4

Symbol:	MCS-418	
Type:	Modified Polyphenyl Ether (C-ether)	
Source:	Monsanto Company	
Properties:	Viscosity at 38C, m^2/s	25×10^{-6}
	Viscosity at 99C, m^2/s	4.1×10^{-6}
	Density at 38C, kg/m^3	1180
	Density at 99C, kg/m^3	1140
	Pour Point	-29

Symbol:	MCS-460	
Source:	Monsanto Company	
Type:	Synthetic Hydrocarbon	
Properties:	Viscosity at 37.8C, m^2/s	37.2×10^{-6}
	Viscosity at 98.9C, m^2/s	4.0×10^{-6}
	Viscosity at 148.9C, m^2/s	1.9×10^{-6}
	Pour Point, C	-29 to -32
	Density 25C, Kg/m^3	932.7

Symbol:	MCS-1218	
Source:	Monsanto Company	
Type:	Cycloaliphatic Hydrcarbon	
Properties:	It is a combination of two components each have a molecular weight less than 1000.	
	Viscosity at 37.8C, m^2/s	1418×10^{-6}
	Viscosity at 98.9C, m^2/s	18.37×10^{-6}
	Density at 23.9C, Kg/m^3	940

Symbol:	FYRQUEL 150 R & O	
Type:	Tri-Aryl Phosphate	
Source:	Stouffer Chemical Company	
Properties:	Density at 15.6C, kg/m^3	1165
	Pour Point,	-23
	Viscosity at 37.8C, Pas	36.9×10^{-3}
	Viscosity at 98.9C, Pas	4.83×10^{-3}

Symbol:	DN-600	
Source:	Continental Oil Company	
Type:	Polyalkyl Aromatic	
Properties:	Viscosity at 37.8C, m^2/s	30×10^{-6}
	Viscosity at 98.9C, m^2/s	5.0×10^{-6}
	Viscosity at 148.9C, m^2/s	2.3×10^{-6}
	Density at 37.8C, Kg/m^3	851
	Pour Point, C	- 60
	Specific Heat at 37.8C, J/Kg K	1624

Symbol:	S1-Diester	
Source:	Rohm and Haas Company	
Type:	Diester-Plexol 201 di-2-ethyl hexyl sebacate (PL 5159)	
Properties:	Viscosity at -53.9C, m^2/s	7990×10^{-6}
	Viscosity at 37.8C, m^2/s	12.8×10^{-6}
	Viscosity at 98.9C, m^2/s	3.32×10^{-6}
	Cloud Point (ASTM D-2500)	below -54C
	V.I. (ASTM D-974)	150
	Flash point, C	216
	Fire point, C	232
	Pour point, C	< -62
	Specific gravity 15.6C/15.6C	0.912

Symbol:	S2	
Source:	American Oil Company	
Type:	Polybutene LF-5193	
Properties:	Viscosity at -17.8C, m^2/s	$18,800 \times 10^{-6}$
	Viscosity at 37.8C, m^2/s	109×10^{-6}
	Viscosity at 98.9C, m^2/s	10.6×10^{-6}
	Density at 25C, Kg/m^3	844.3
	V.I. (ASTM D-2270)	87
	Polymer Number Average Molecular Weight	409
	Diluent oil content	0

Symbol:	Krytox 143-AB (Lot 10)	
Type:	Perfluorinated polyether	
Source:	DuPont Company	
Properties:	Viscosity at 37.8C, m^2/s	96.6×10^{-6}
	Viscosity at 98.9C, m^2/s	11.5×10^{-6}
	Density at 24C, kg/m^3	1890
	Density at 98.9C, kg/m^3	1760
	V.I. (ASTM D-2270)	116
	Pour point, C	-40
	Flammability	does not burn

Symbol:	Brayco, Micronic 815Z	
Type:	Perfluorinated polyphenyl ether	
Source:	Bray Oil Company	
Properties:	Viscosity 98.9C, m^2/s	40×10^{-6}
	Viscosity 37.8C, m^2/s	129×10^{-6}
	Density at 15.5C, kg/m^3	1866
	Pour point, C	-73

Symbol:	Advanced Ester	
Source:	Shell Oil Company	
Type:	Based on Pentaerythritol (Aeroshell Turbine Oil 555 Base Oil)	
Properties:	Viscosity at 37.8C, m^2/s	25.8×10^{-6}
	Viscosity at 98.9C, m^2/s	5.1×10^{-6}
	Viscosity at 148.9C, m^2/s	2.3×10^{-6}
	Density at 37.8C, Kg/m^3	979
	Flash point, C	260

Table I. Least-square Expressions for the Glass Transition Temperature as a Function of Pressure for Experimental Lubricants Based on Formation History B. T_g in C and P_g in GPa.

Experimental Lubricants	Range of Measurements GPa	Least Square Expression for T_g
5P4E	0.16 - 0.41	$T_g = -4.74 + 182.9\ P_g$
MCS-1218	0.16 - 0.46	$T_g = -4.66 + 197.4\ P_g$
N1	0.46 - 0.70	$T_g = -32.79 + 120.8\ P_g$
N2	0.43 - 0.70	$T_g = -33.40 + 134.5\ P_g$

Table II. Glass Transition Temperature, T_g, At Atmospheric Pressure

(Approximate cooling rates from 0.6 to 1.7 c/min.)

FLUID	T_g C
N1	-81.5
N2	-81
N3	-82
Nap 2	-73
P1	-96
FN 2961	-72
XRM 177F	-96
Mobil 1	-92
Santotrac 50	-83
5P4E	-30.5
MCS 418	-67.5
MCS 460	-71.5
MCS 1218	-49
Fyrquel 150 R&O	-60
DN 600	-95
S1	-127
S2	-82
Krytox	-81

Table IIIa. Temperature and Traction Measurements for Fluid 5P4E (Smooth ball: .011 μm R_a, P_H = 1.02 GPa).

V_b m/s	V_{sa} m/s	$\bar{V}$ m/s	Σ	T_{bath} C	T_b at center C	ΔT_b at center C	TC
.36	.36	.36	0	30	39	9	.029
.38	.34	.36	.111	30	39	9	.050
.41	.31	.36	.278	30	41	11	.064
.72	0	.36	2	33	79	46	.070
.5	.5	.50	0	31	41.5	10.5	.019
.52	.48	.50	.08	31	41.5	10.5	.032
.55	.45	.50	.2	31	42	11	.051
.57	.43	.50	.28	31	42	11	.067
1.0	0	.50	2	35	97	62	.070

Table IIIb. Film Thickness Measurements for Fluid 5P4E (Smooth ball: .011 μm R_a, P_H = 1.02 GPa).

V_b	V_{sa}	$\bar{V}$	Σ	T_{bath}	h_c		h_m	
m/s	m/s	m/s		C	μ-in	μm	μ-in	μm
.36	.36	.36	0	32	48.1	1.21	36.4	.91
.38	.34	.36	.111	32	48.1	1.21	36.4	.91
.42	.30	.36	.278	33	51.9	1.30	38.0	.95
.72	0	.36	2	36	13.4	.34	5.4	.13
.5	.5	.50	0	35	48.1	1.21	36.4	.91
.52	.48	.50	.08	35	48.1	1.21	36.4	.91
.55	.45	.50	.2	34	48.1	1.21	36.4	.91
.57	.43	.50	.28	33	55.1	1.38	36.4	.91
1.0	0	.50	2	35	13.4	.34	6.4	.16

Table IV. Summary of Stationary Ball Surface Temperature

(Smooth ball: 0.011 μm R_a, Fluid N1, P_H = 1.02 GPa, Σ = -2)

V_b	V_{sa} (= V_s)	T_{bath}	T_b @ Center (= $T_{b,max}$)	ΔT_b ($T_b - T_{bulk}$)*
m/s	m/s	C	C	C
0	0.82	28	92.5	50.5
0	1.20	28	108	66
0	1.24	28	109.5	67.5
0	1.50	28	118	76
0	1.70	28	125	83
0	1.85	26	128	86
0	1.98	26	131	89
0	2.58	28	146	104

*T_{bulk} ≈ 42 C for all the experiments (T_{bulk} = T_b two to three Hertzian diameters before the contact).

Table V. Normal Load Sharing Between Asperities and the EHD Film

(Medium rough ball: .076 μm R_a, Fluid N1, V_s = 1.0 m/s, V_{sa} = 0)

Contact Total (Both Lubricant Film and Asperities)				Portion Supported by Lubricant Film for Stated Average Asperity Slope, σ_θ			
				σ_θ = .0349		σ_θ = .122	
W	P_H	P_{avg}	Λ	W_{avg}	P_{avg}	W_{avg}	P_{avg}
N	GPa	GPa		N	GPa	N	GPa
8.9	.52	.348	4.33	8.89	.348	8.86	.347
17.8	.65	.435	3	17.8	.435	17.7	.433
25.4	.74	.493	2.5	25.2	.489	24.7	.479
40.0	.86	.573	2	39.0	.559	36.8	.527
66.7	1.02	.678	1.5	62.4	.636	54.3	.552
215	1.51	1.00	1	192	.900	152	.715
222	1.52	1.02	.8	191	.876	142	.649
254	1.59	1.06	.6	208	.872	144	.602
293	1.67	1.11	.4	228	.866	146	.556
307	1.70	1.13	.33	234	.857	146	.536

Table VI. Experimental Study of Starvation Failure of a Sapphire on Steel Ball Contact

(Smooth ball: 0.011 μm R_a, Fluid N1, V_{sa} = 0)

	Experiment	T_{bath} (C)	W (N)	V_s (m/s)	TC	T_b @ center (C)
1.	Steady State 1	30	67	1.5	0.06	92
	Starved State 2 (unsteady)		(P_H = 1.02 GPa)	1.37	-	-
	Transient			-	-	650
	Post failure State 3 (unsteady)			1.1	0.21	135
2.	Steady State 1	32	67	2.36	0.05	105
	Starved State 2 (unsteady)		(P_H = 1.02 GPa)	2.1	-	-
	Transient			-	-	690
	Post failure State 3 (unsteady)			1.75	0.19	150
3.	Steady State 1	45	67	4.0	0.04	133
	Starved State 2 (unsteady)		(P_H = 1.02 GPa)	3.7	-	-
	Transient			-	-	700
	Post failure State 3 (unsteady)			3.11	0.16	185
4.	Steady State 1	36	118.3	2.38	0.055	130
	Starved State 2 (unsteady)		(P_H = 1.24 GPa)	1.95	-	-
	Transient			-	-	850
	Post failure State 3 (unsteady)			1.89	0.2	193
5.	Steady State 1	53	118.3	4.26	0.045	165
	Starved State 2 (unsteady)		(P_H = 1.24 GPa)	3.92	-	-
	Transient			-	-	1100
	Post failure State 3 (unsteady)			3.87	0.19	240

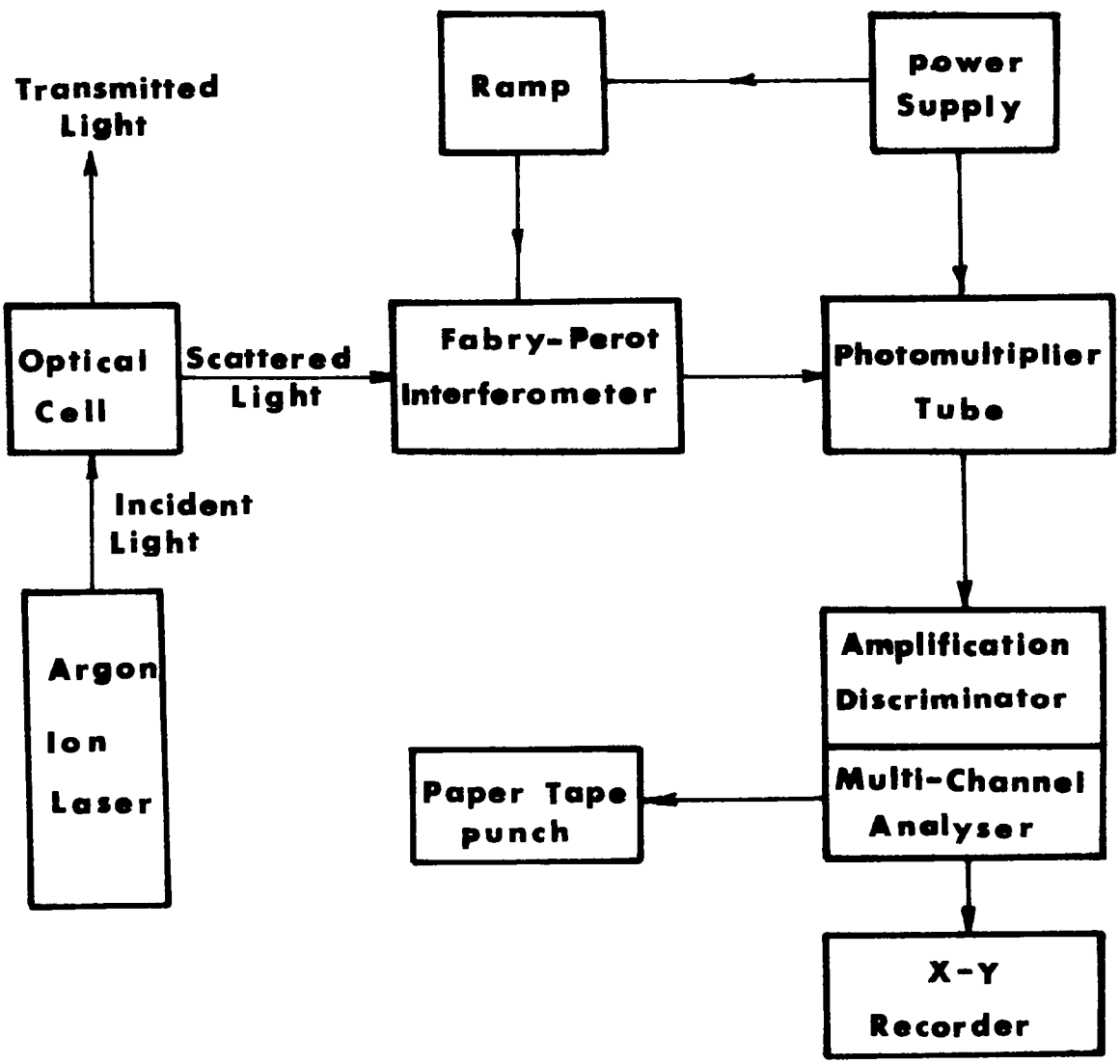

Figure 1a. Schematic Arrangement of the Light-Scattering Experiment.

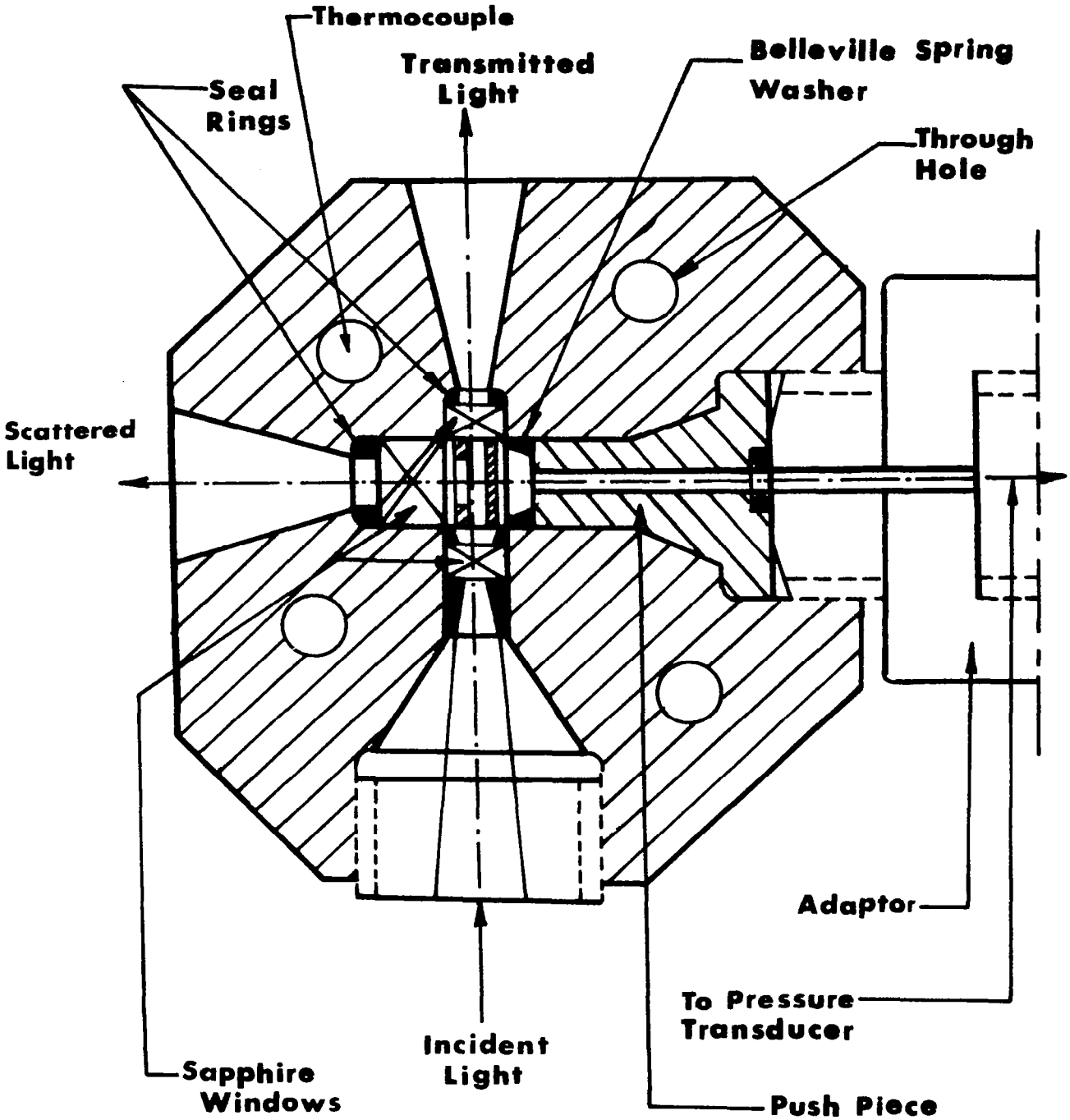

Figure 1b. Schematic Arrangement of the Light-Scattering Cell. The Intensifier is attached Perpendicular to the Plane of the figure at the centerline of the cell.

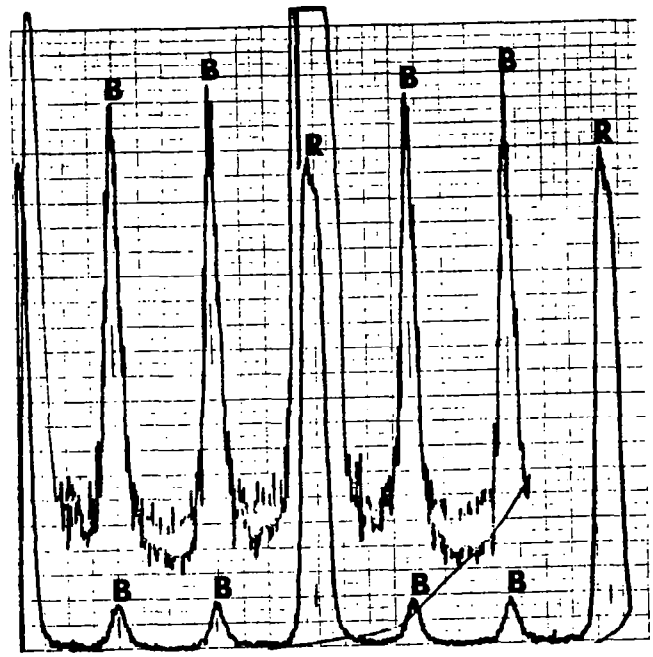

Figure 2. Frequency Spectrum of N1 obtained by History A at 0.277 GPa and 24C. B and R represents the Brillouin and Rayleigh Components respectively (the two signal levels represent two system amplifications for clarity).

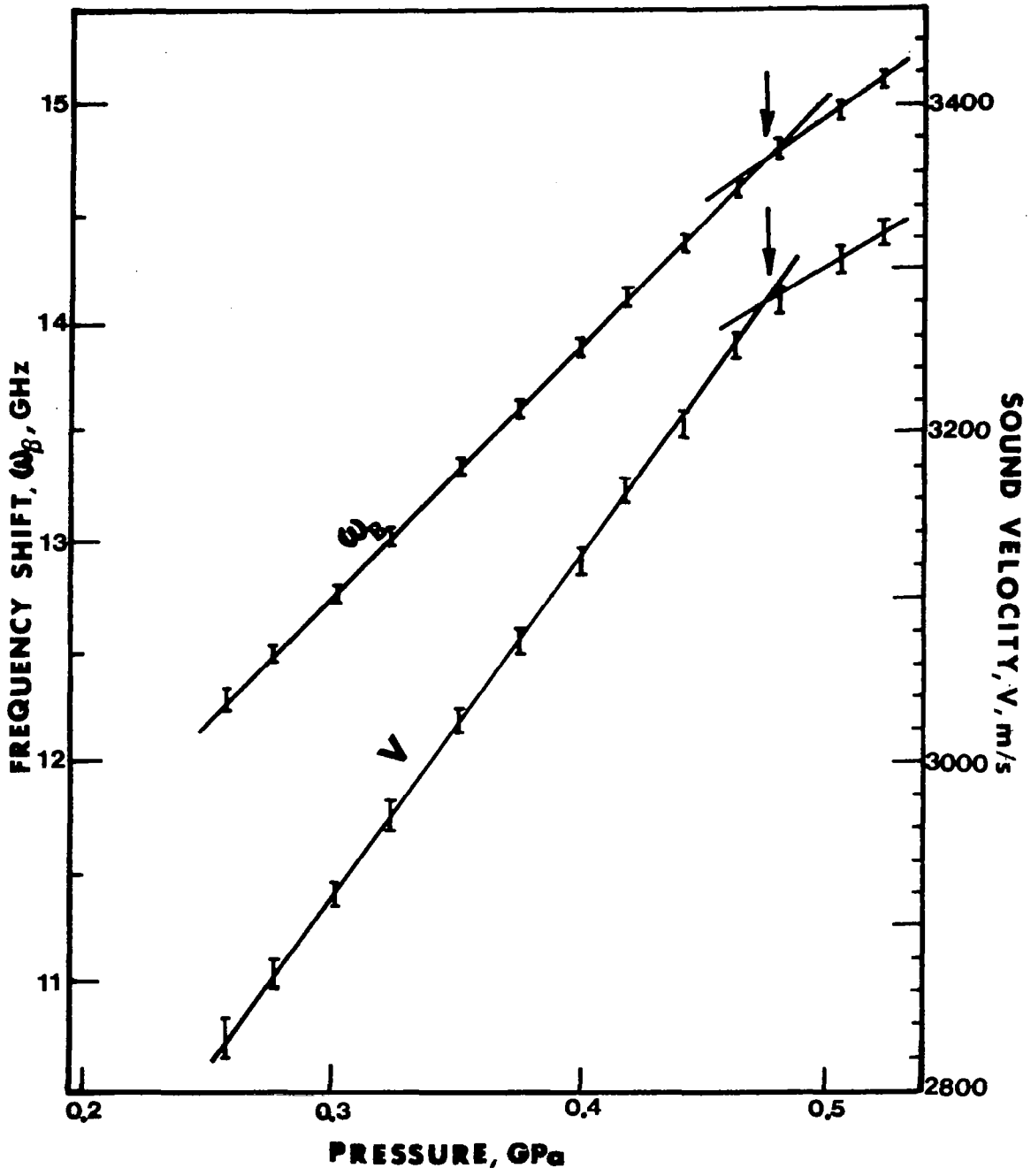

Figure 3. Variation of Frequency Shift (ω_B) and Sound Velocity (V) with Pressure at 24C for Naphthenic Mineral Oil (N1) (History B). Arrows indicate glass transition pressure (P_g).

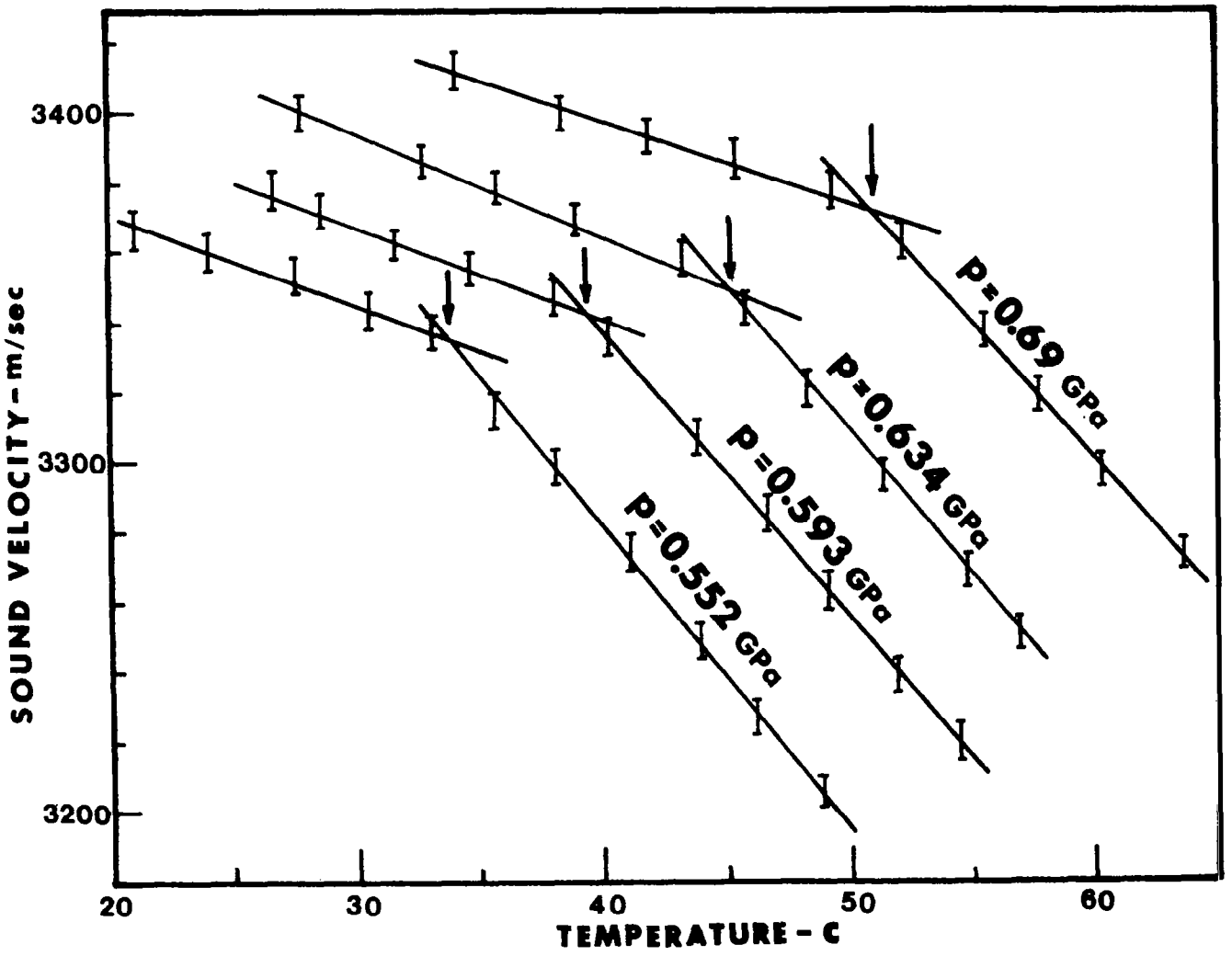

Figure 4. Velocity of Sound (V) as a function of Temperature at Different Pressures for Naphthenic Mineral Oil (N1) (History B). Arrows indicate Glass Transition Temperature (T_g).

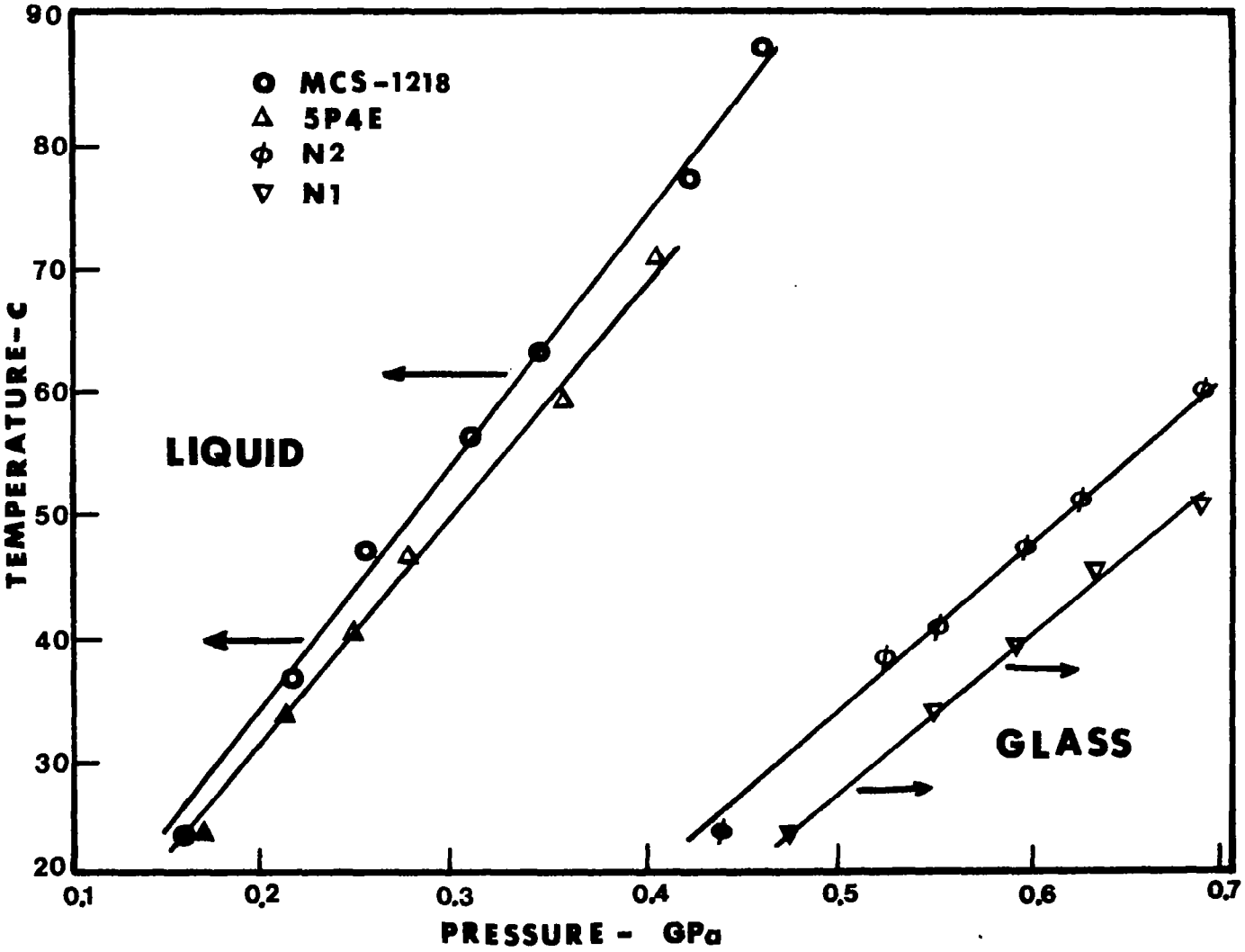

Figure 5. Transition Diagram for Four Experimental Fluids. Solid and Open Symbols are for Histories A and B respectively. Glassy state is to the right and below Transition lines and liquid state is to left and above transition lines based on Light-Scattering Technique.

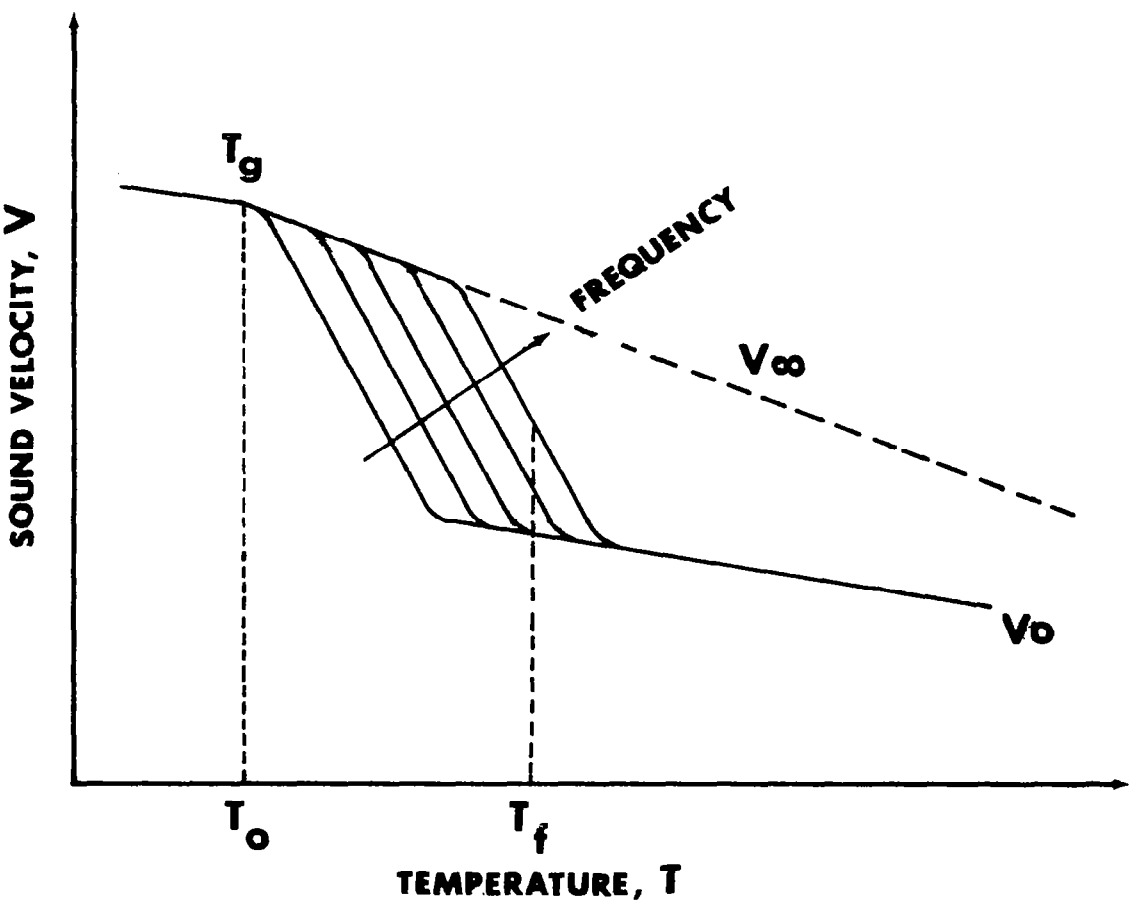

Figure 6. Typical Sound Velocity as a Function of Temperature and Frequency at Constant Pressure V_∞ and V_o are limiting High and Low Frequency Sound Velocities Respectively.

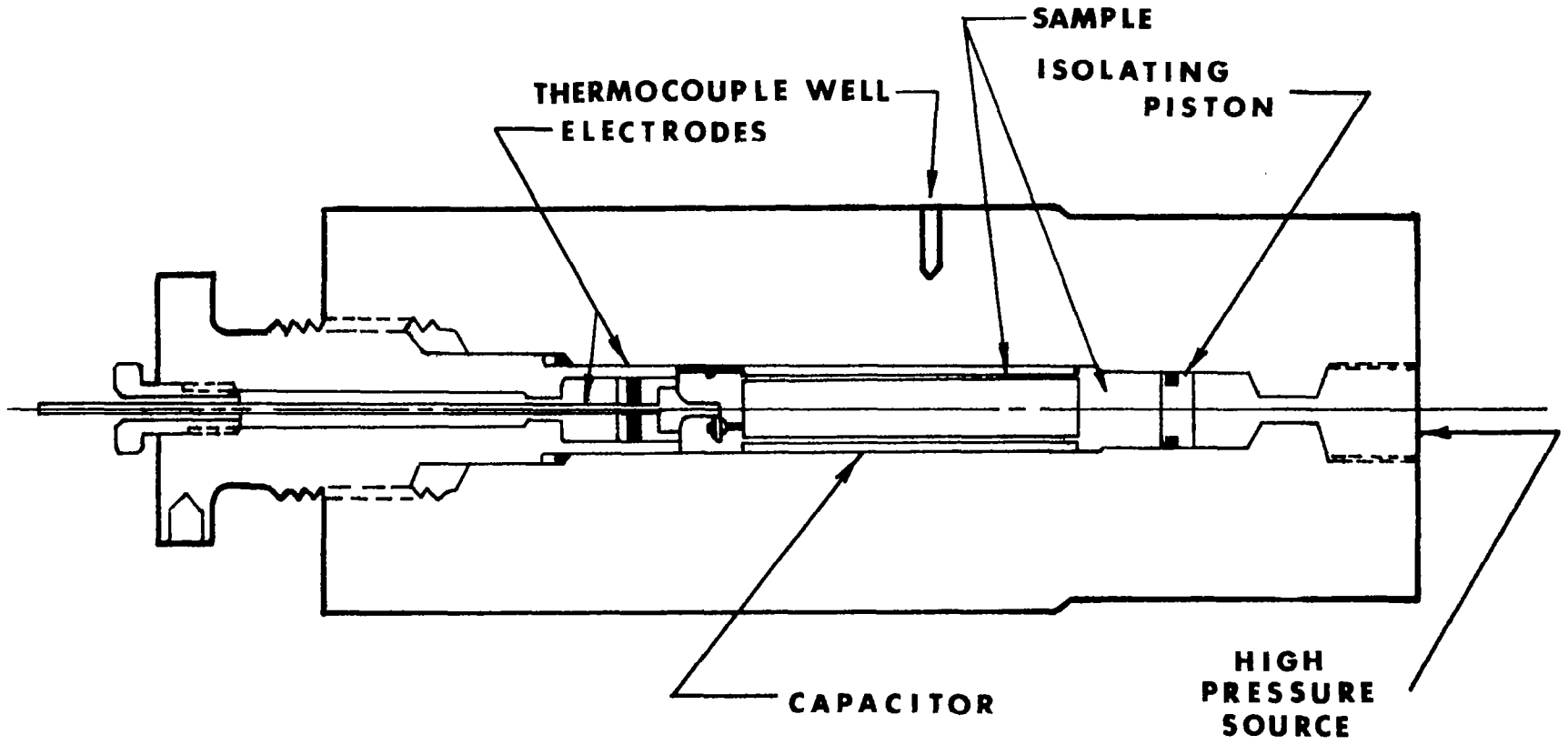

Figure 7. Schematic of Dielectric Cell.

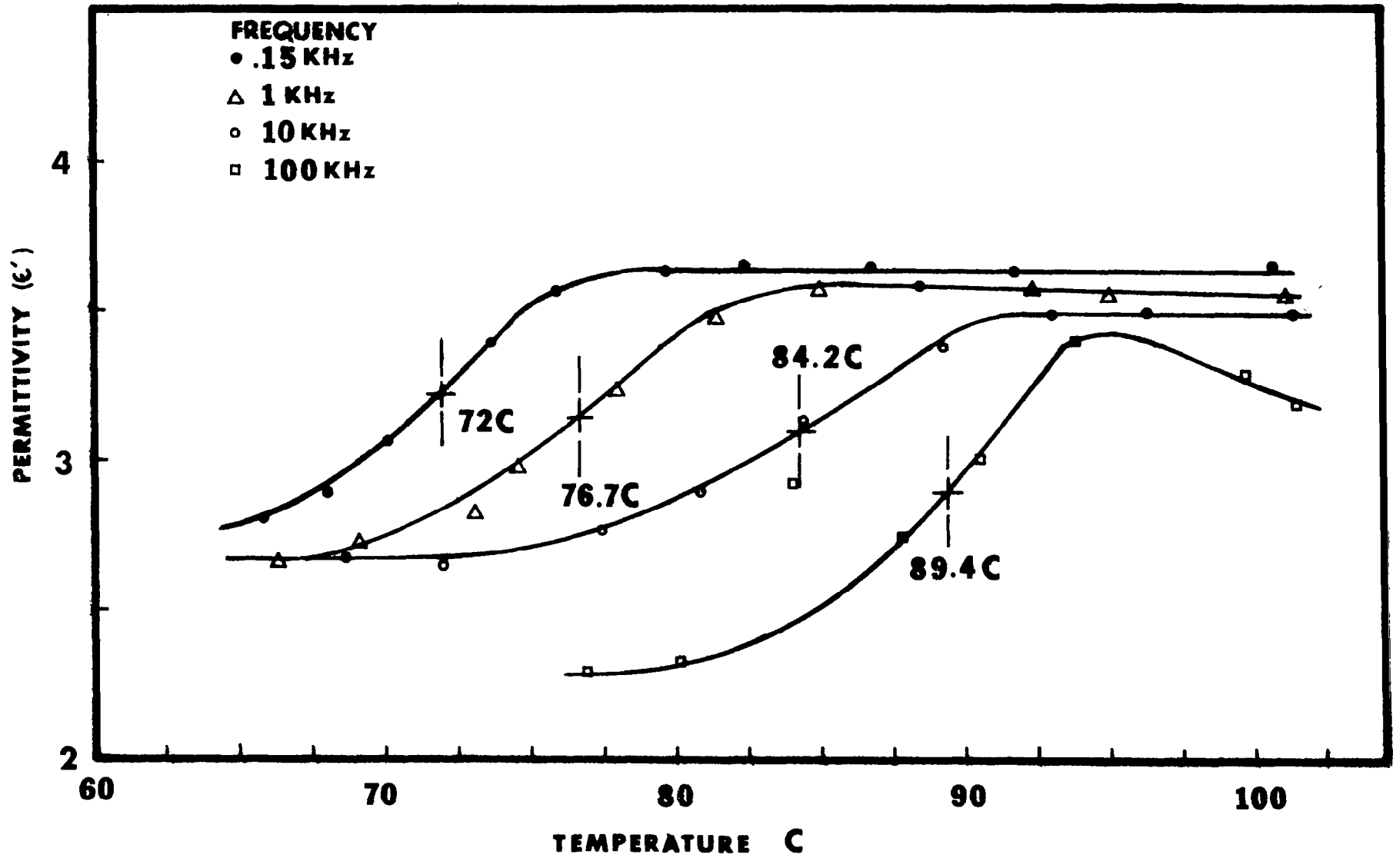

Figure 8. Permittivity (ε') of Polyphenyl Ether (5P4E) at 0.414 GPa (60 kpsi).

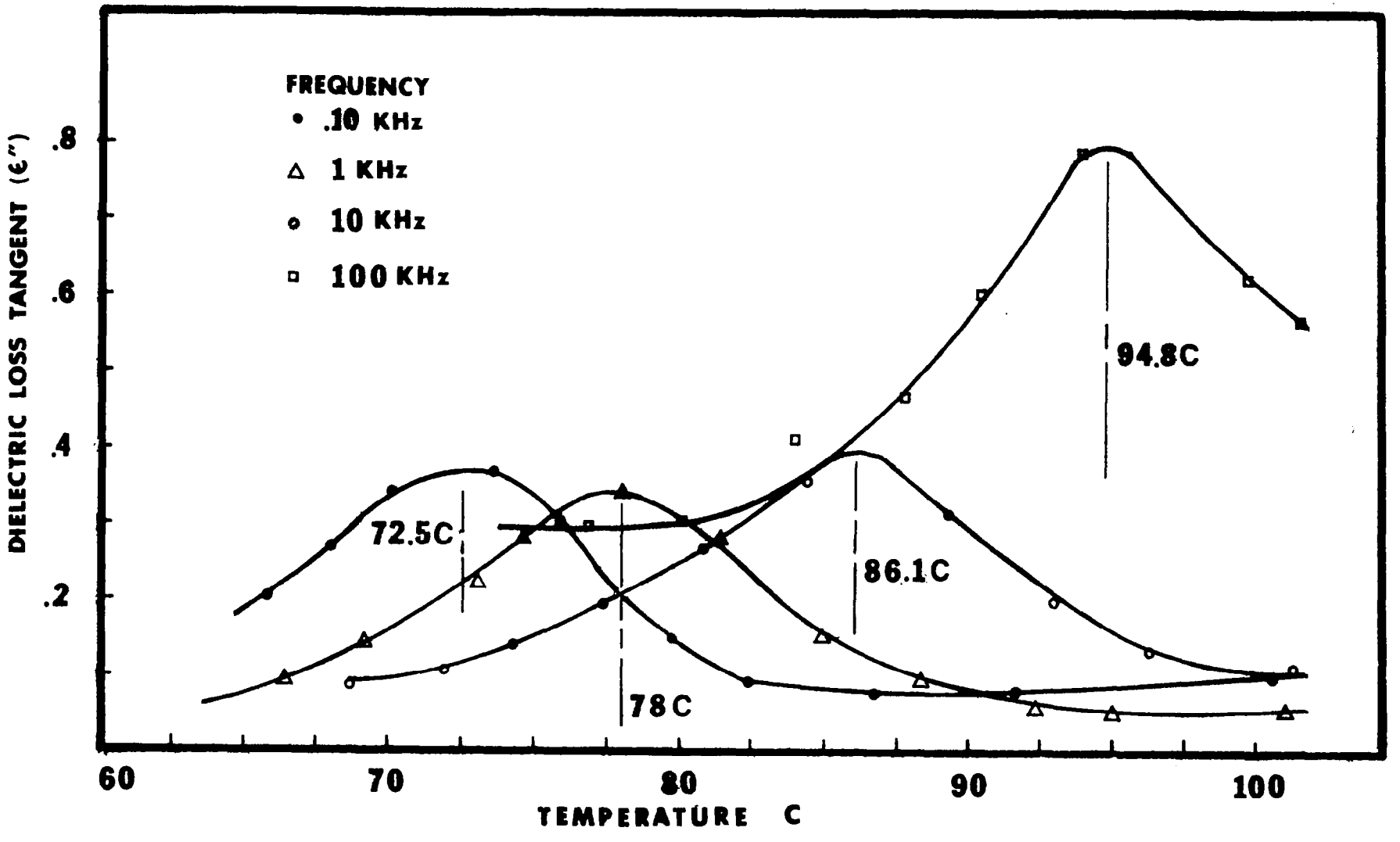

Figure 9. Dielectric Loss Tangent (ε") of Polyphenyl Ether (5P4E) at 0.414 GPa (60 kpsi).

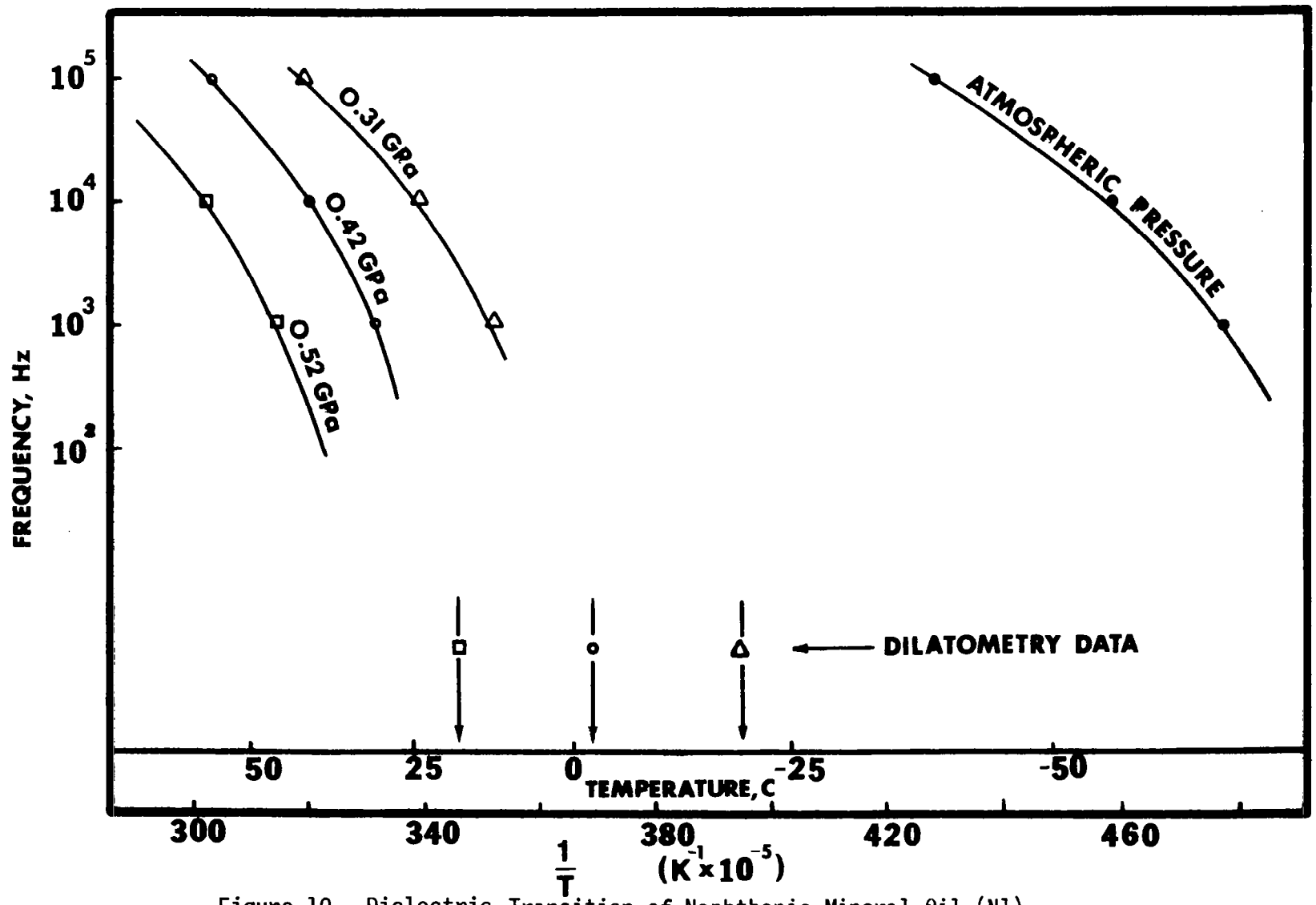

Figure 10. Dielectric Transition of Naphthenic Mineral Oil (N1).

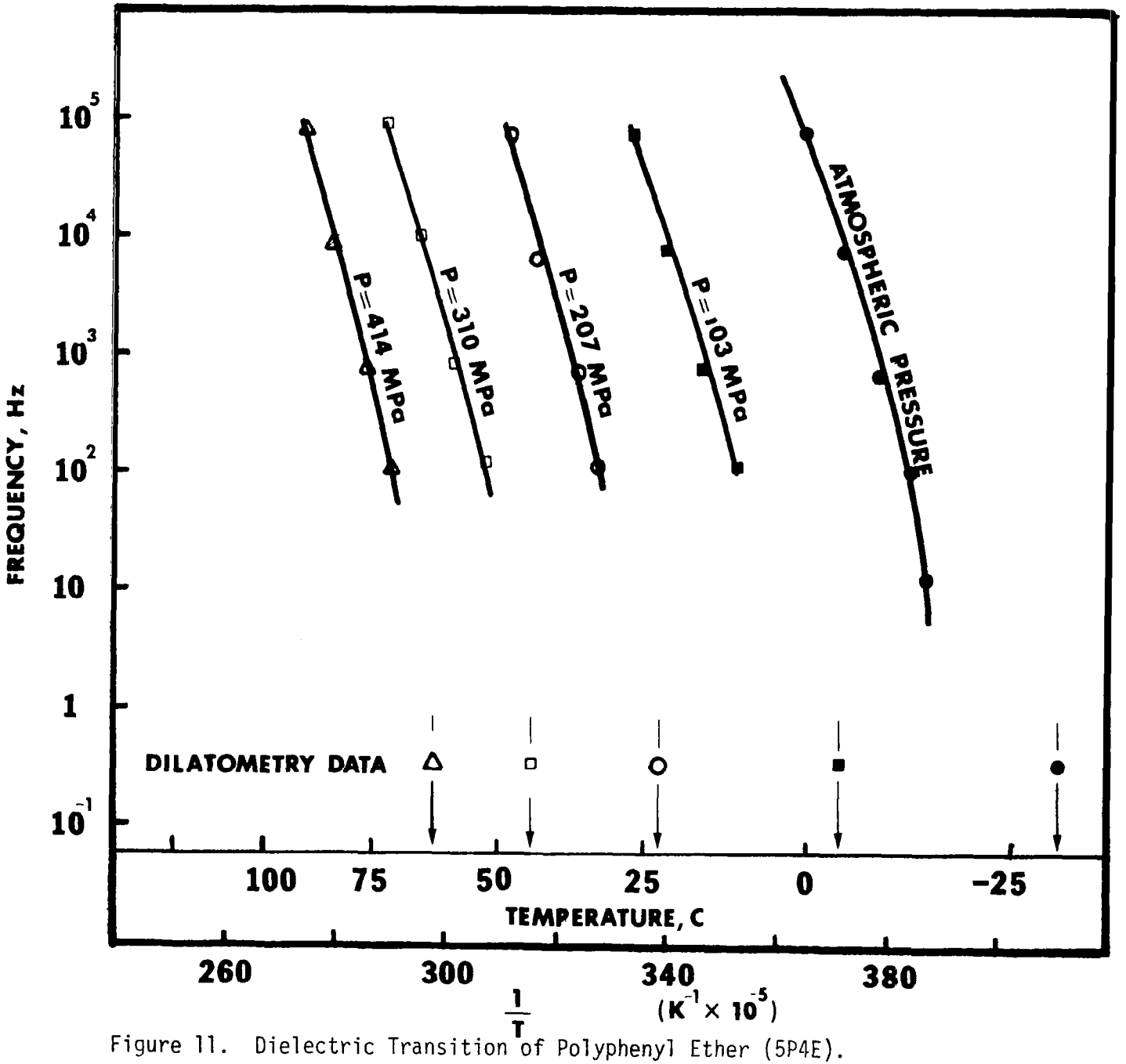

Figure 11. Dielectric Transition of Polyphenyl Ether (5P4E).

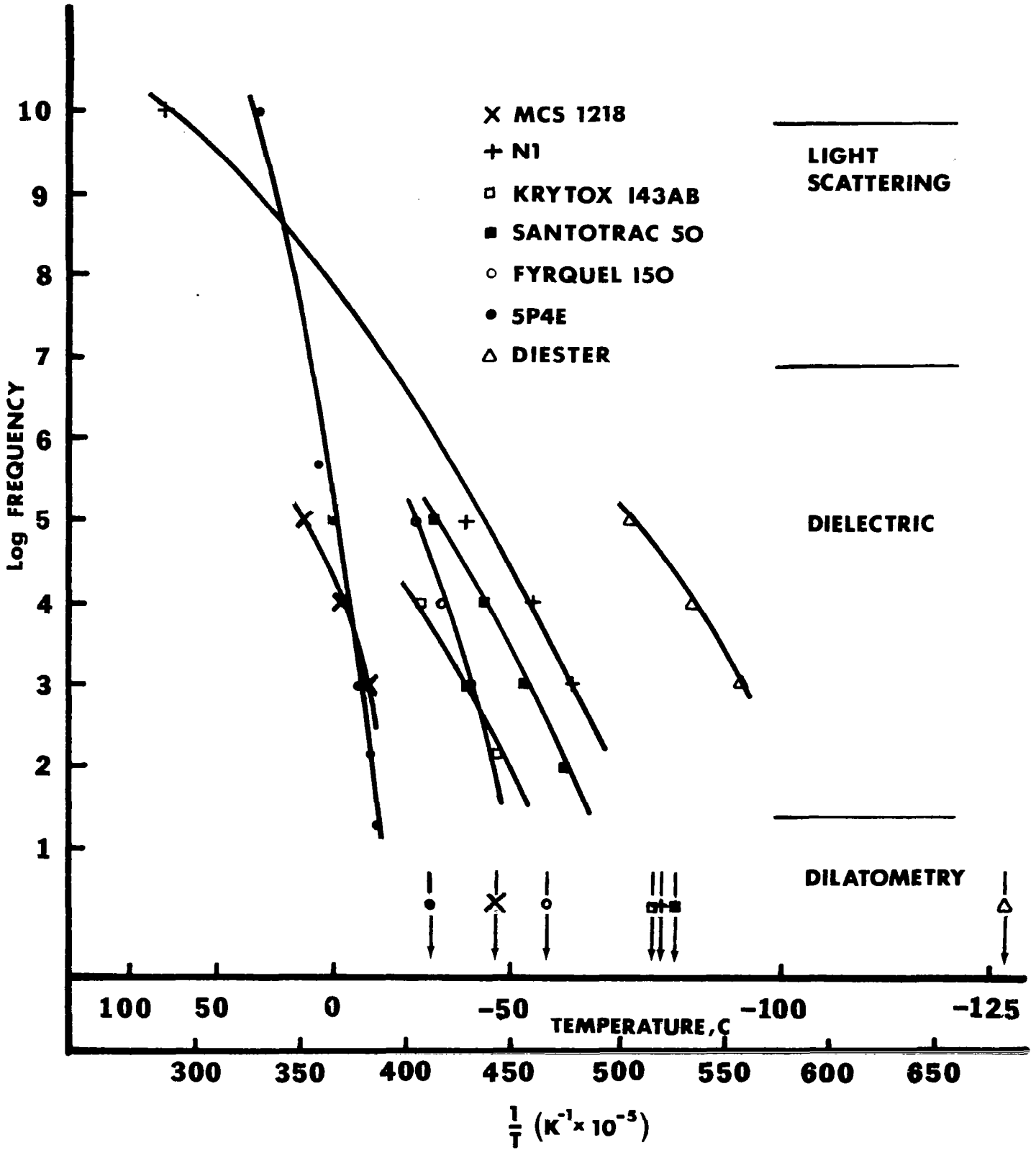

Figure 12. Dielectric ($10 \leq Hz \leq 10^6$), Low Rate Dilatometry (arrows) and Light Scattering ($Hz = 10^{10}$) Transition Data at Atmospheric Pressure.

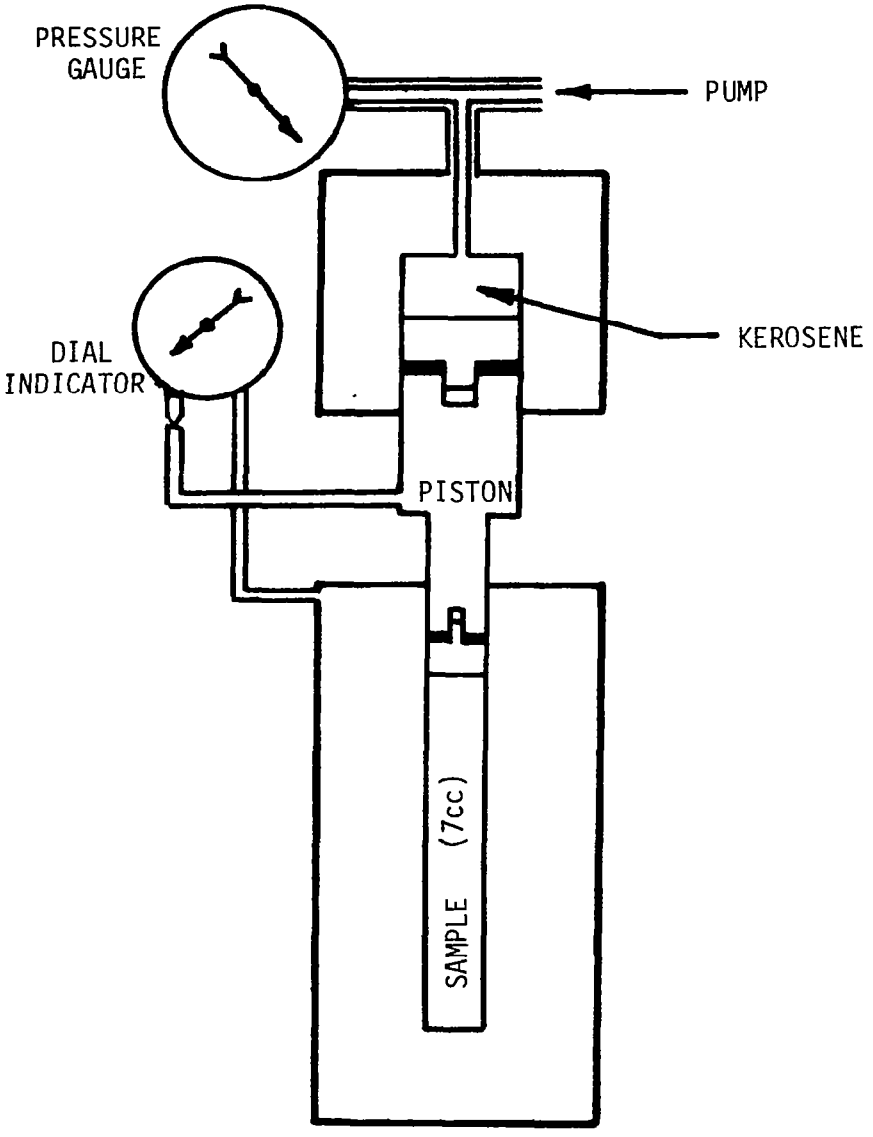

Figure 13. Schematic of High Pressure Dilatometer (0.35 to 1.75 GPa).

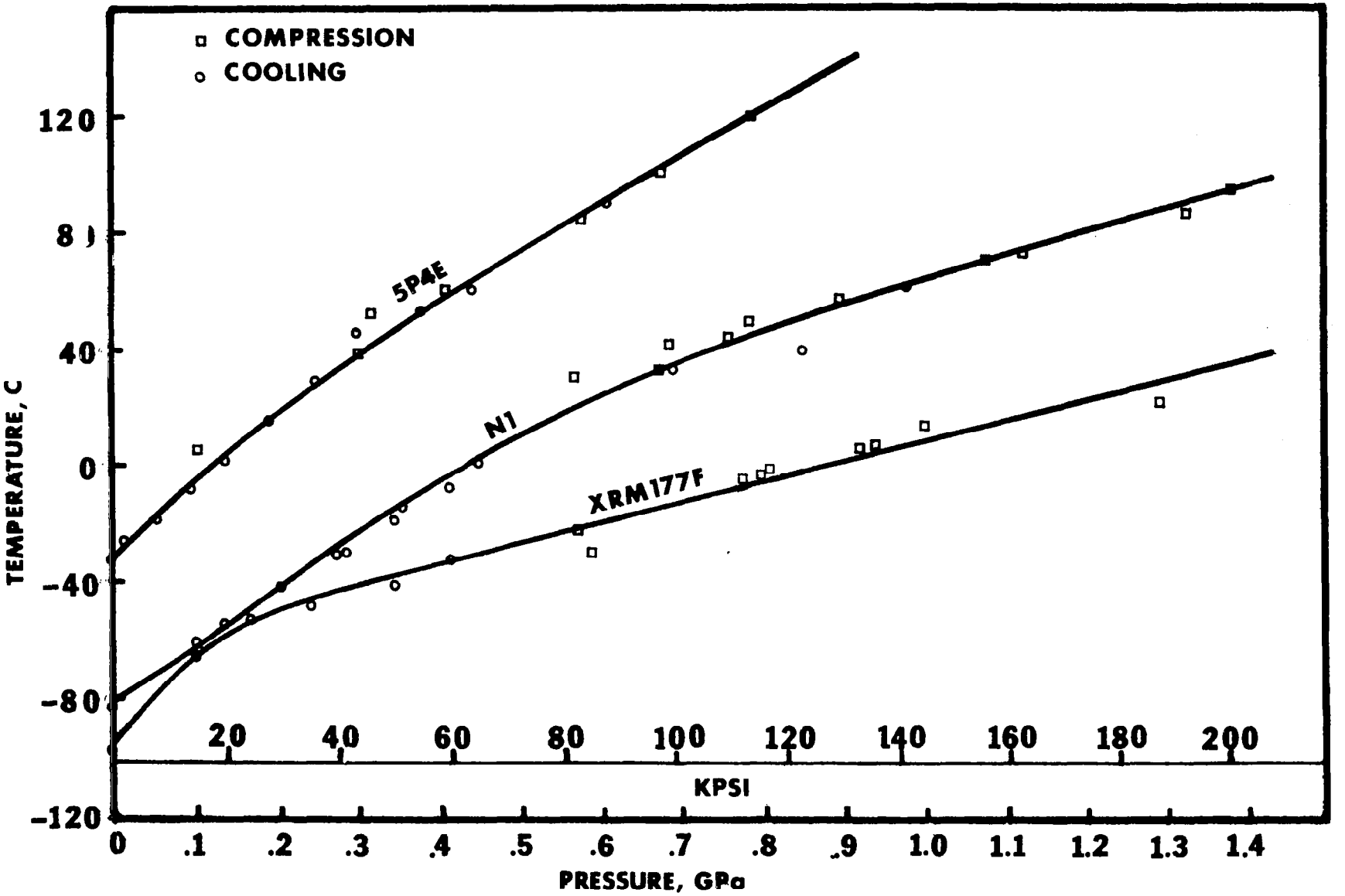

Figure 14. Volume Dilatometry Transition Diagram for Polyphenyl Ether (5P4E), Naphthenic Mineral Oil (N1), Synthetic Paraffinic Mineral Oil (XRM 177F).

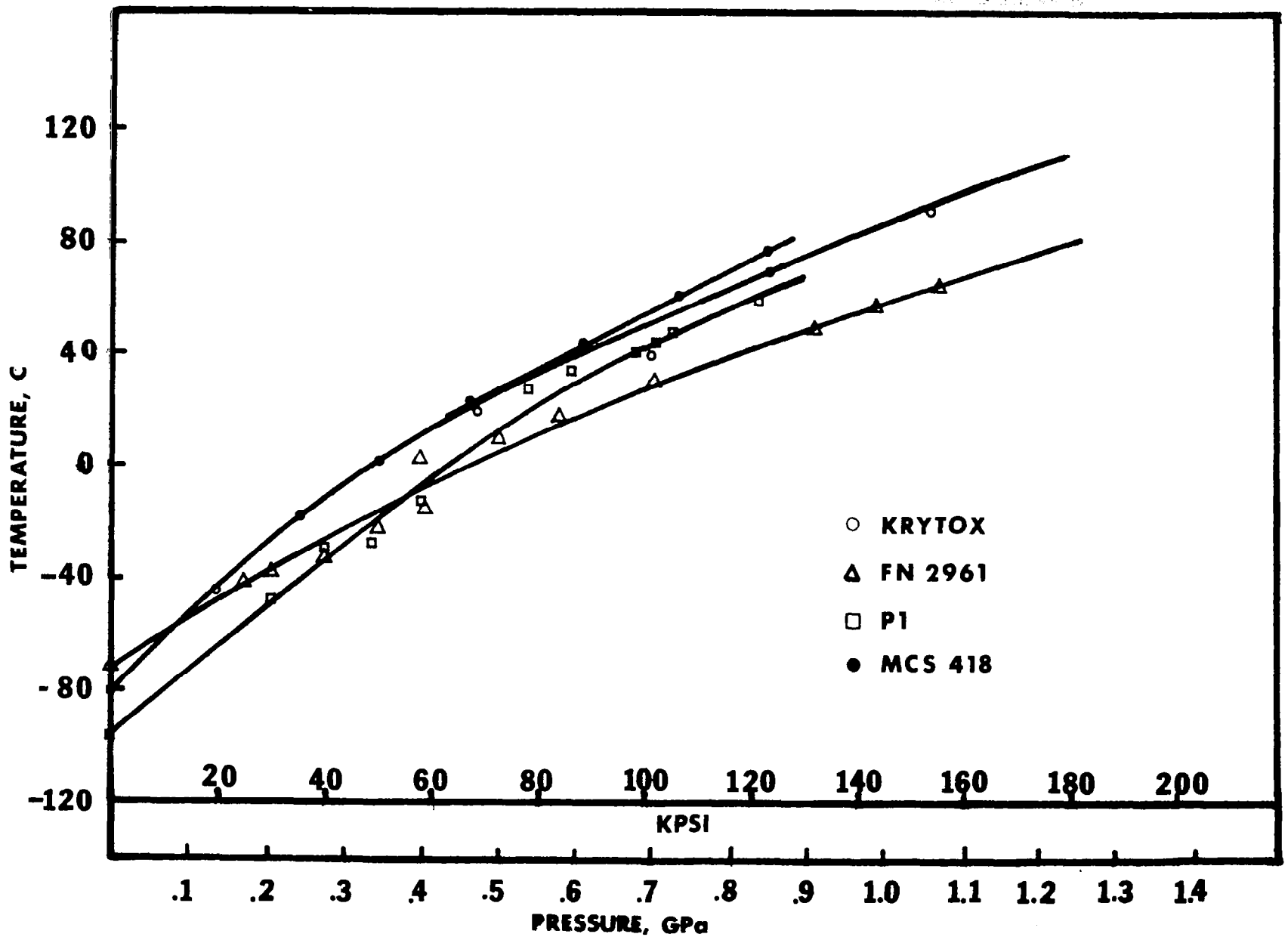

Figure 15. Volume Dilatometry Transition Diagram for Perfluorinated Poly ether (Krytox 143-AB), Super refined Naphthenic Mineral Oil (FN 2961), Paraffinic Mineral Oil (P1) Modified Polyphenyl Ether (C-ether) (MCS-418).

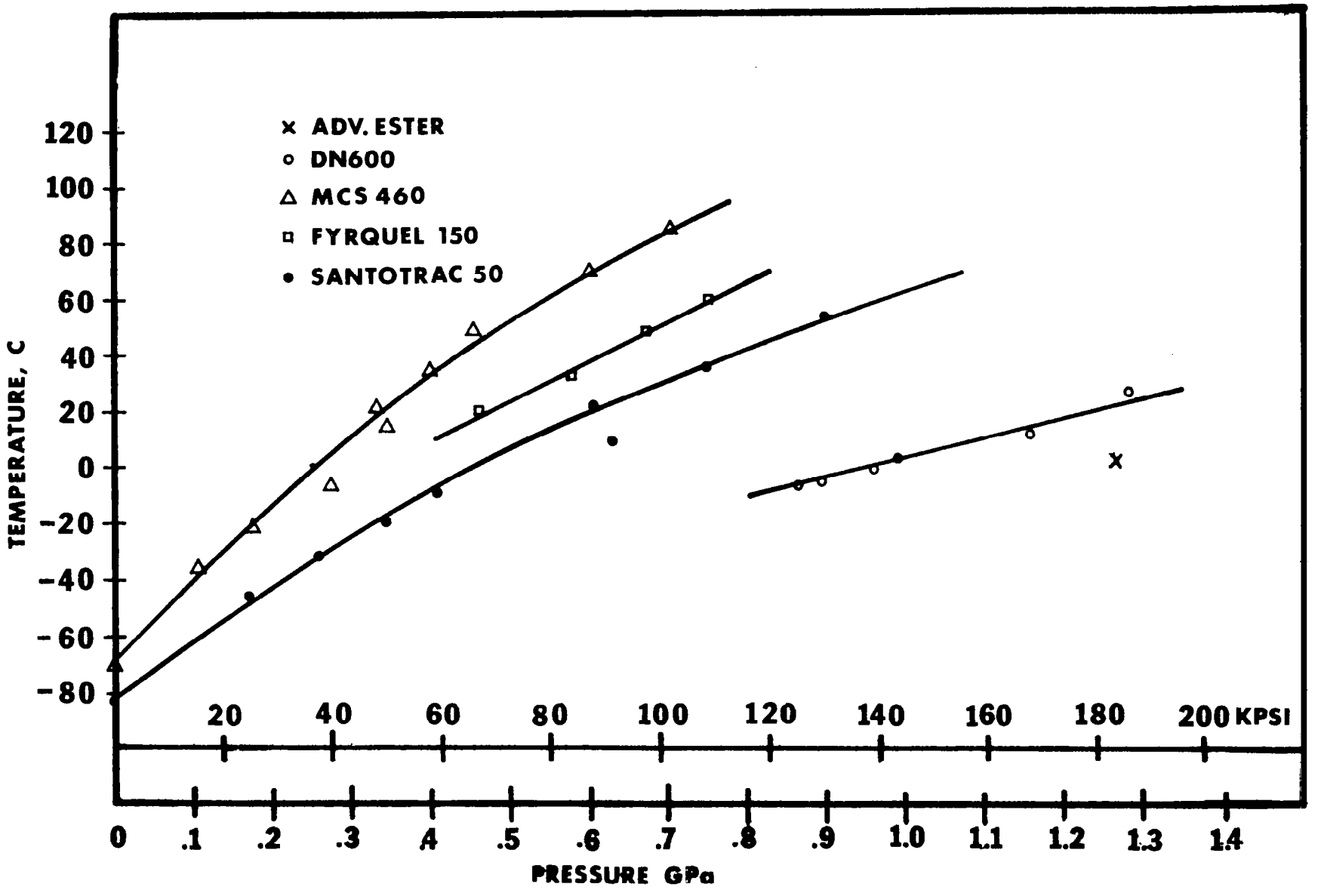

Figure 16. Volume Dilatometry Transition Diagram for Pentaerythritol (Advanced Ester), Polyalkyl aromatic (DN 600), Synthetic hydrocarbon (MCS 460), Tri-aryl phosphate ester (Fyrquel 150), Synthetic cycloaliphatic hydrocarbon (Santotrac 50).

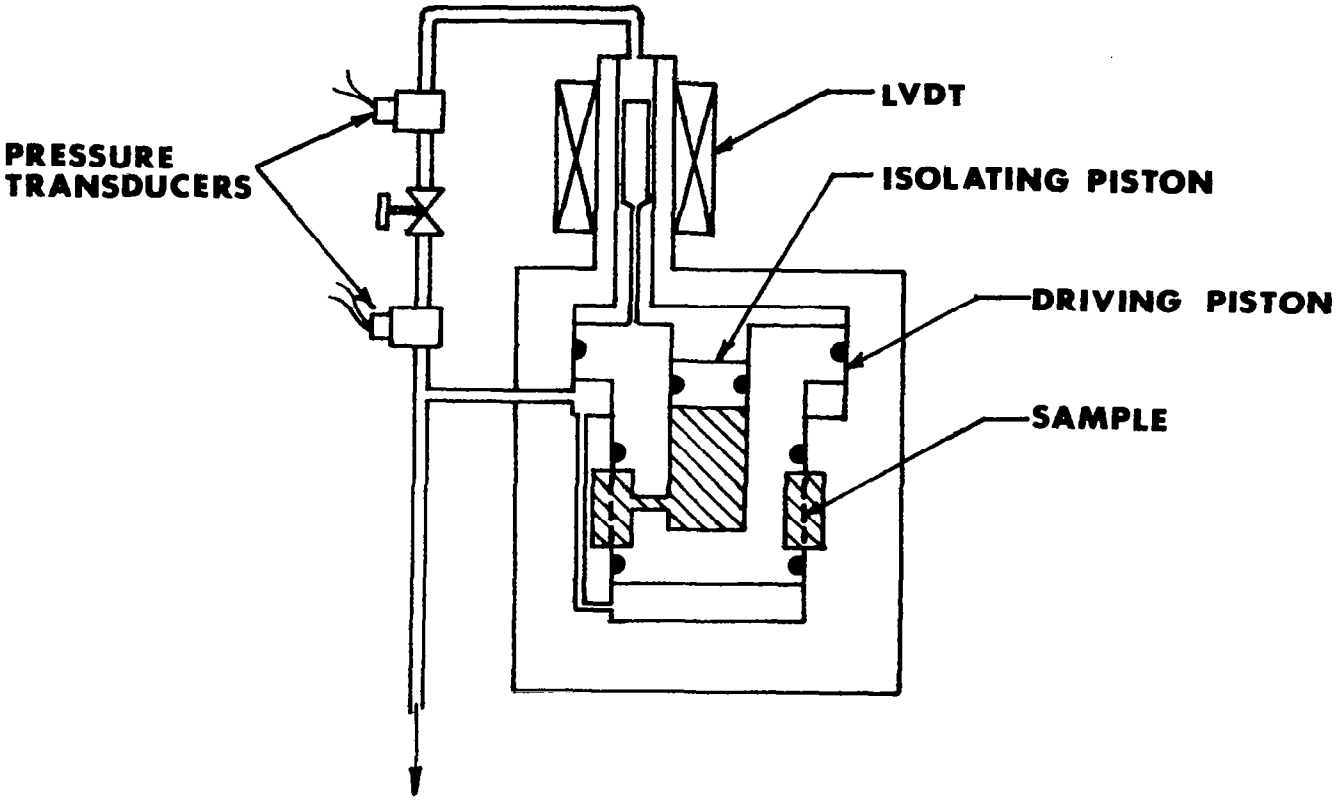

Figure 17. Schematic of Shear Stress Apparatus, 0.7 GPa (100 kpsi).

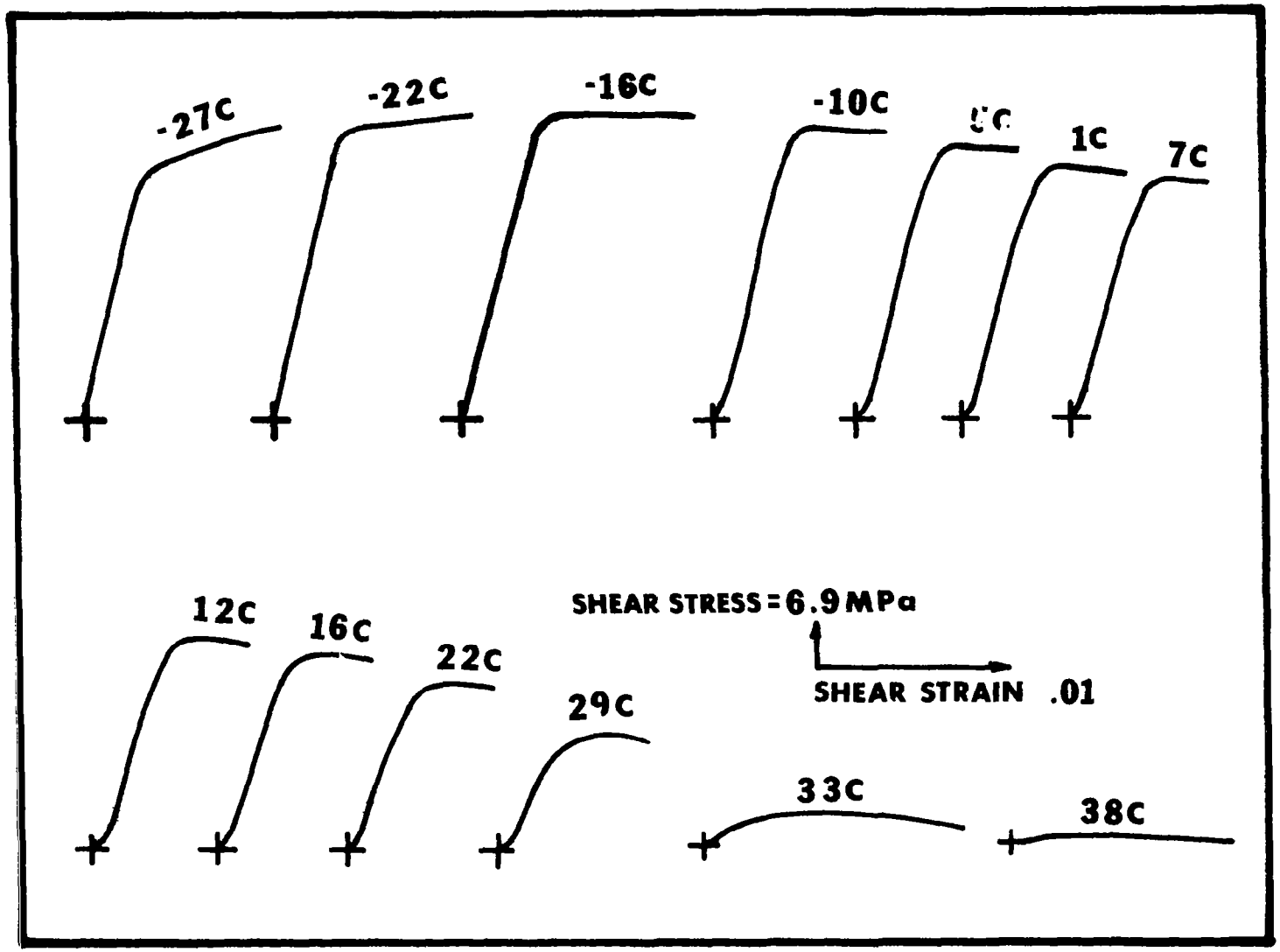

Figure 18. Recorder Plot of Shear Stress versus Shear Strain for Polyphenyl ether (5P4E) at 0.275 GPa (40 kpsi) and Indicated Temperatures.

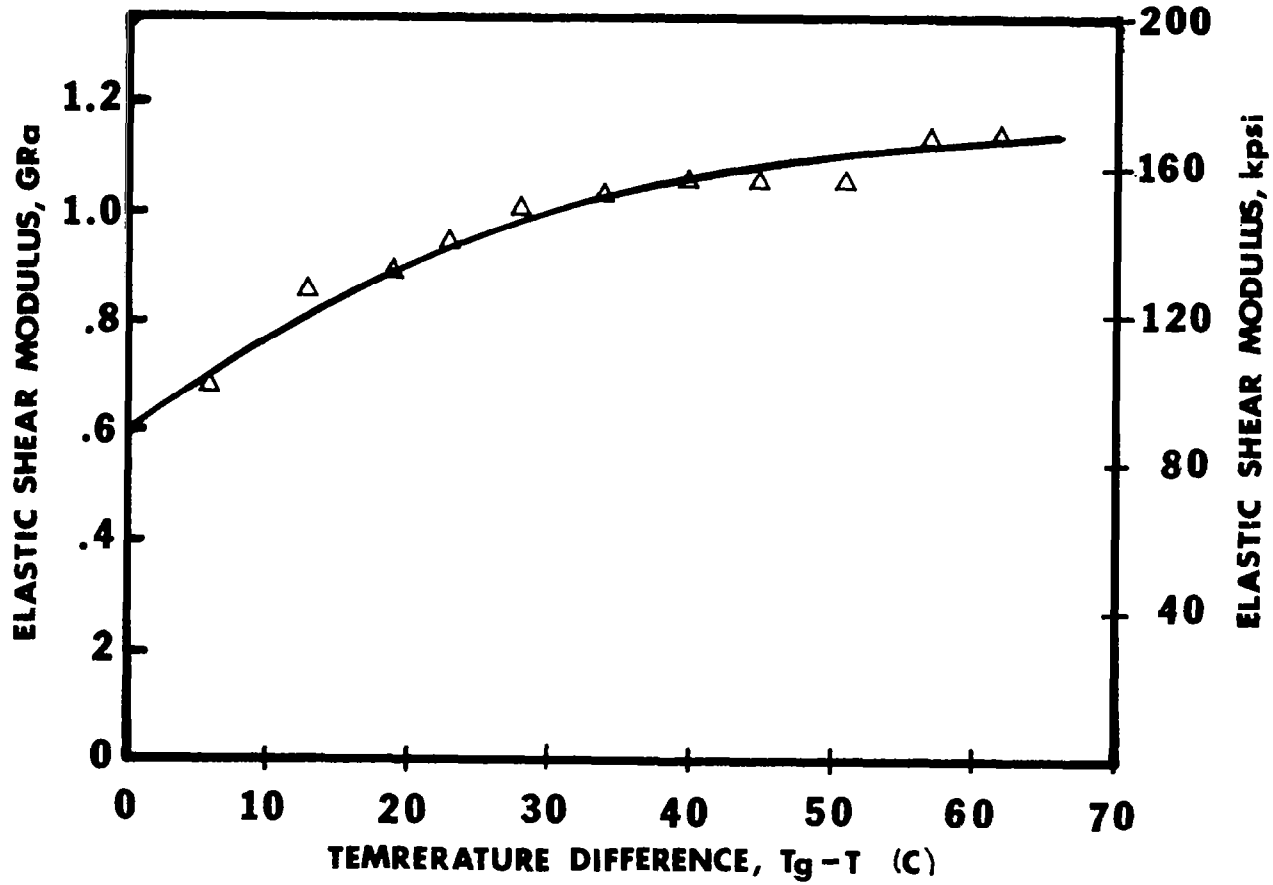

Figure 19. Elastic Shear Modulus of Polyphenyl Ether (5P4E) at 0.275 GPa in (40 kpsi) in Amorphous Glassy Region.

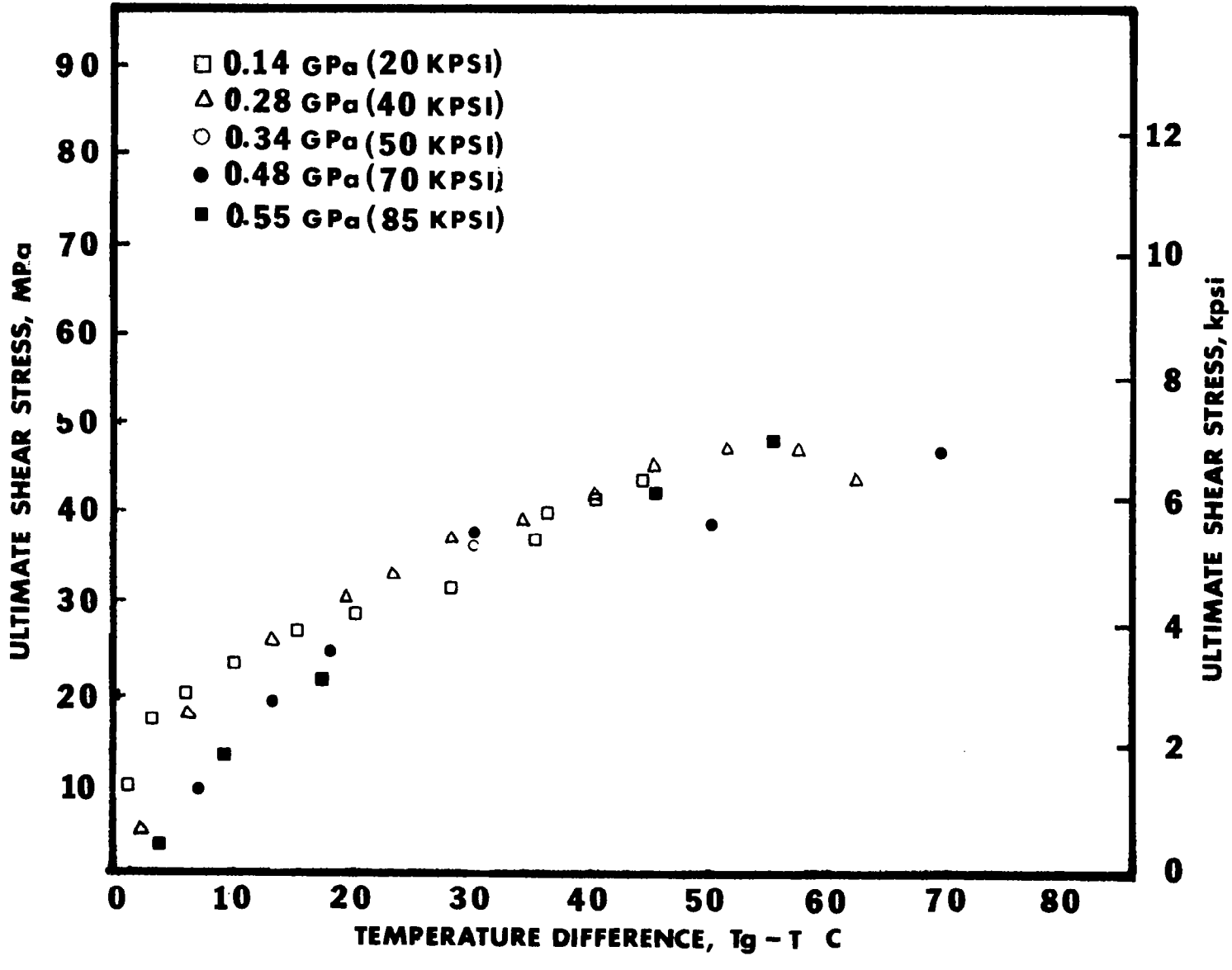

Figure 20. Ultimate Shear Stress of Polyphenyl Ether 5P4E.

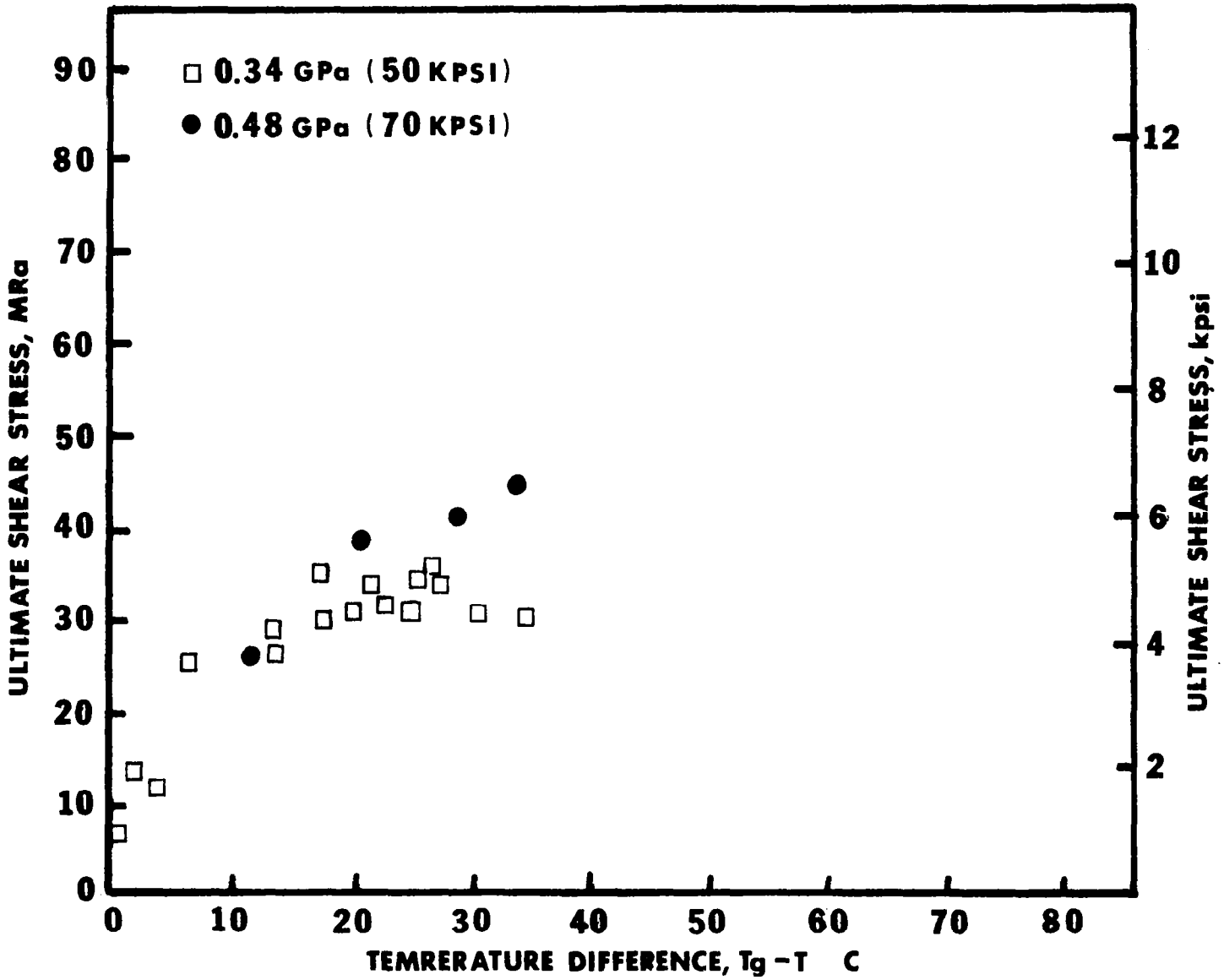

Figure 21a. Ultimate Shear Stress for Naphthenic Mineral Oil (N1).

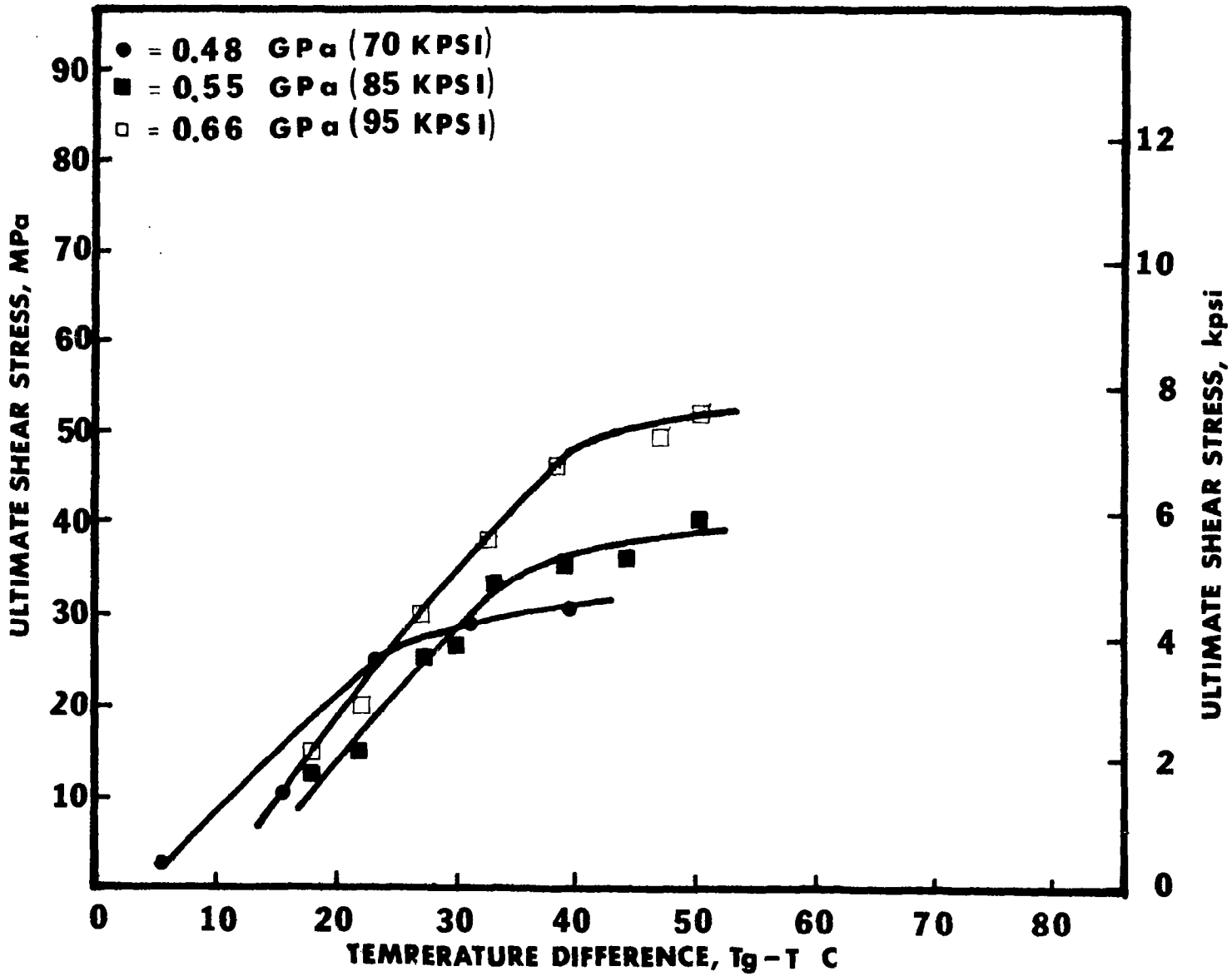

Figure 21b. Ultimate Shear Stress for Naphthenic Mineral Oil (N1).

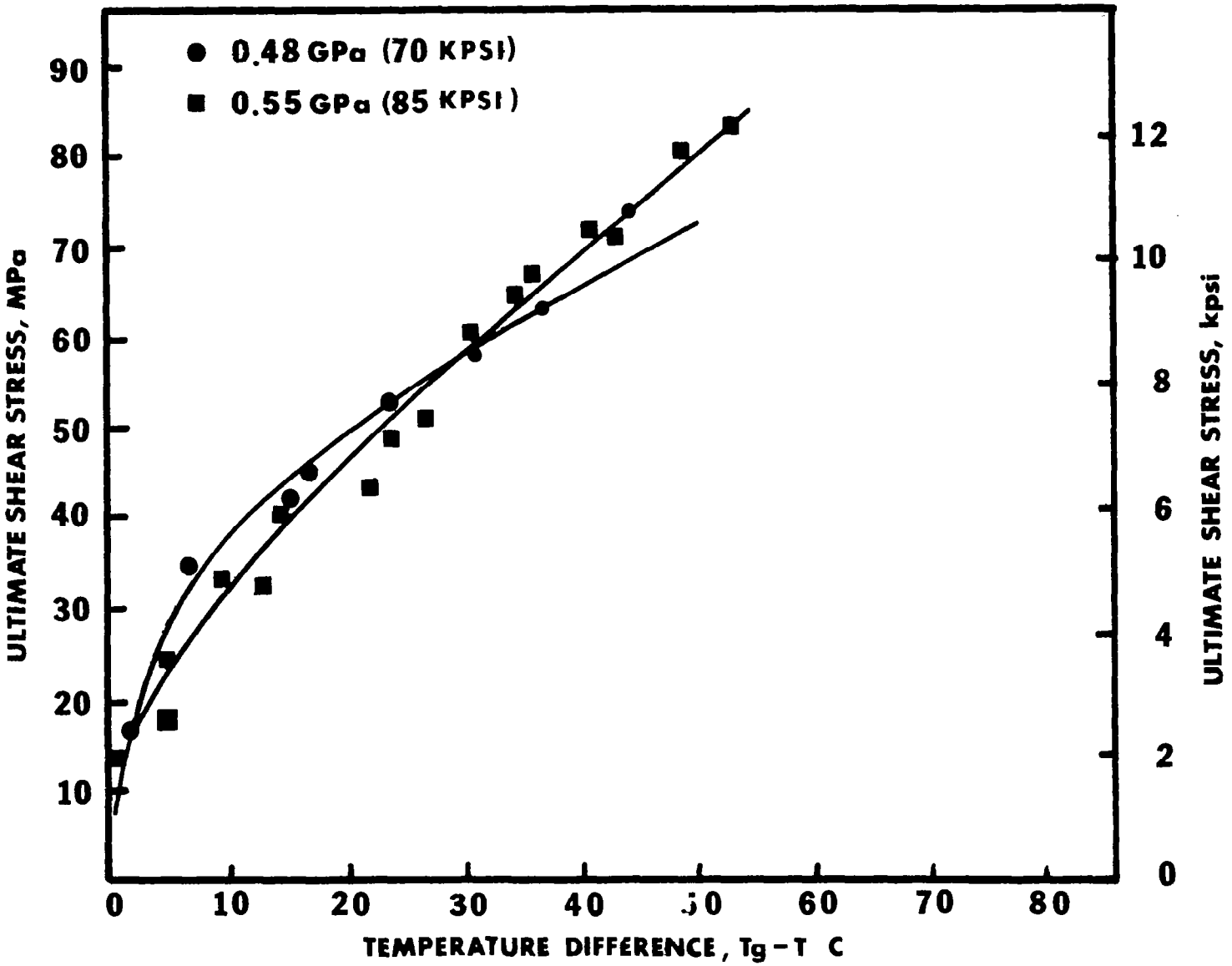

Figure 22. Ultimate Shear Stress for Synthetic Cycloaliphatic Hydrocarbon (Santotrac 50).

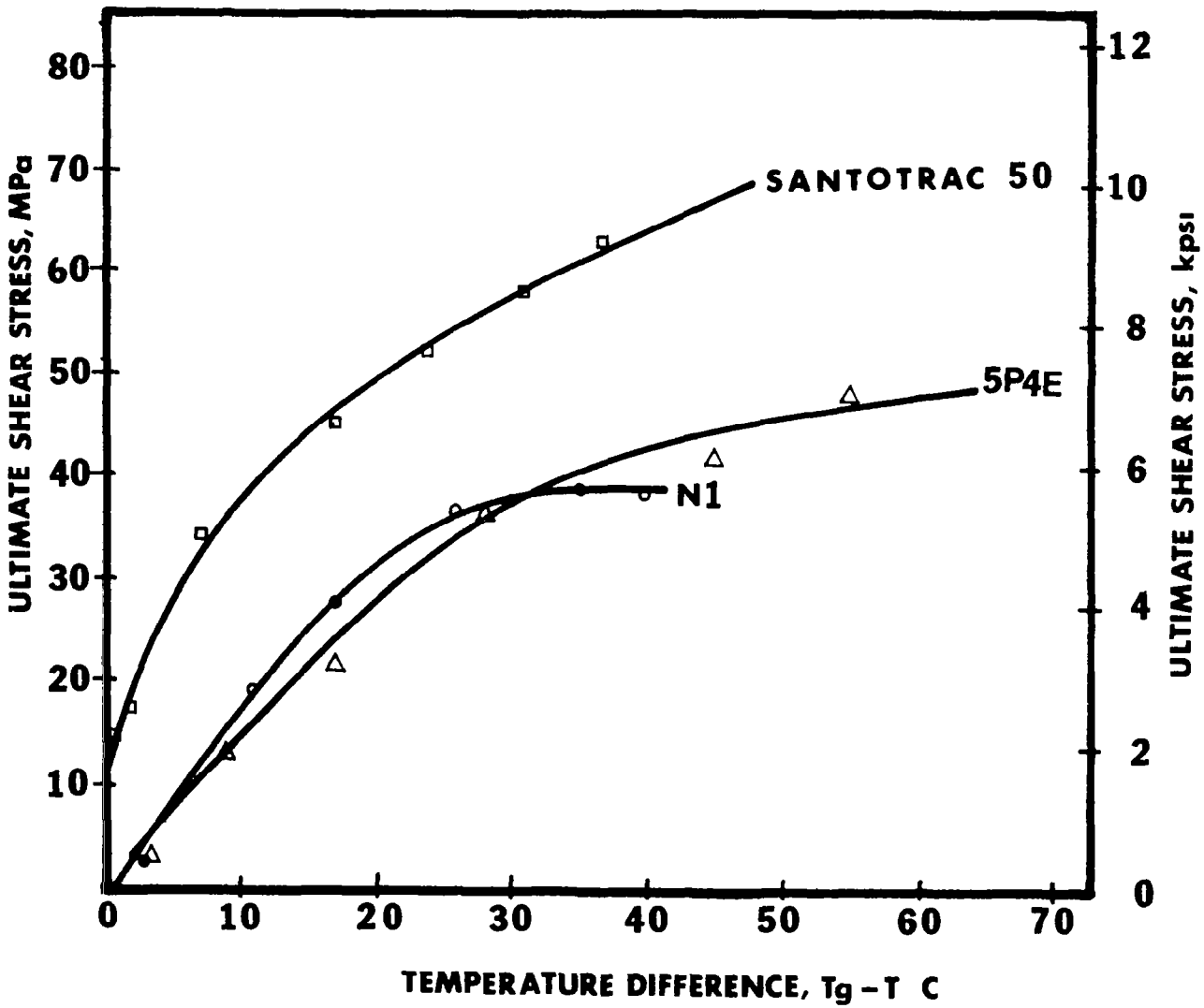

Figure 23. Ultimate Shear Stress for Synthetic Cycloaliphatic Hydrocarbon (Santotrac 50), Polyphenyl Ether (5P4E), Naphthenic Mineral Oil (N1) at 0.48 GPa (70 kpsi).

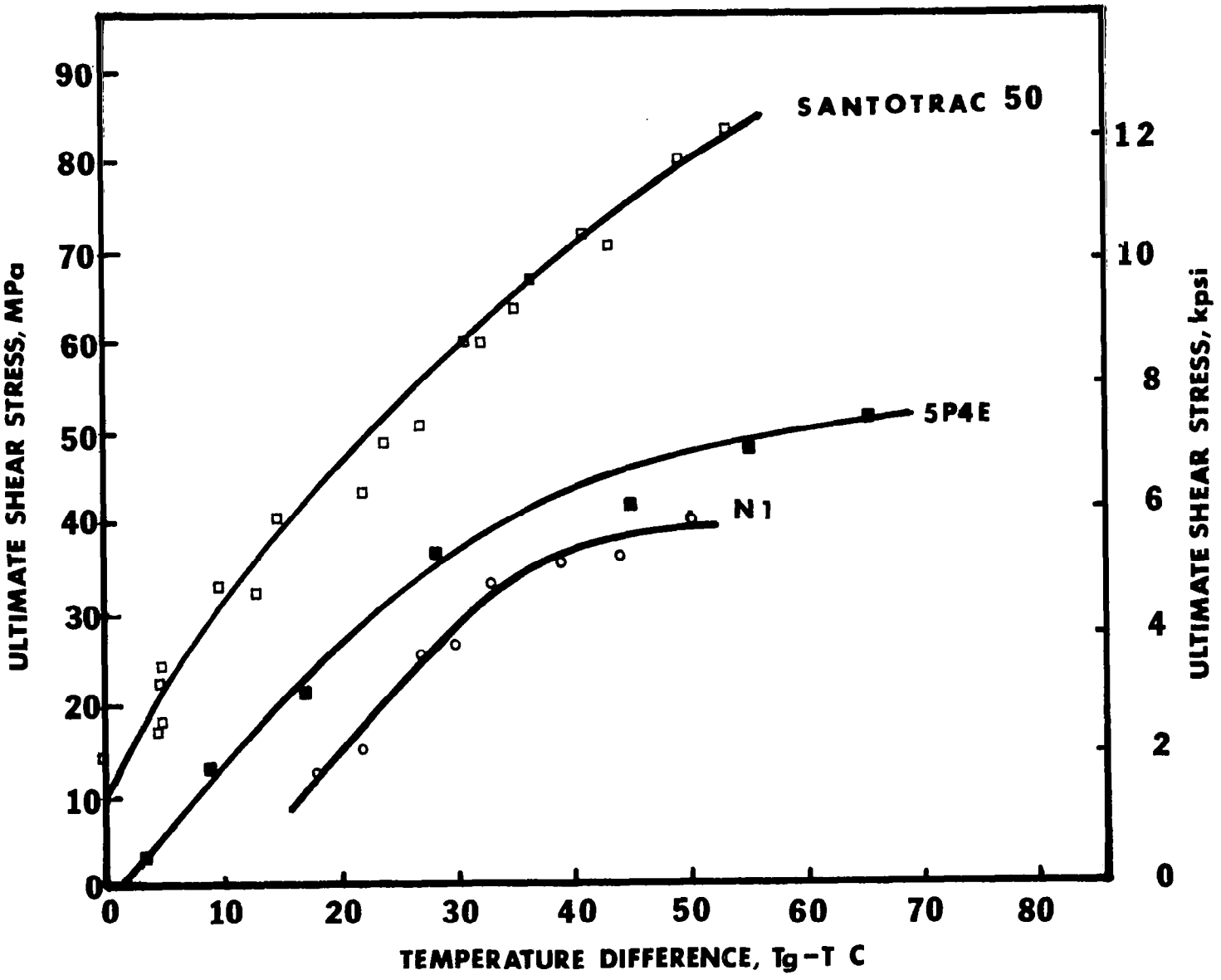

Figure 24. Ultimate Shear Stress for the Three Lubricants at 0.59 GPa.

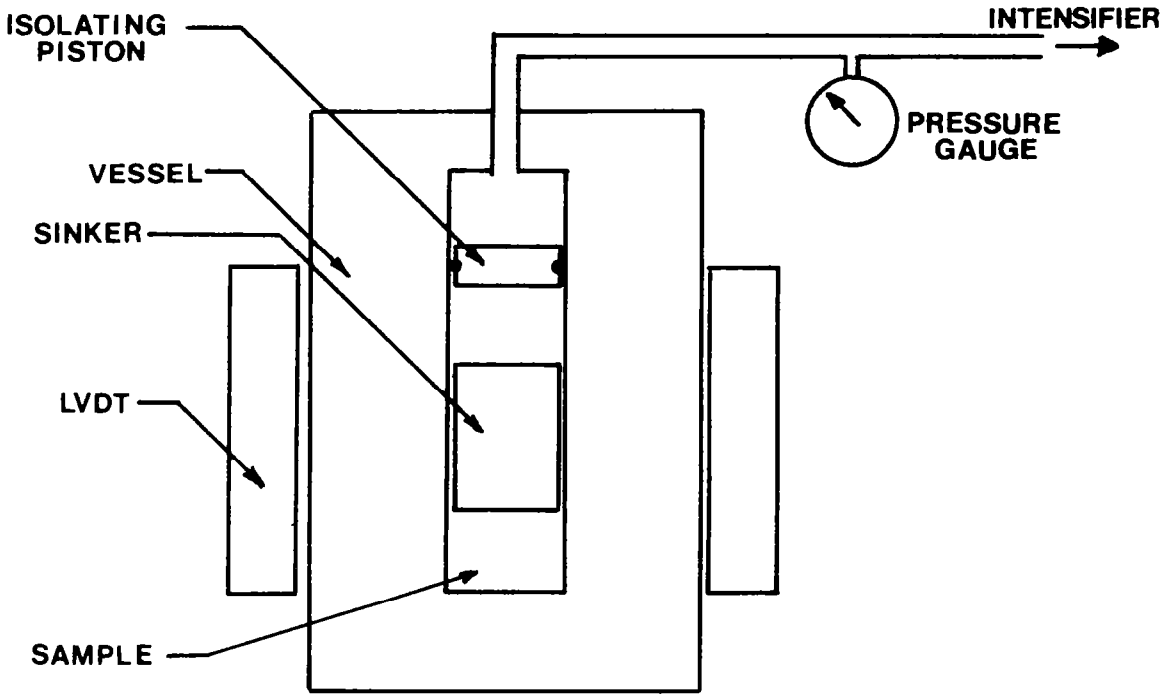

Figure 25. Schematic of High Pressure Falling Body Viscometer (0.63 GPa, 90 kpsi).

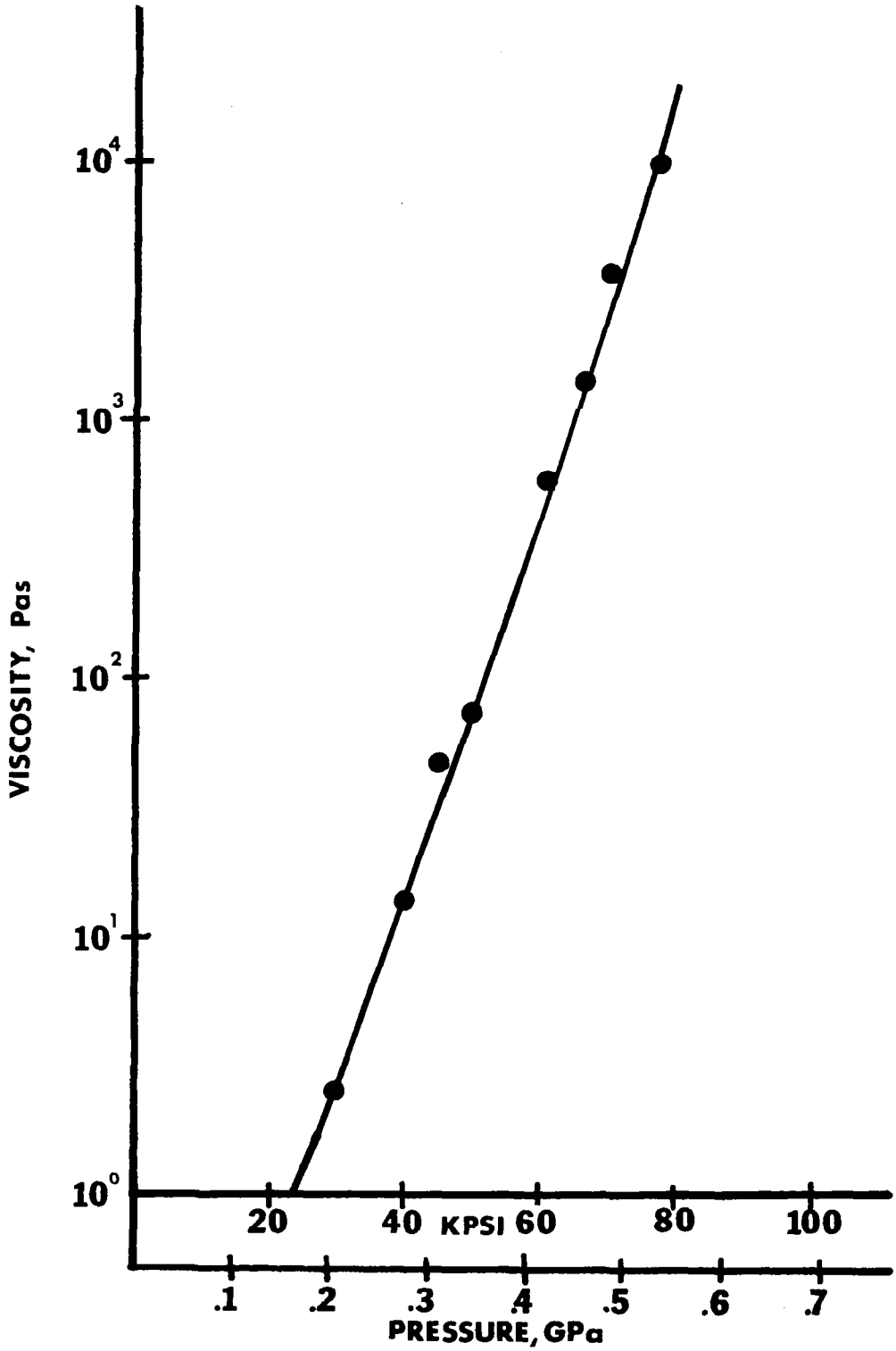

Figure 26. Pressure-Viscosity Isotherm Naphthenic Mineral Oil (N1) at 40C.

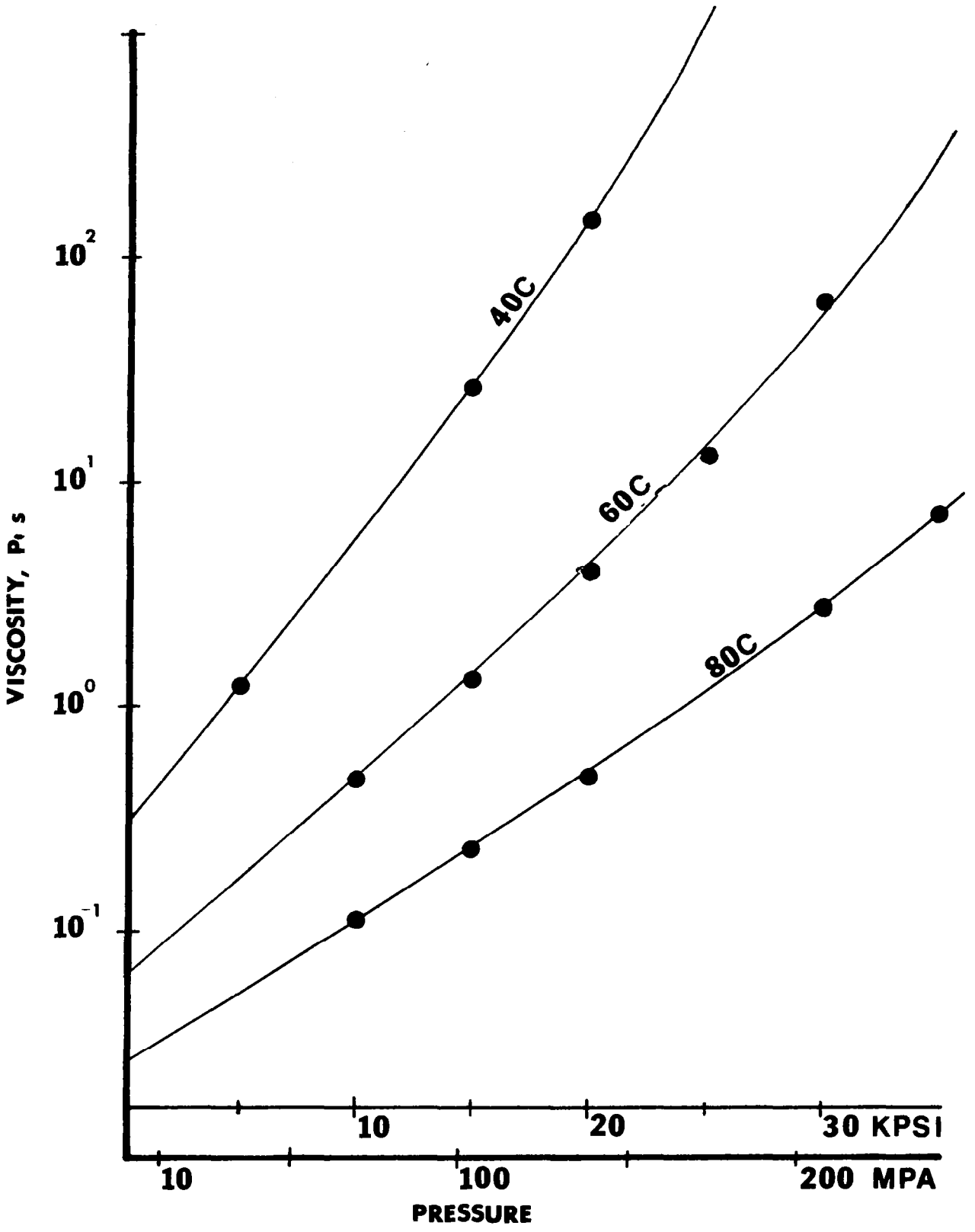

Figure 27a. Pressure-Viscosity Isotherms for Polyphenyl ether (5P4E).

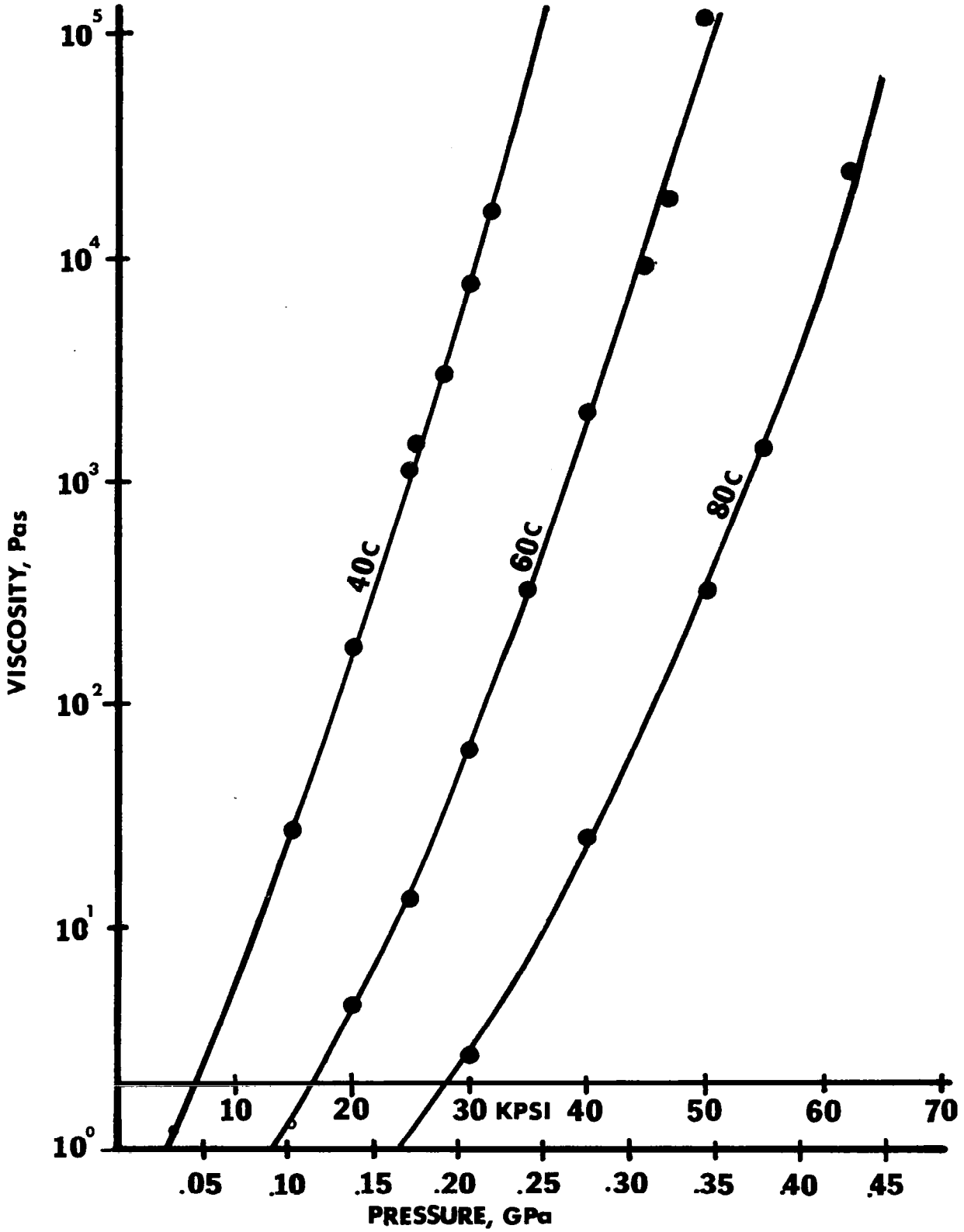

Figure 27b. Pressure-Viscosity Isotherms for Polyphenyl ether (5P4E).

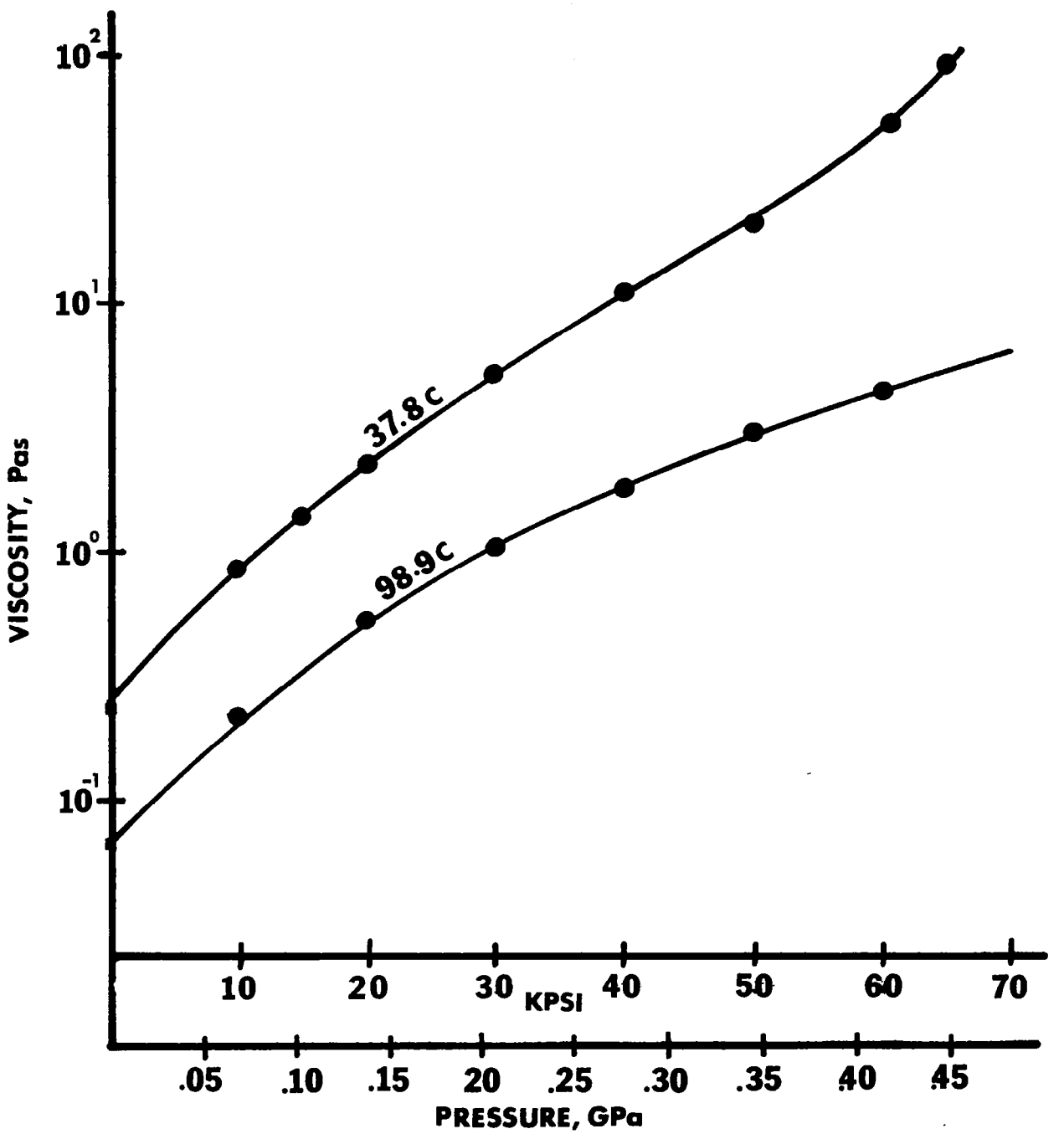

Figure 28. Pressure-Viscosity Isotherms for Perfluorinated Polyether (Brayco, 815Z).

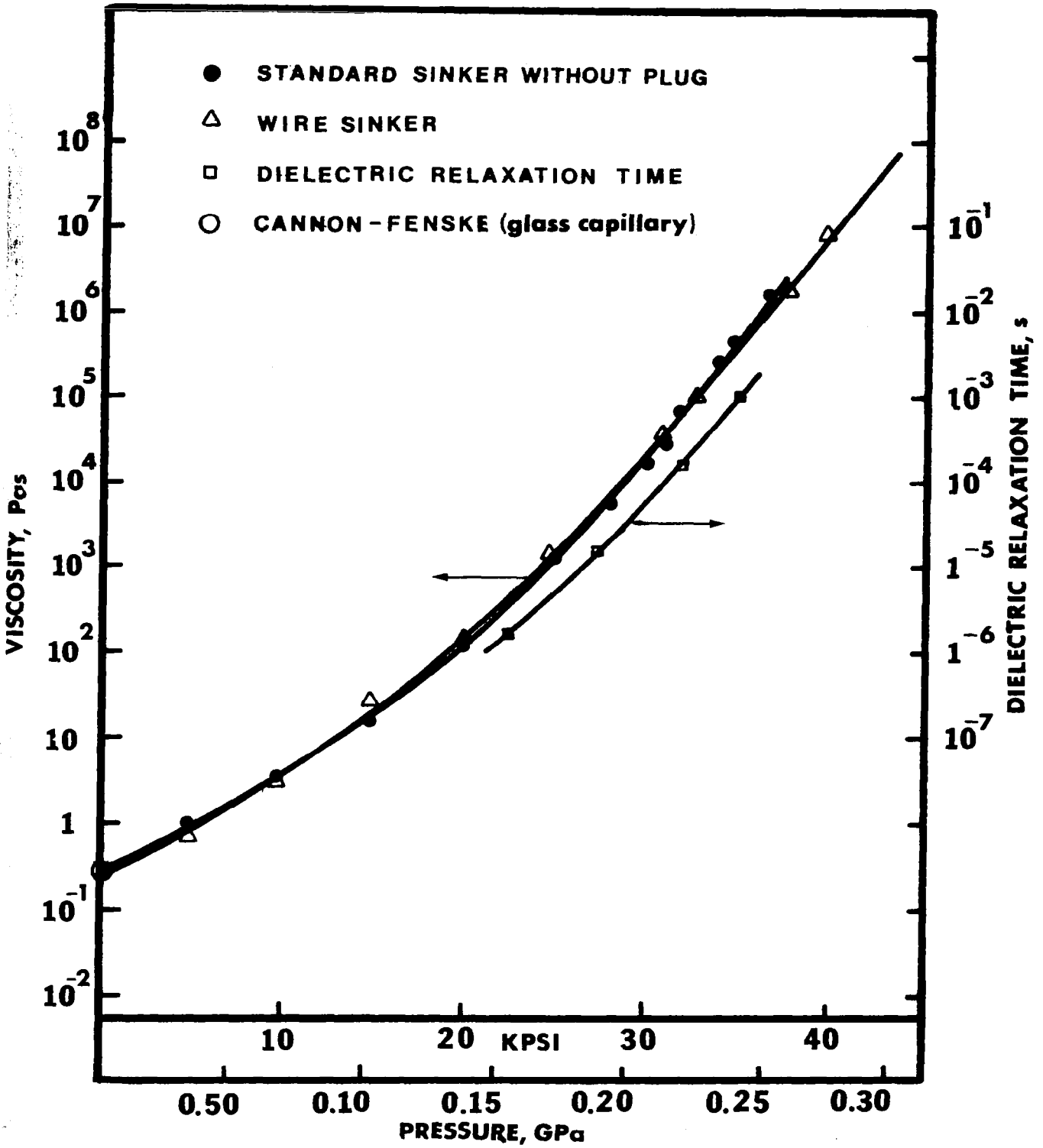

Figure 29. Low Shear Viscosity-pressure and Dielectric Relaxation Time Isotherms for Polyphenyl Ether (5P4E) at 40C.

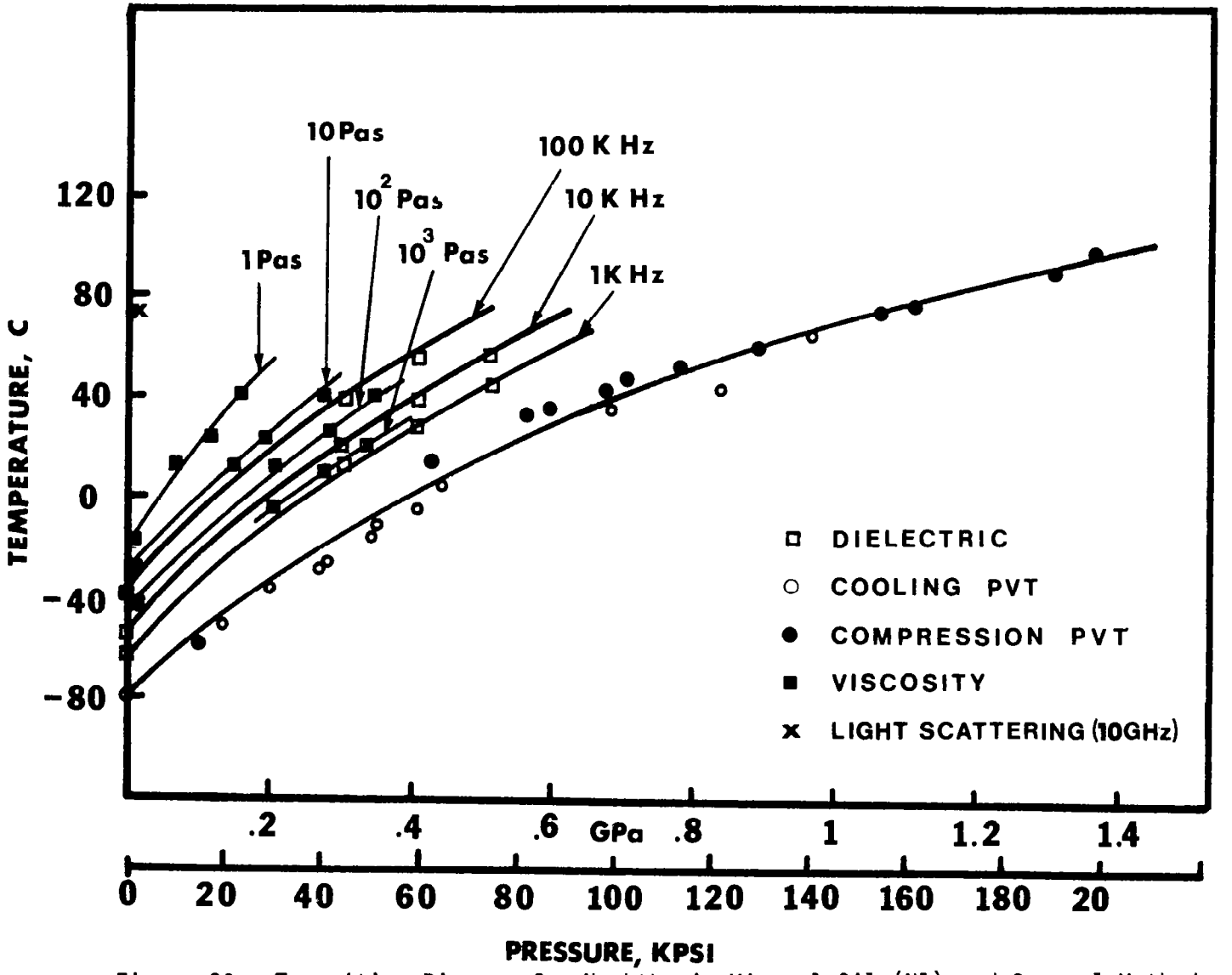

Figure 30. Transition Diagram for Naphthenic Mineral Oil (N1) and Several Methods.

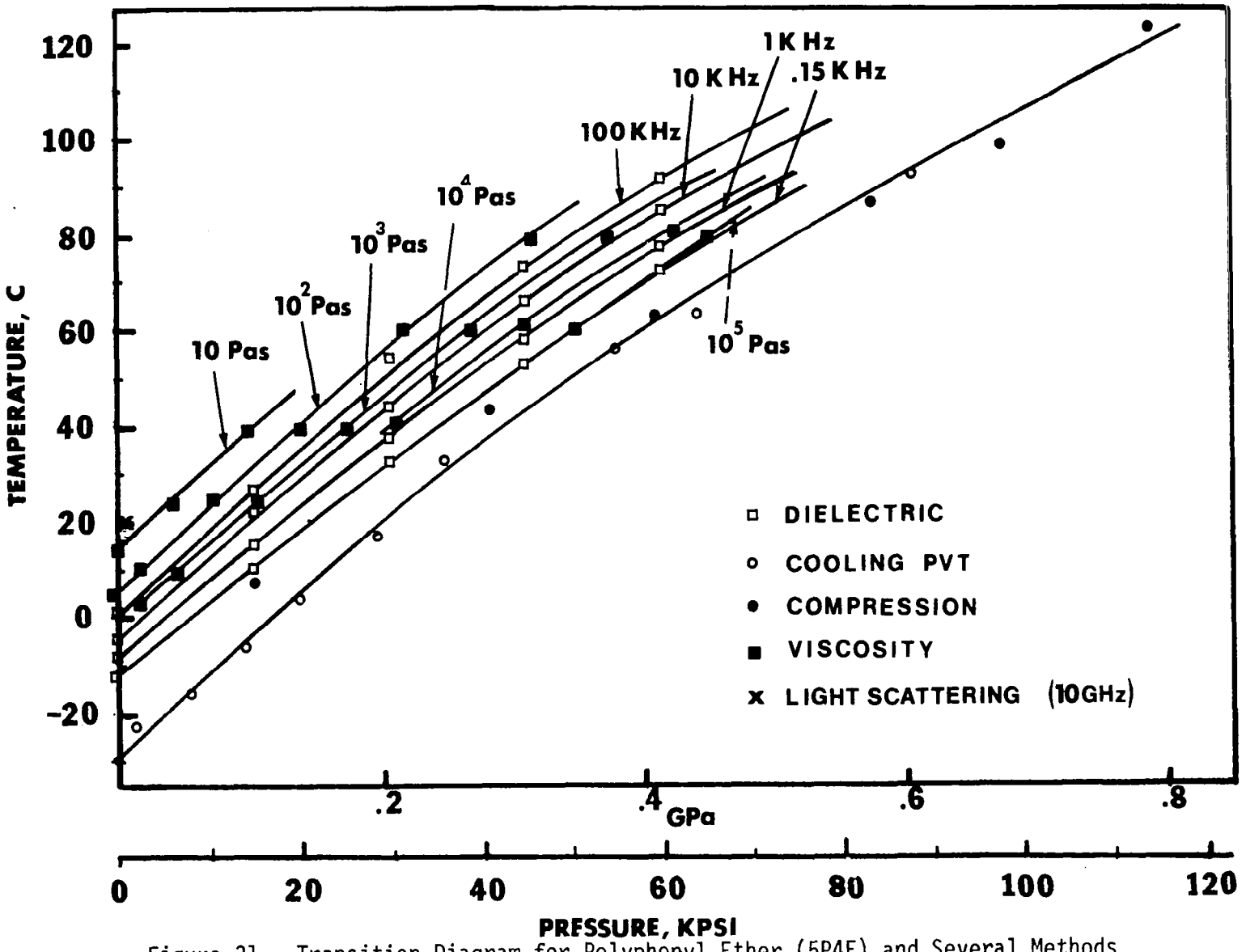

Figure 31. Transition Diagram for Polyphenyl Ether (5P4E) and Several Methods.

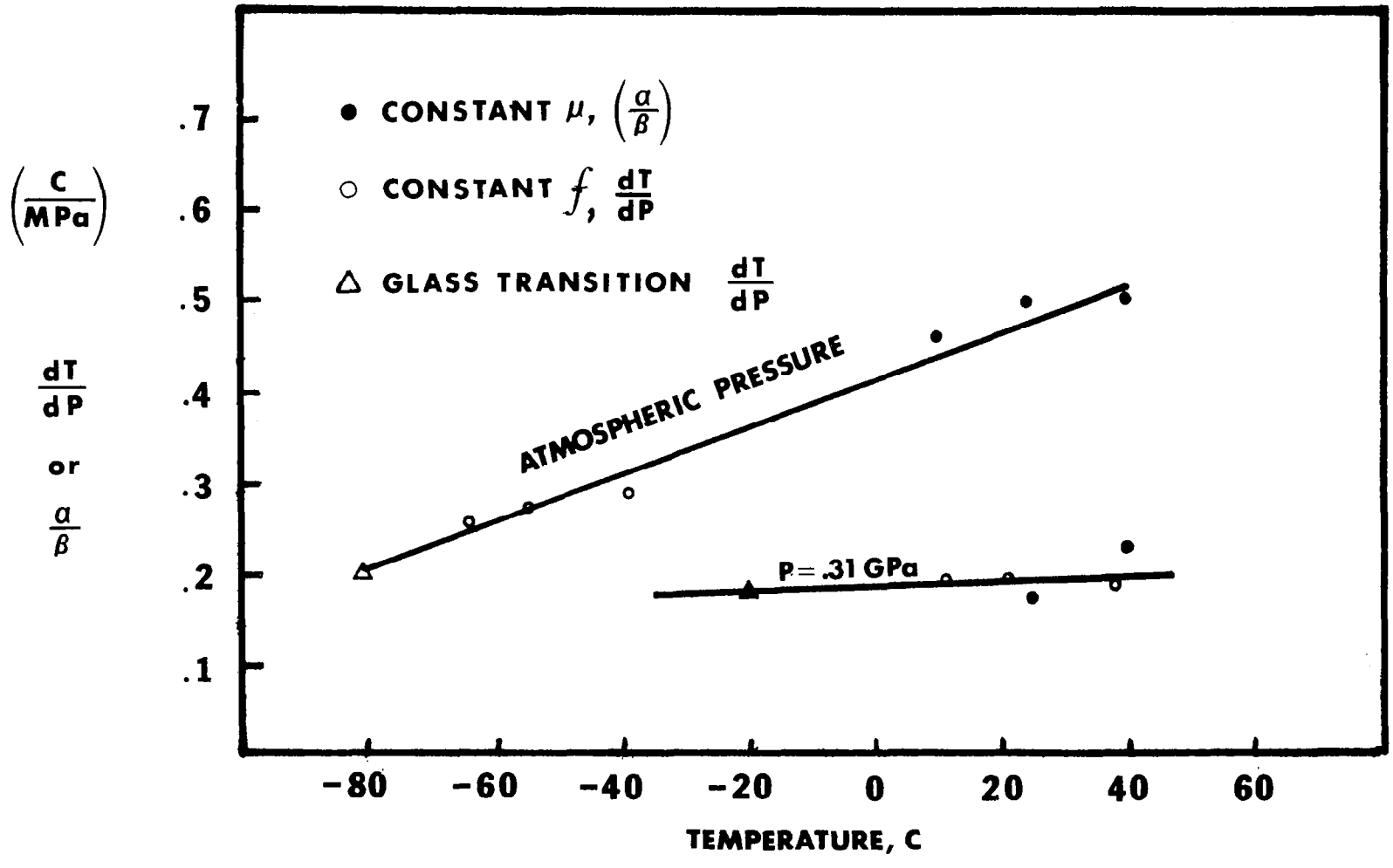

Figure 32. Comparison of Pressure-temperature Dependence at Constant Viscosity (μ) or Frequency (f) for Naphthenic Mineral Oil (N1).

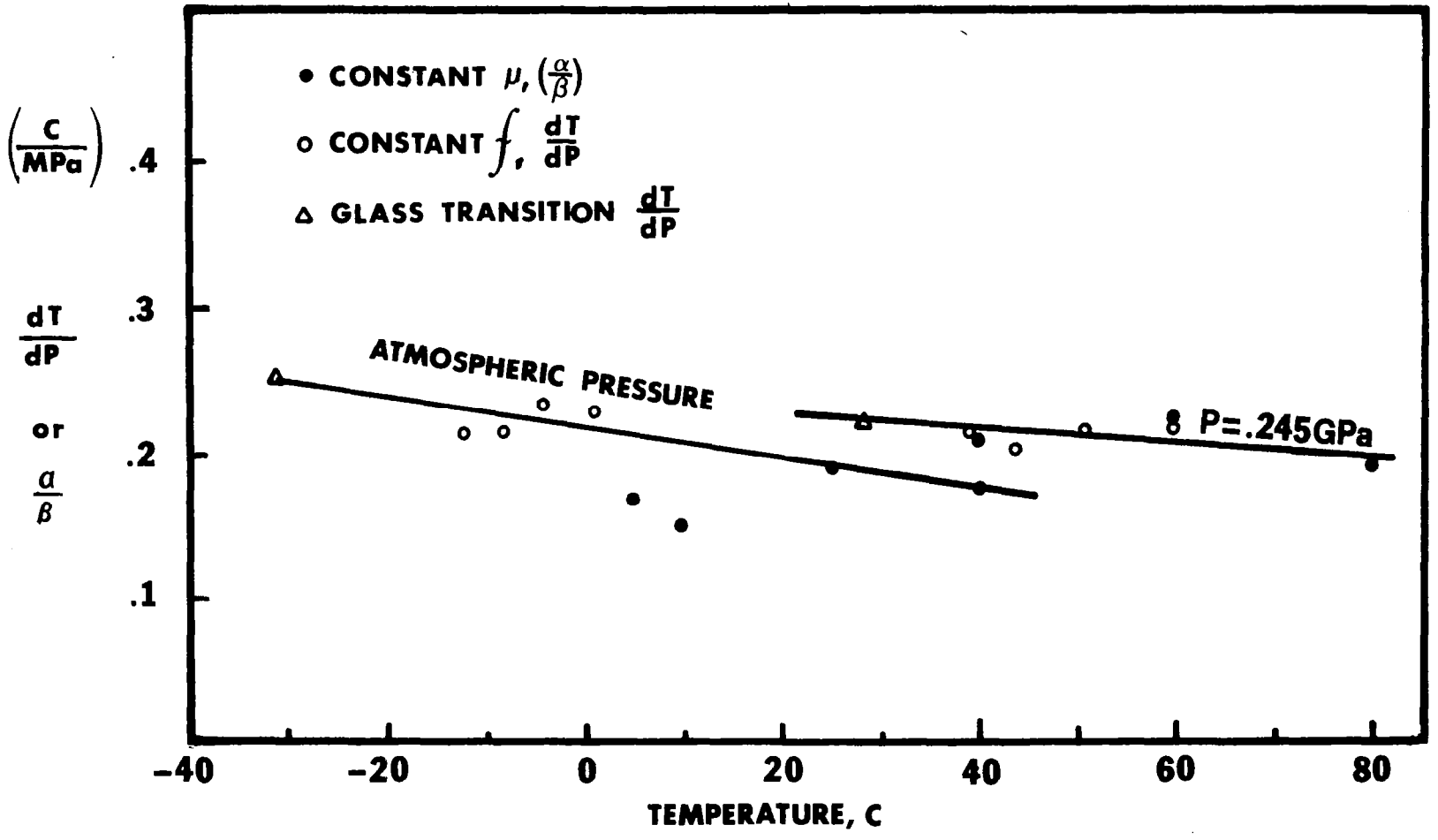

Figure 33. Comparison of Pressure-Temperature Dependence at constant Viscosity (μ) or frequency (f) for Polyphenyl ether (5P4E).

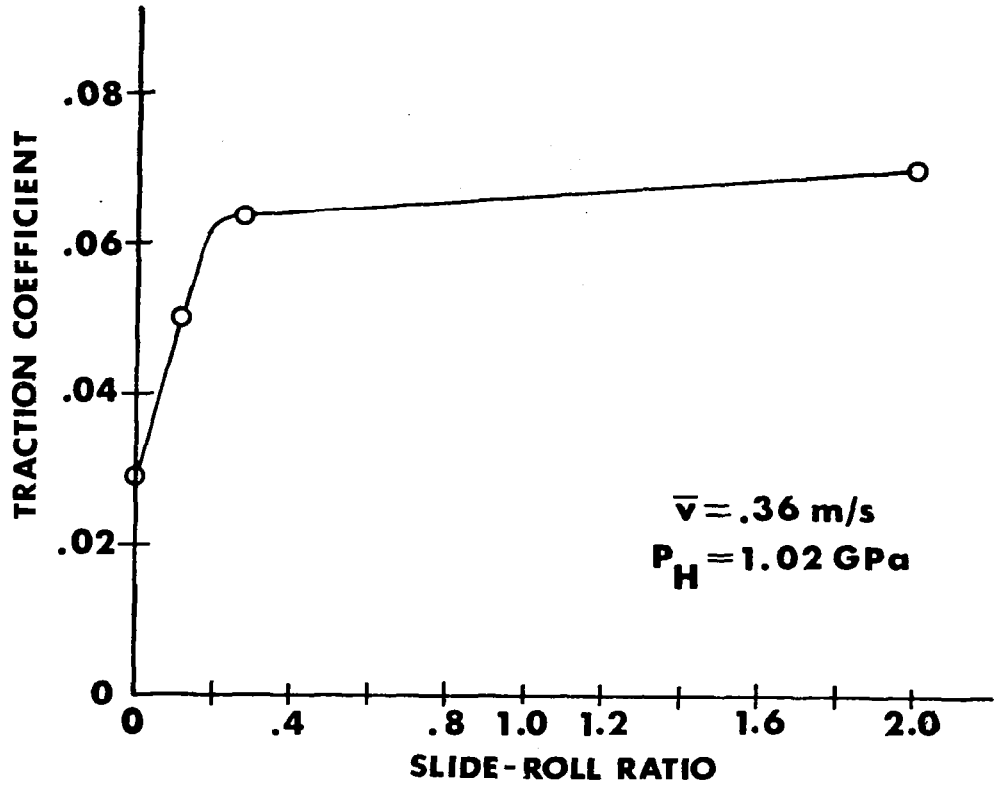

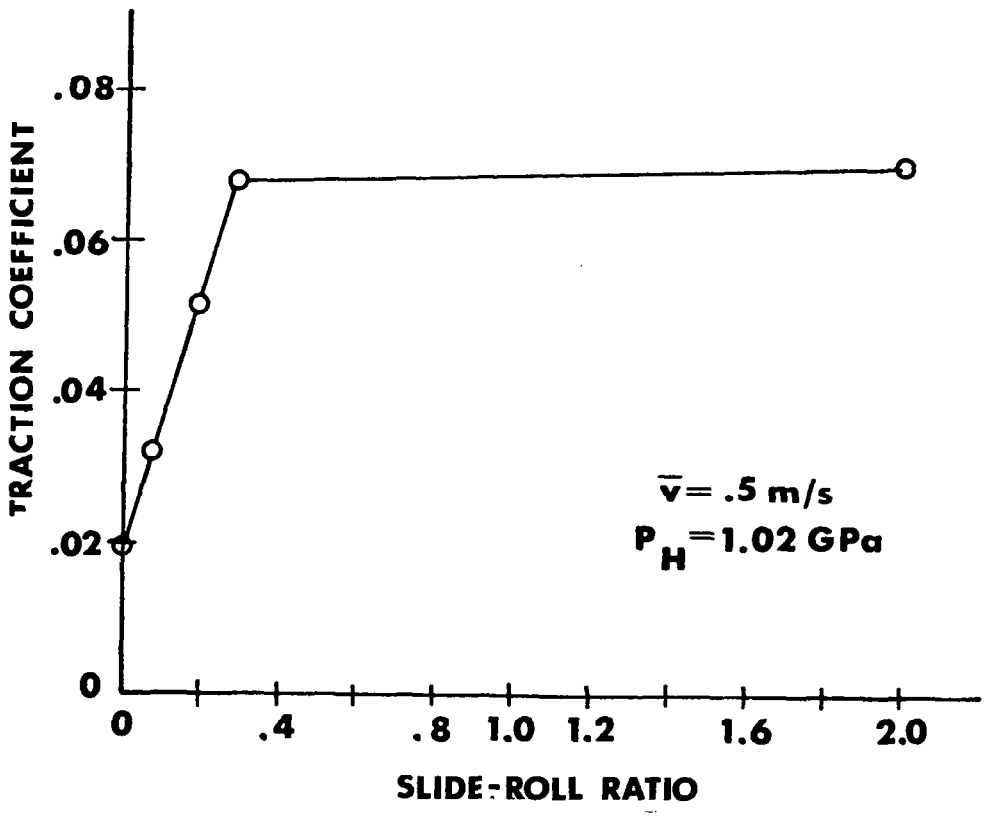

Figure 34. Traction Coefficient versus Slide-roll Ratio for Polyphenyl ether (5P4E).

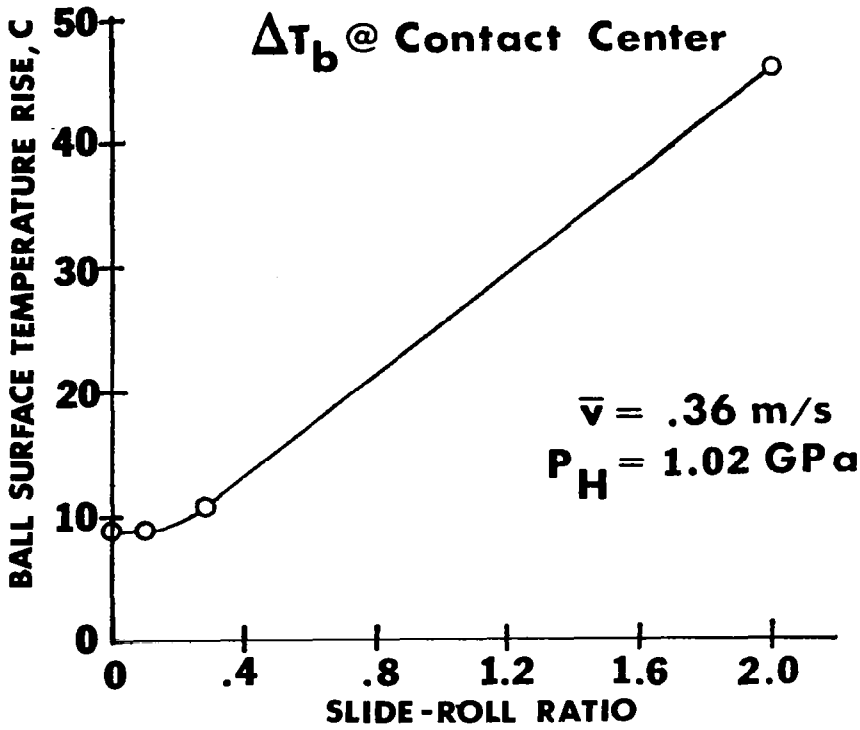

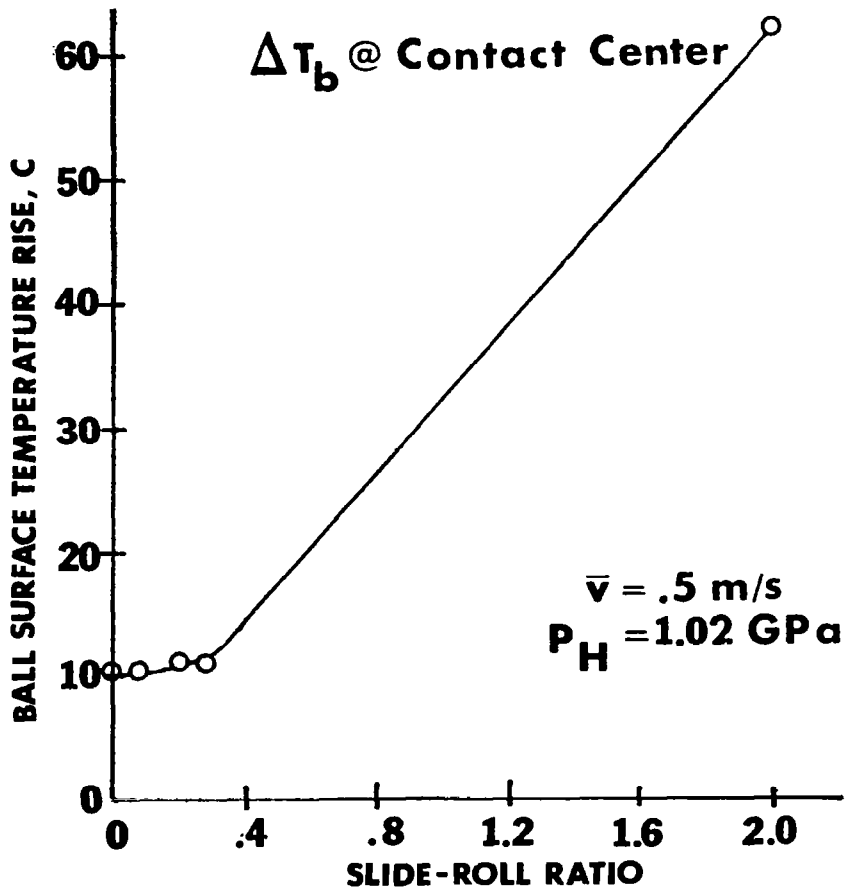

Figure 35. Ball Surface Contact Center Temperature Rise for Polyphenyl Ether (5P4E).

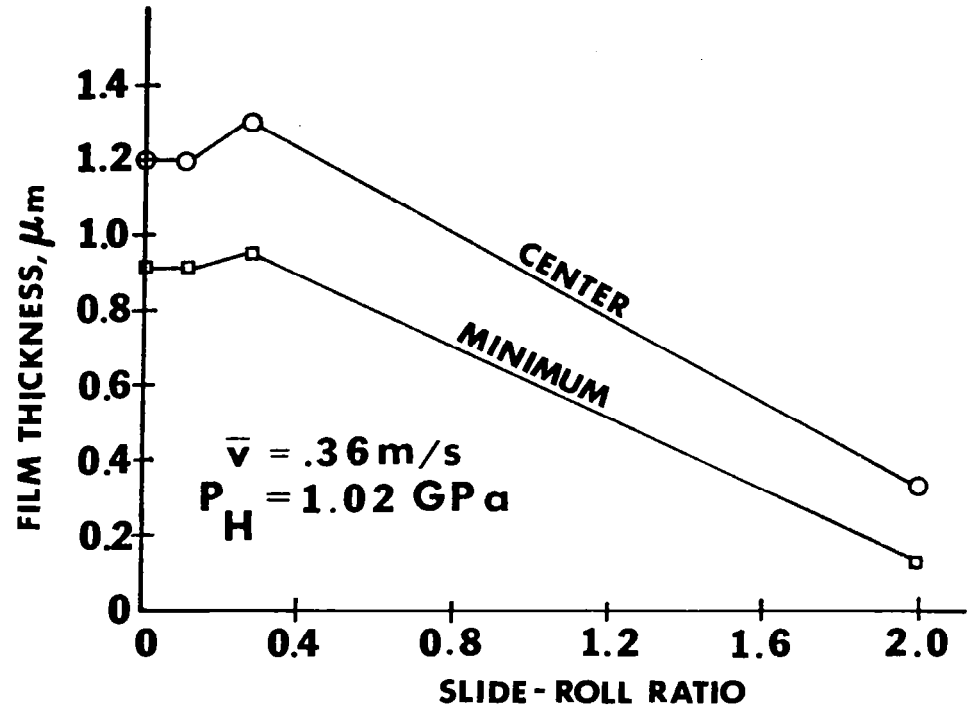

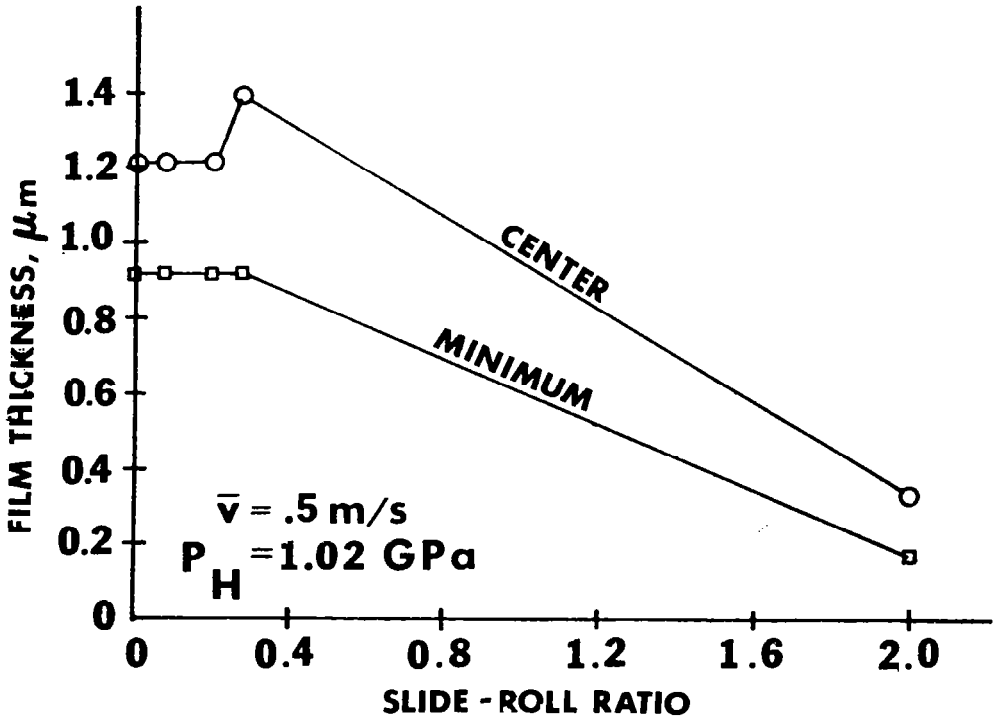

Figure 36. Film Thickness for Polyphenyl Ether (5P4E).

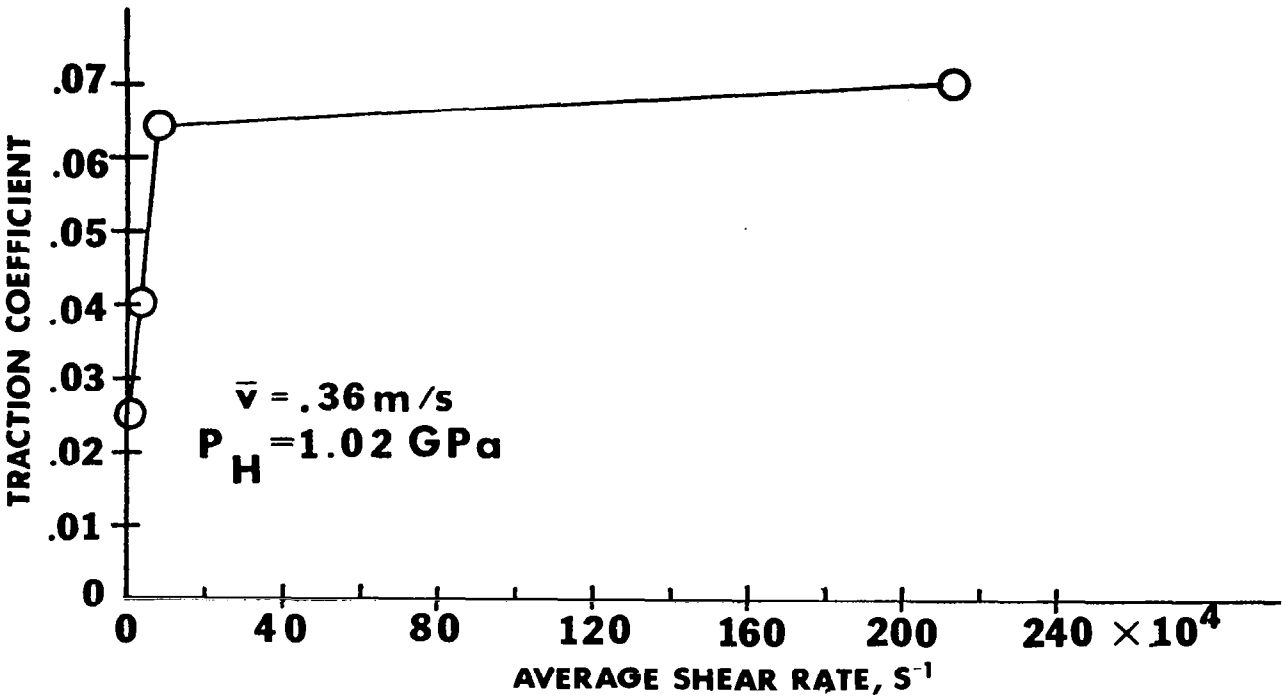

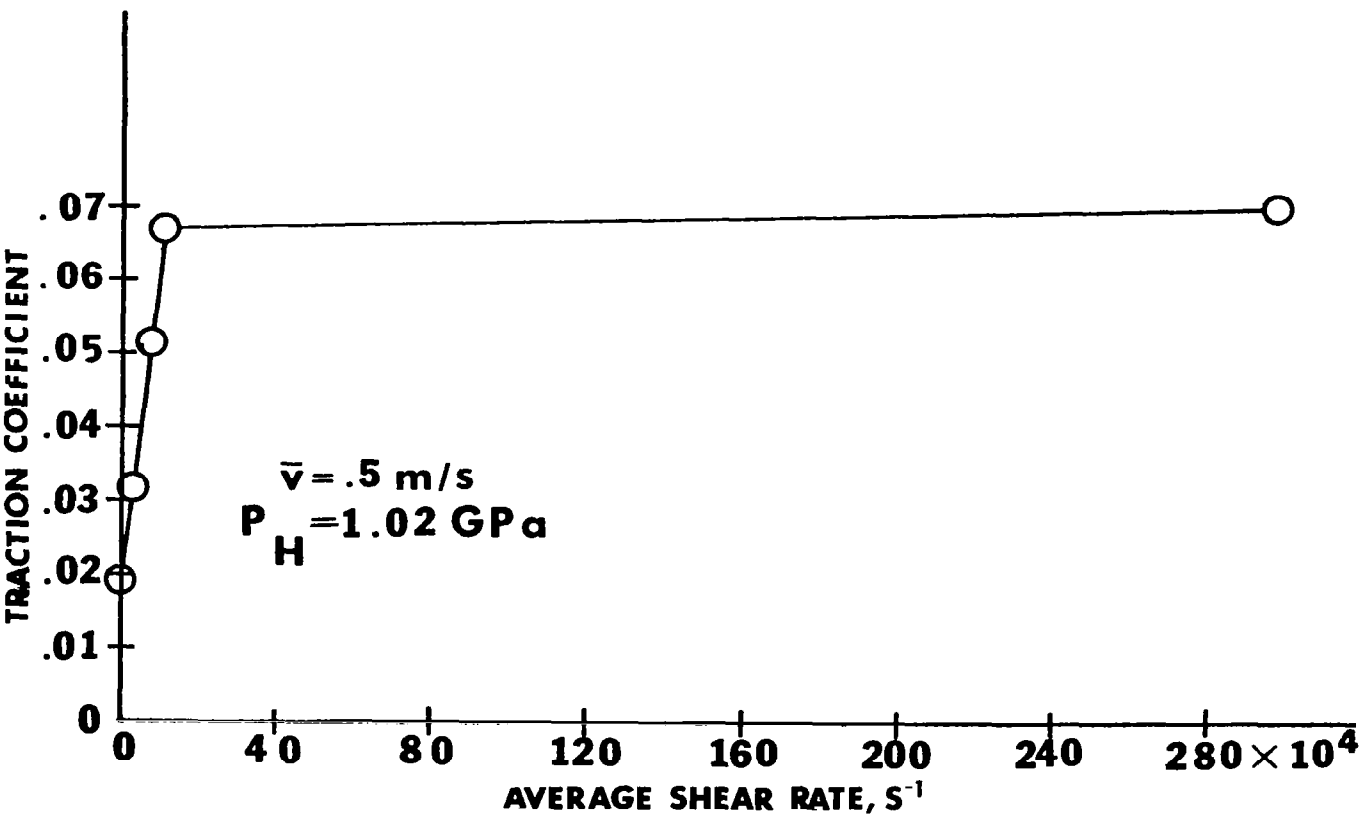

Figure 37. Traction Coefficient as a Function of Shear Rate, Polyphenyl Ether (5P4E).

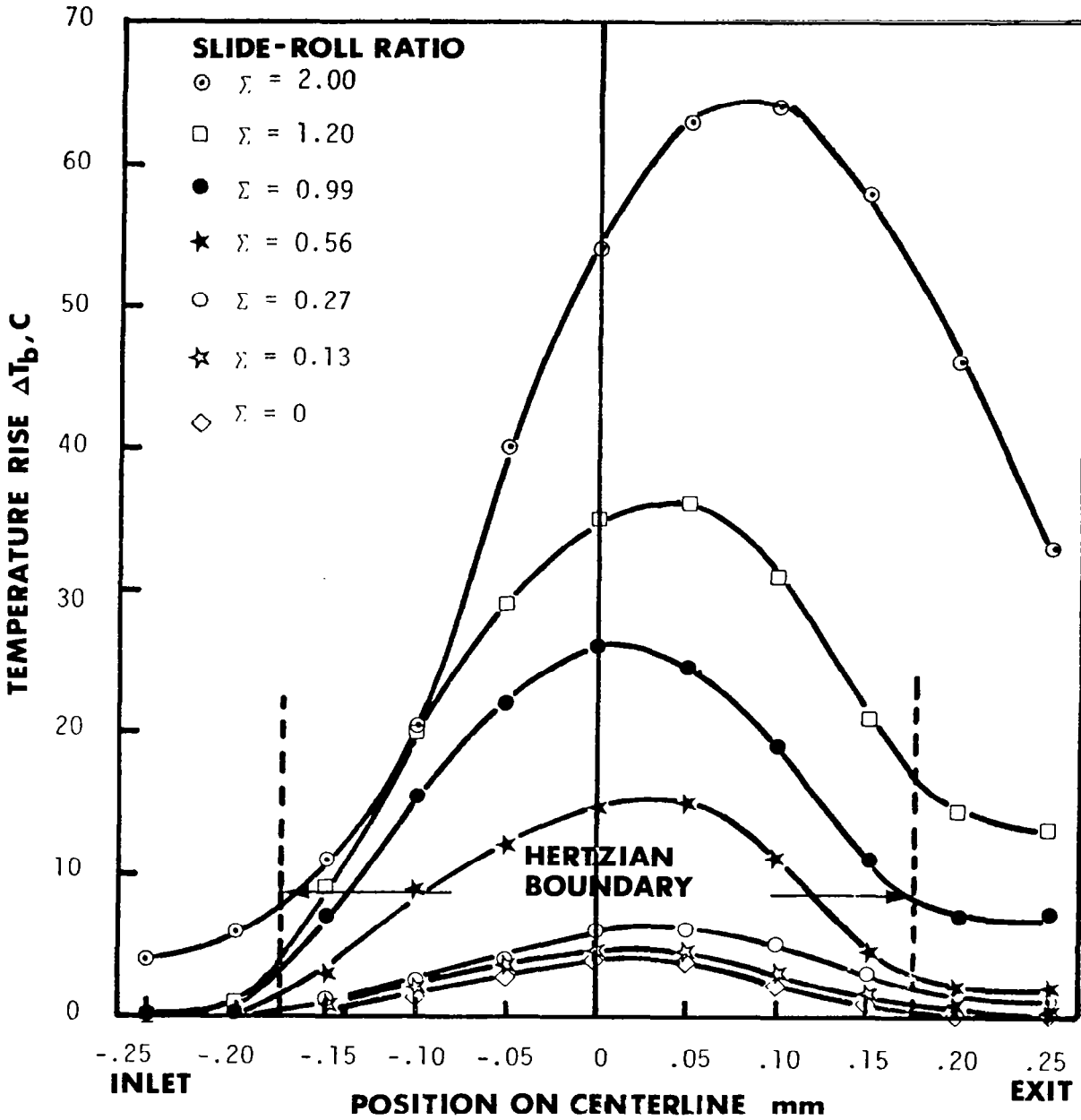

Figure 38. Ball Surface Temperature Rise Along the Contact Centerline (.011 μm R_a Roughness, P_H = 1.02 GPa, $\bar{V}$ = 0.75 m/s) for Naphthenic Mineral Oil (N1).

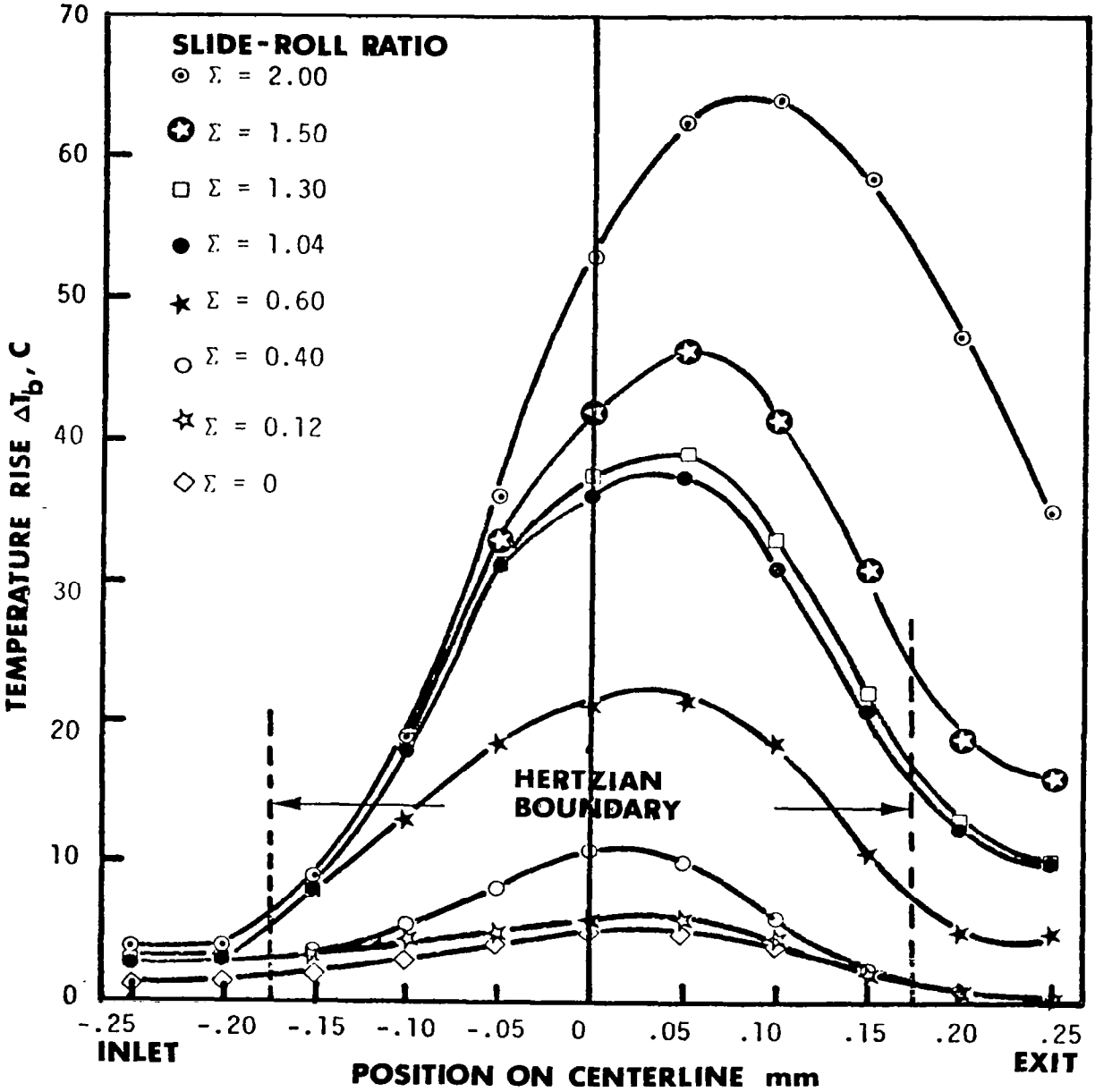

Figure 39. Ball Surface Temperature Rise Along the Contact Centerline (.011 μm R_a Roughness, P_H = 1.02 GPa, $\bar{V}$ = 1.00 m/s) for Naphthenic Mineral Oil (N1).

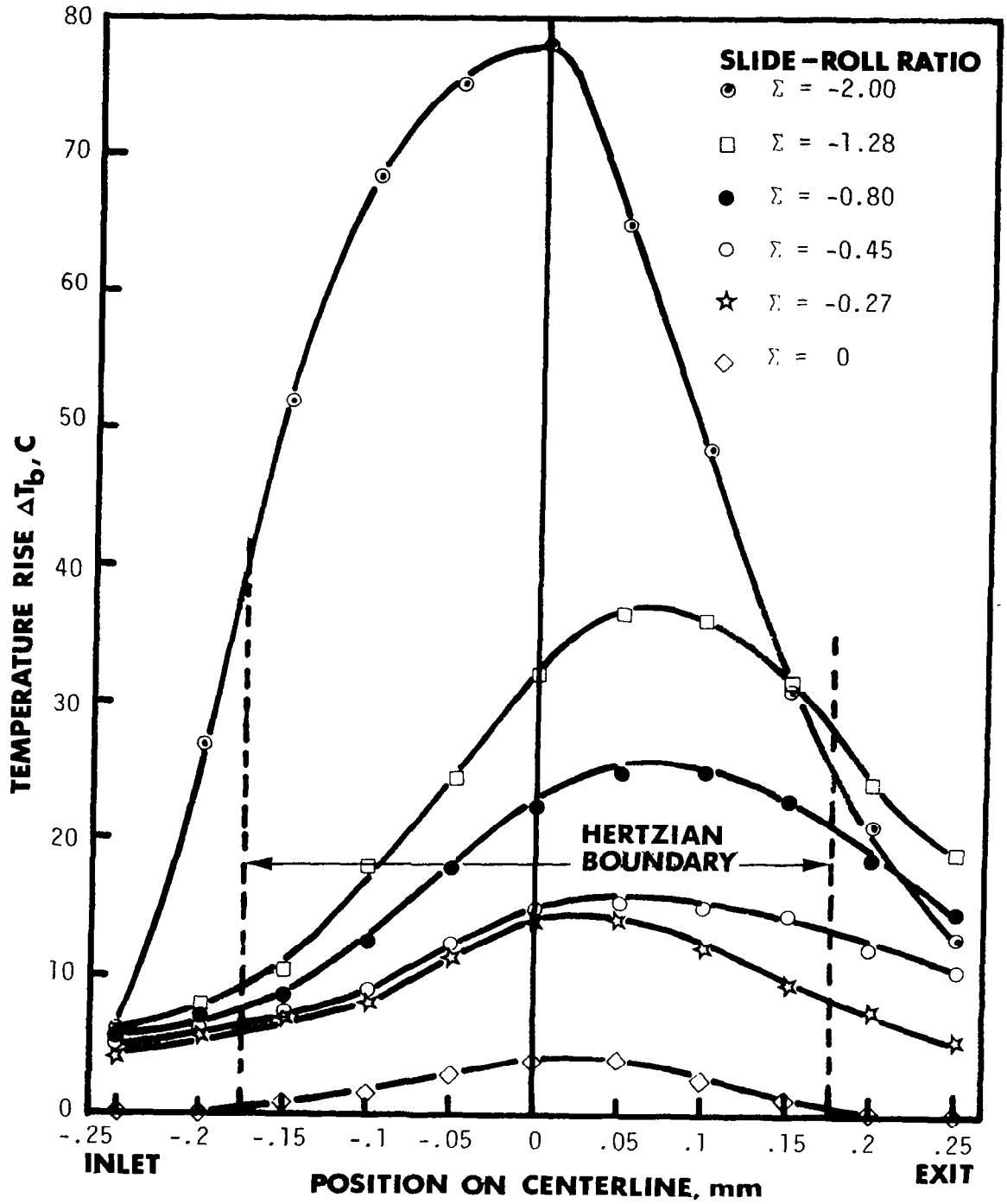

Figure 40. Ball Surface Temperature Rise along the Contact Centerline (Smooth ball 0.011 μm R_a, P_H = 1.02 GPa, $\bar{V}$ = 0.75 m/s) for Naphthenic Mineral Oil (N1).

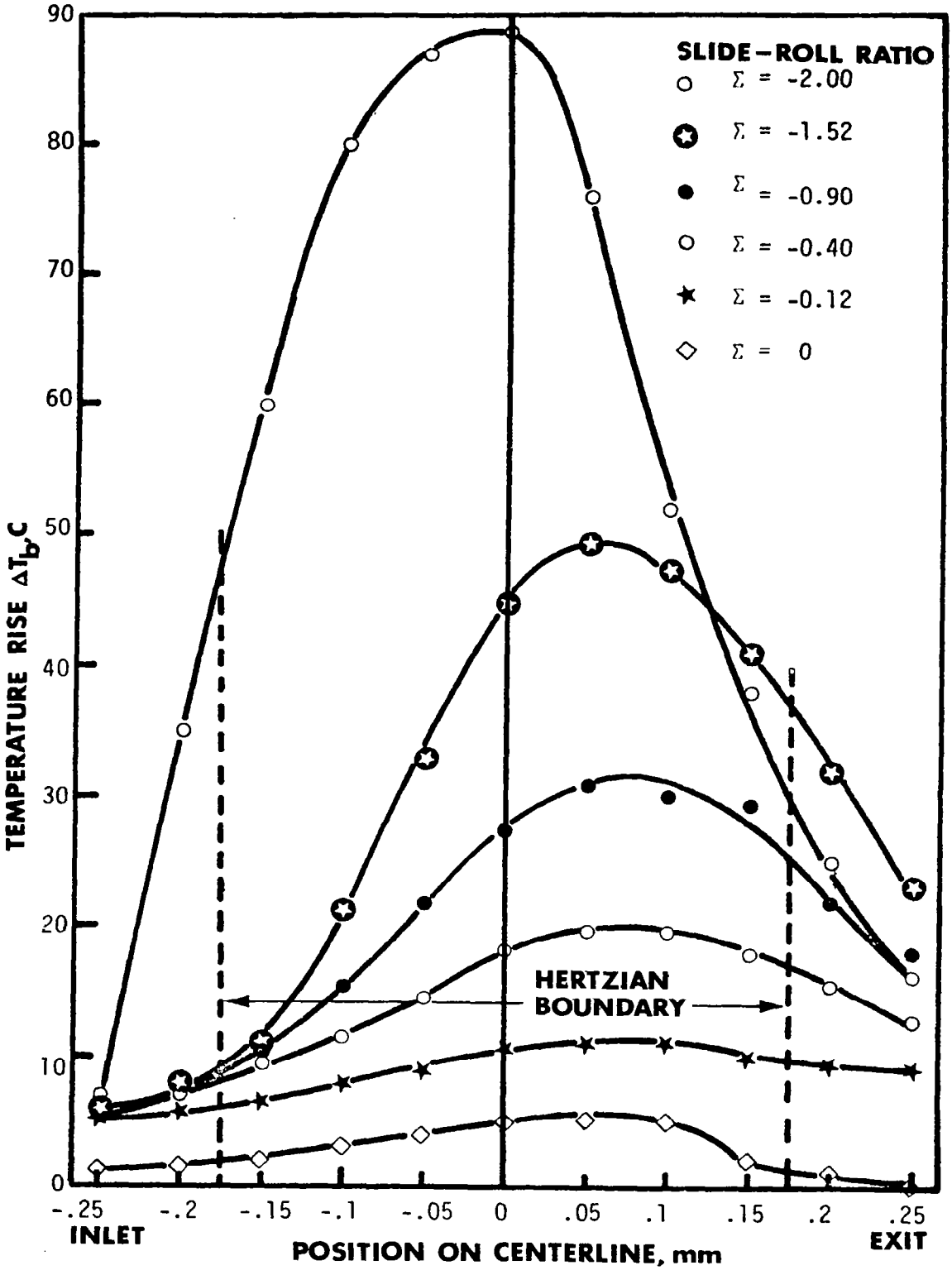

Figure 41. Ball Surface Temperature Rise along the Contact Centerline (Smooth ball 0.011 μm R_a, P_H = 1.02 GN/m^2, $\bar{V}$ = 1.0 m/s) for Naphthenic Mineral Oil (N1).

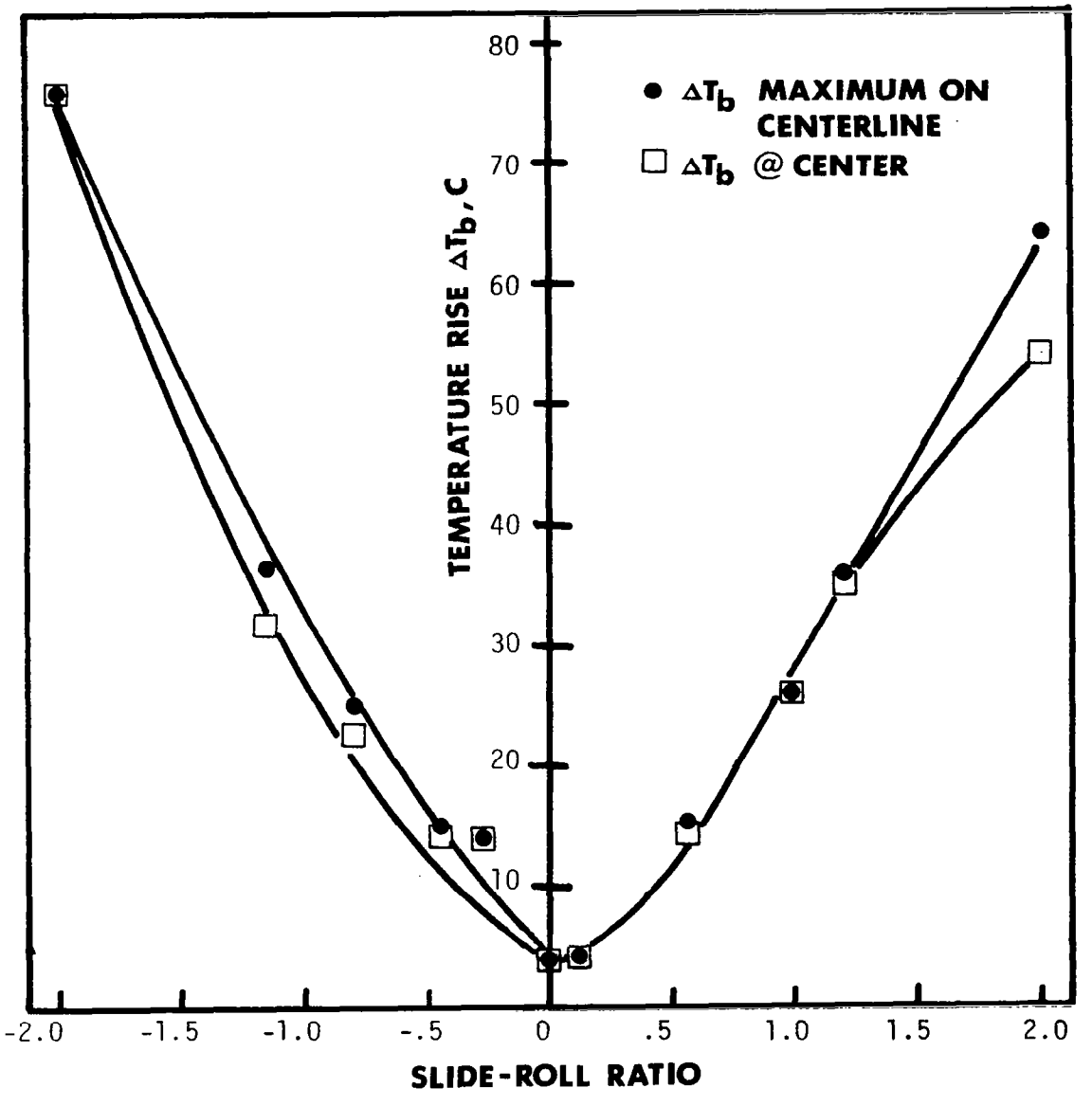

Figure 42. Ball Surface Temperature Rise as a Function of Slide-roll Ratio (-2 to +2) (Smooth ball 0.011 μm R_a, P_H = 1.02 GPa, $\bar{V}$ = 0.75 m/s) for Naphthenic Mineral Oil (N1).

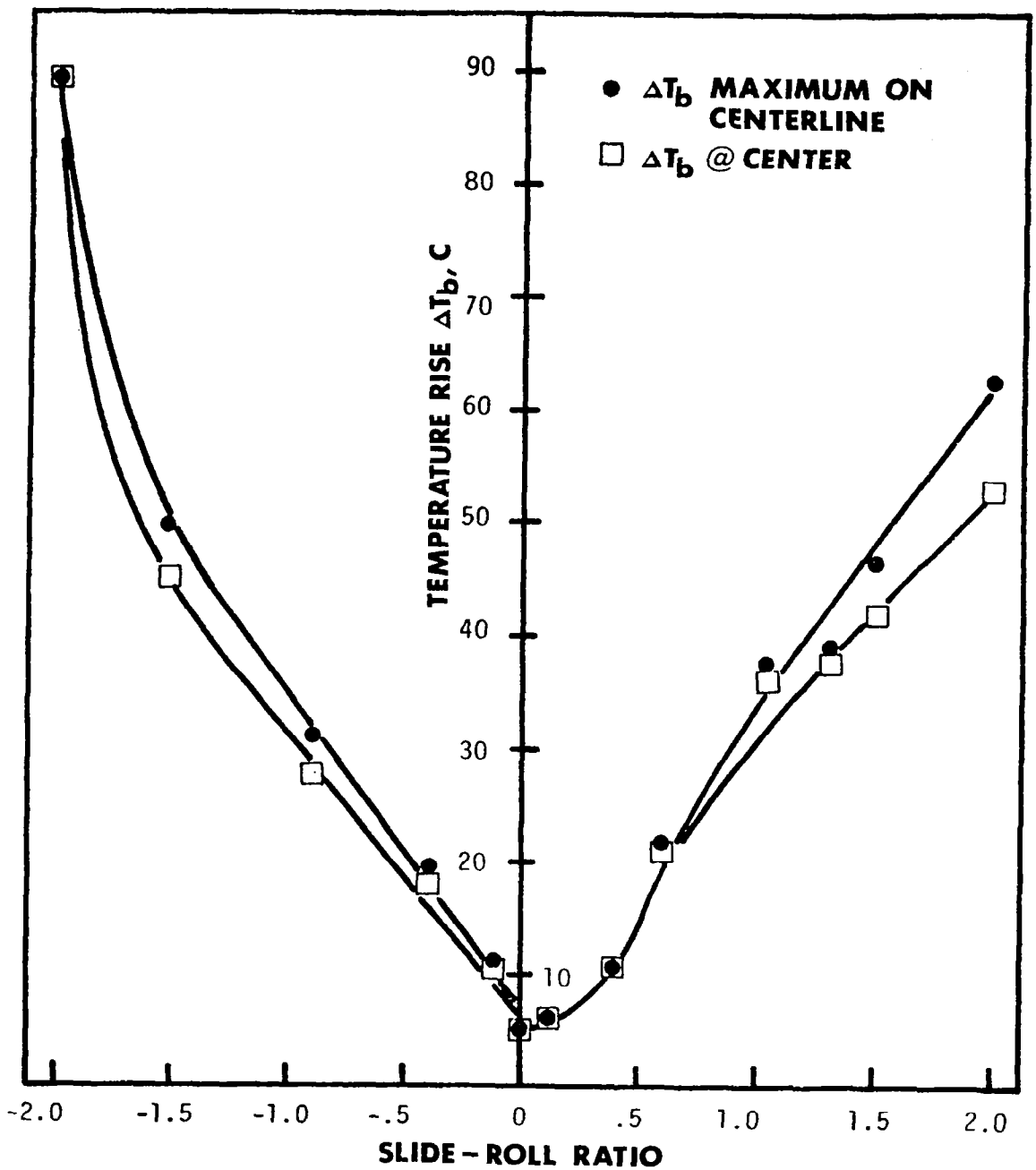

Figure 43. Ball Surface Temperature Rise as a Function of Slide-Roll Ratio (Smooth ball 0.011 μm R_a, P_H = 1.02 GPa, $\bar{V}$ = 1.0 m/s) on Naphthenic Mineral Oil (N1).

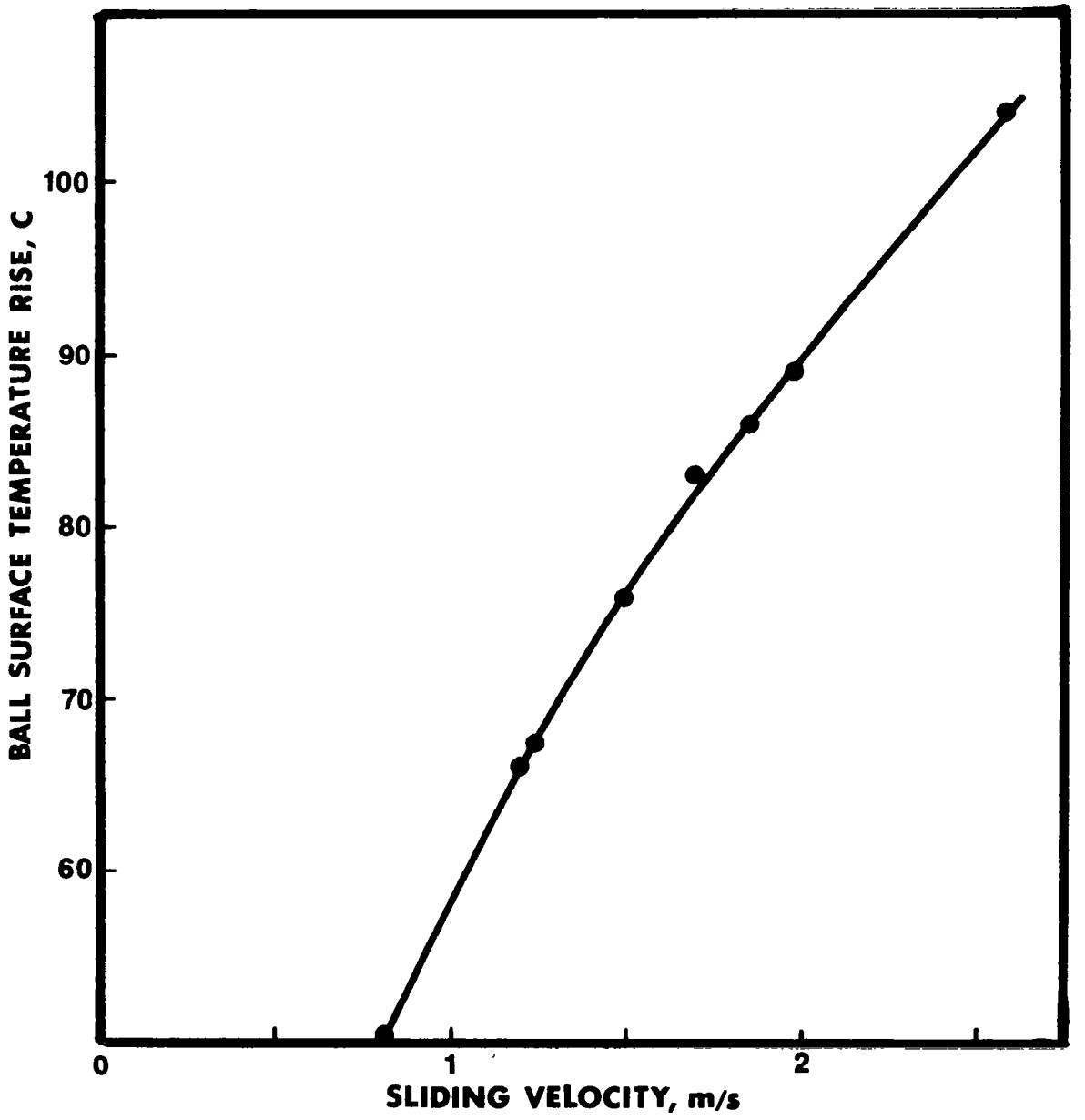

Figure 44. Stationary Ball Surface Temperature Rise, pure sliding, 1.02 GPa Hertz Pressure with Naphthenic Mineral Oil (N1), (See Table IV, p. 63).

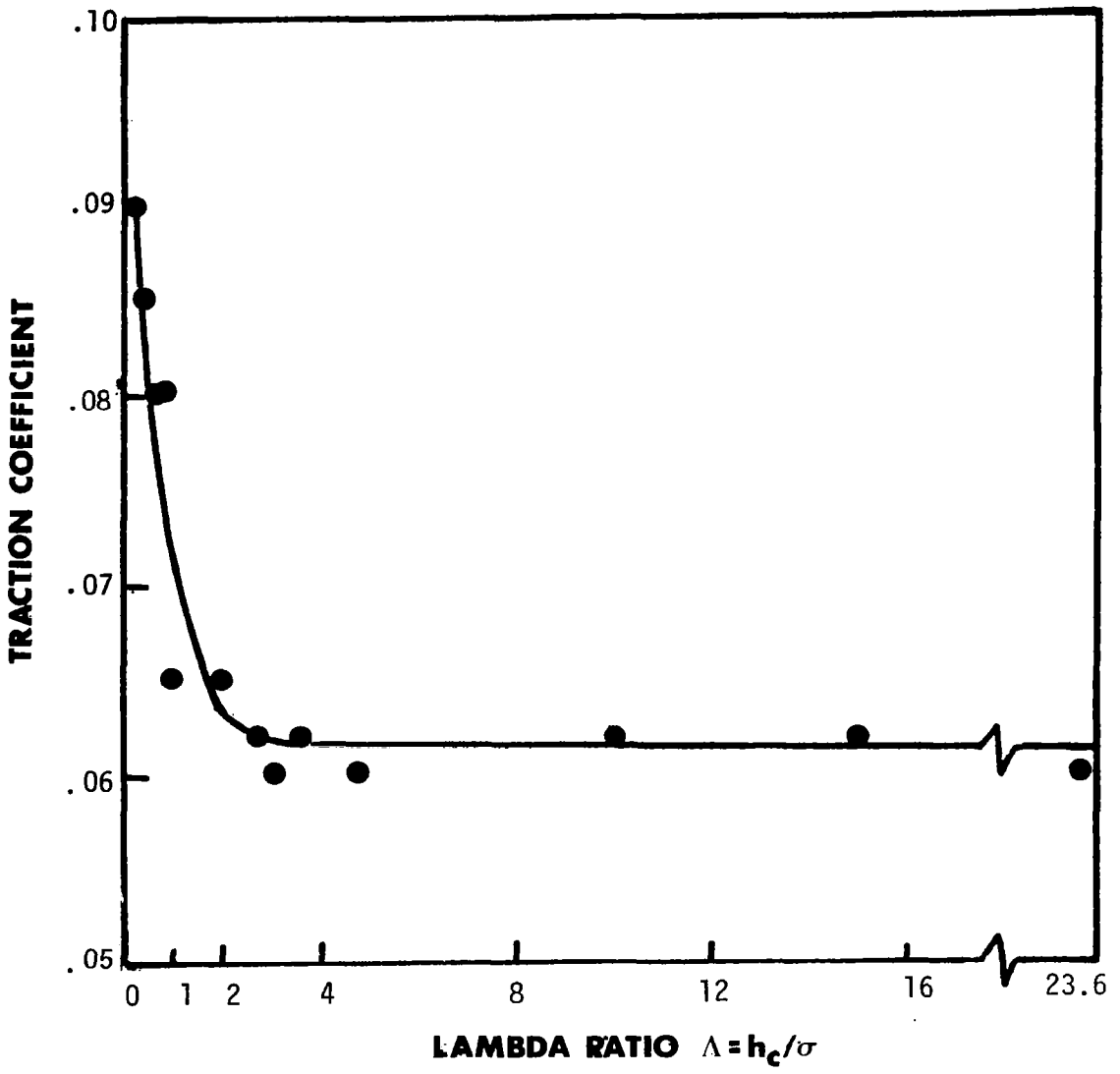

Figure 45. Traction Coefficient as a Function of Λ Ratio. Steel balls with roughnesses of 0.011, 0.076 and 0.38 μm R_a against sapphire flat, Naphthenic Mineral Oil, bulk temperature of 27C, load and sliding speed varied to vary Lambda ratio (Λ).

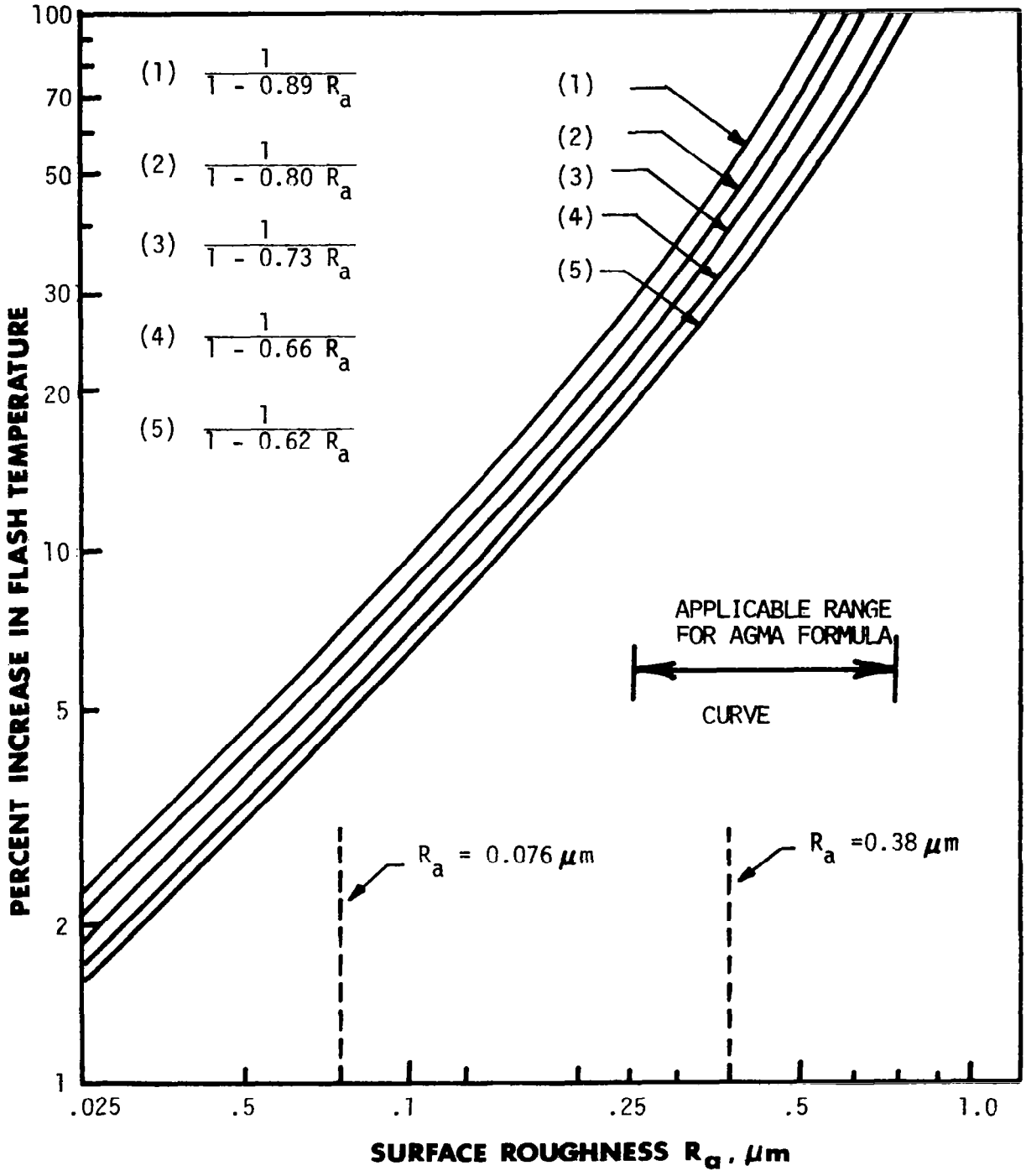

Figure 46. Percent Increase in Flash Temperature Due to Surface Roughness. Curve (2) corresponds to the Factor Recommended by AGMA [51] (For R_a = 0.011 μm increase less than 1%).

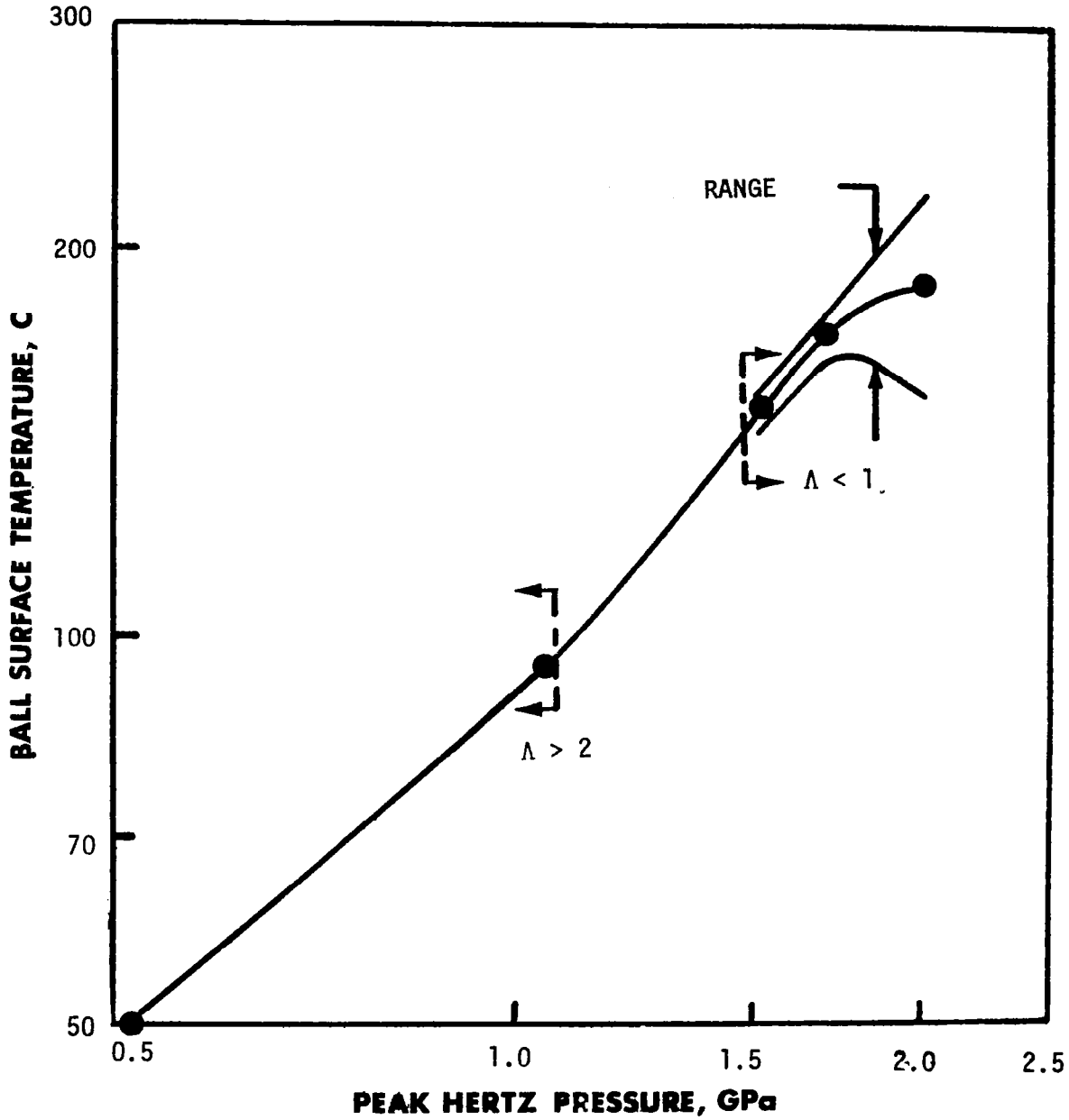

Figure 47. Average Value and Range of Ball Surface Temperature Fluctuation versus Peak Hertz Pressure (Medium Rough Ball: 0.076 μm R_a, Fluid Naphthenic Mineral Oil (N1),

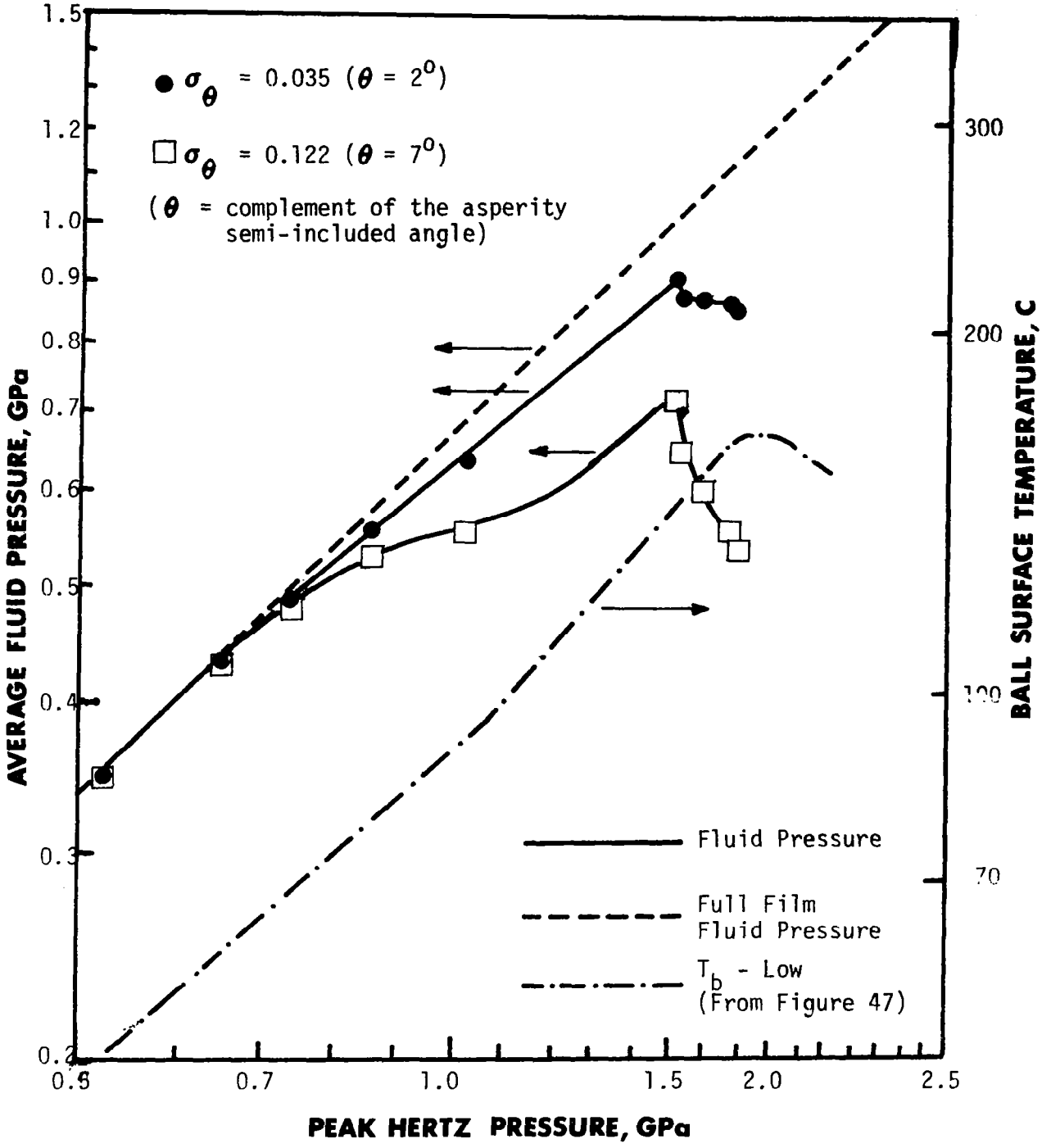

Figure 48. Average Fluid Pressure versus Peak Hertz Pressure under Partial EHD Conditions (Medium Rough Ball: 0.076 μm R_a. Fluid Naphthenic Mineral Oil (N1), Ball Sliding Speed 1.0 m/s).

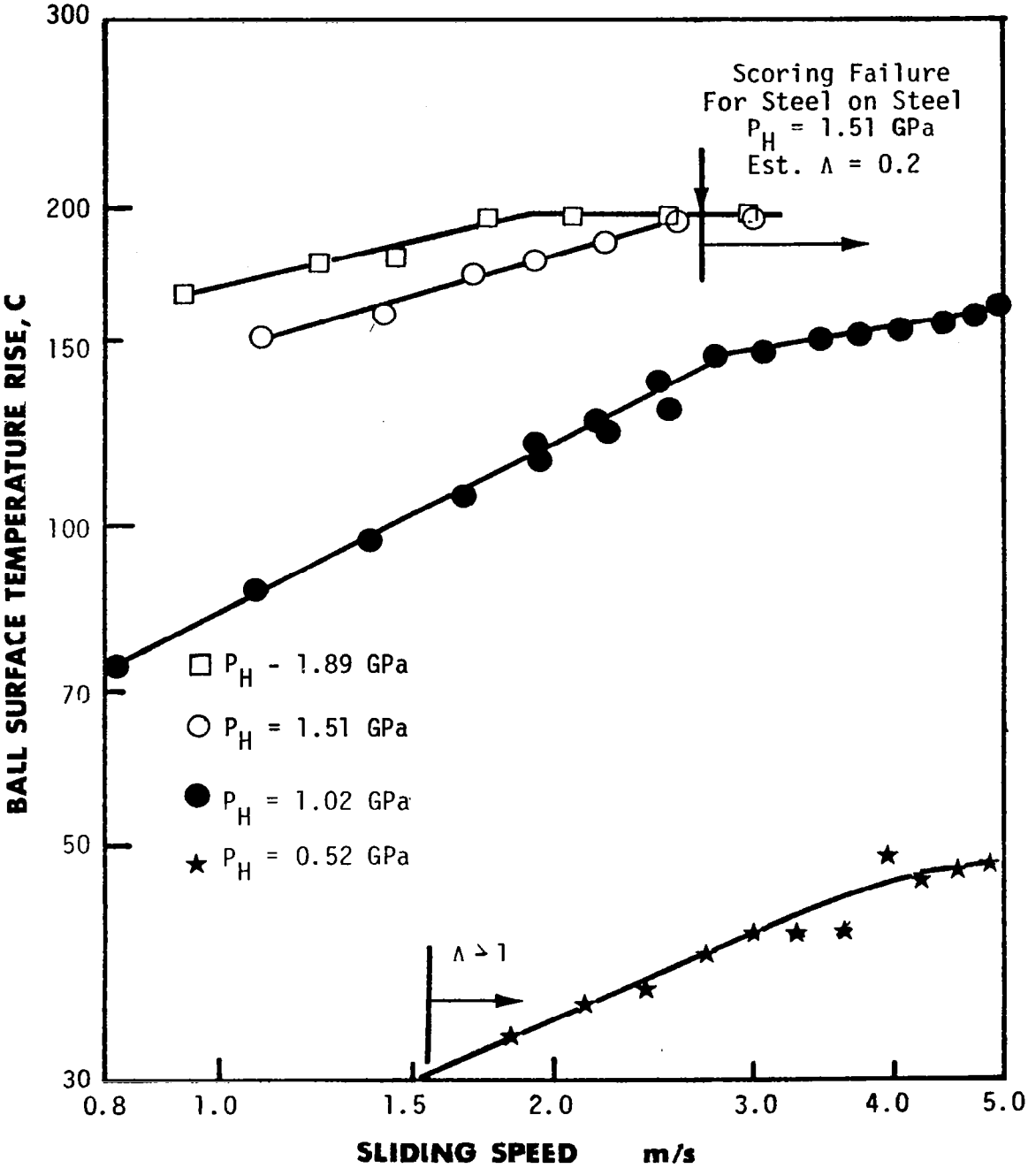

Figure 49. Maximum Ball Surface Temperature Rise versus Sliding Speed for Steel Ball/Sapphire Flat System (Rough Ball: 0.38 μm R_a, Fluid Naphthenic Mineral Oil N1, Flat Surface Stationary, Λ < 1 except as noted) with location of conditions for scoring failure with steel on steel system.

1. Report No.	2. Government Accession No.	3. Recipient's Catalog No.
NASA CR-3031		

4. Title and Subtitle	5. Report Date
SURFACE TEMPERATURES AND GLASSY STATE INVESTIGATIONS IN TRIBOLOGY - PART I	June 1978
	6. Performing Organization Code
7. Author(s)	8. Performing Organization Report No.
Ward O. Winer and David M. Sanborn	
	10. Work Unit No.
9. Performing Organization Name and Address	
Georgia Institute of Technology Atlanta, Georgia 30332	11. Contract or Grant No. NSG-3106
	13. Type of Report and Period Covered
12. Sponsoring Agency Name and Address	Contractor Report
National Aeronautics and Space Administration Washington, D.C. 20546	14. Sponsoring Agency Code

15. Supplementary Notes

Final report. Project Manager, William R. Jones, Jr., Fluid System Components Division, NASA Lewis Research Center, Cleveland, Ohio 44135.

16. Abstract

The research in this report is divided into two categories: (1) lubricant rheological behavior, and (2) thermal behavior of a simulated elastohydrodnamic contact. The studies of the lubricant rheological behavior consists of high pressure, low shear rate viscosity measurements, viscoelastic transition measurements, by volume dilatometry, dielectric transitions at atmospheric pressure and light scattering transitions. Lubricant shear stress-shear strain behavior in the amorphous glassy state has been measured on several fluids. It appears clear from these investigations that many lubricants undergo viscoplastic transitions in typical EHD contacts and that the lubricant has a limiting maximum shear stress it can support which in turn will determine the traction in the contact except in cases of very low slide-roll ratio. The thermal studies in elastohydrodynamic simulators were a continuation of the infrared temperature work previously reported from this laboratory. Surface temperature measurements were made for a naphthenic mineral oil and a polyphenyl ether. The maximum surface temperature in these experiments was approximately symmetrical about the zero slide-roll ratio except for absolute values of slide-roll ratio greater than about 0.9 in which case the slower moving surface had higher temperatures than the faster moving surface in the contact. Additional surface temperature measurements were made in contacts with rough surfaces where the composite surface roughness was approximately equal to the EHD film thickness. A regression analysis was done to obtain a predictive equation for surface temperatures as a function of pressure, sliding speed, and surface roughness. A correction factor for surface roughness effects to the typical flash temperature analysis was found which is very similar to that recommended by the American Gear Manufacturer's Association.

17. Key Words (Suggested by Author(s))	18. Distribution Statement
Liquid lubricants Elastohydrodynamic lubrication Glass transition Surface temperature	Unclassified - unlimited STAR Category 27

19. Security Classif. (of this report)	20. Security Classif. (of this page)	21. No. of Pages	22. Price*
Unclassified	Unclassified	126	A07

* For sale by the National Technical Information Service, Springfield, Virginia 22161

NASA-Langley, 1978